Repair of GFRP Reinforced Concrete Bridge Barriers

by

Mohammad Rubiat Islam

A Thesis submitted to the Faculty of Graduate Studies of

The University of Manitoba

in partial fulfillment of the requirements of the degree of

MASTER OF SCIENCE

Department of Civil Engineering

University of Manitoba

Winnipeg, Manitoba, Canada

Copyright © 2012 by Mohammad Rubiat Islam

ABSTRACT

In present days both concrete bridge decks and barriers are being internally reinforced with corrosion free glass fiber-reinforced polymer (GFRP) bars. The design of bridge decks and barriers with internal GFRP reinforcement is well established and incorporated in current CAN/CSA-S6-06 code provisions. However, no test results are available on repairing GFRP-RC bridge barriers in case of damage caused by vehicle accidents. Therefore, this present research is aimed to conduct experiments on repairing full-scale GFRP-RC bridge barriers and provide much needed guidelines to repair such barriers. To do so, three full-scale 6-m long Performance Level-2 (PL-2) concrete bridge barriers (used in moderate to high traffic volume highways) totally reinforced with GFRP bars as per CAN/CSA-S6-06 were constructed. Then these barriers were tested at the middle and two edges of the barrier by applying monotonic load up to failure simulating vehicle crash test. Two different repair techniques, Splicing (Planting) and Near Surface Mounted (NSM), were used to repair the damaged barriers, and finally retested under the identical load condition that of intact barriers to evaluate the efficiency of the repair techniques. Test results were compared and discussed in terms of barrier wall capacity, mode of failure, deflection and strains in GFRP bars to evaluate the performance of intact barrier walls as well as efficiency of the repair techniques. It was concluded that GFRP-RC bridge barrier can be repaired using either Splicing (Planting) technique or NSM technique.

ACKNOWLEDGEMENT

I would like to express my deepest and sincere gratitude to my supervisor Dr. Ehab El-Salakawy Ph.D., P.Eng., Canada Research Chair in Durability and Modernization of Civil Structures in the Department of Civil Engineering at the University of Manitoba, for his guidance, continuous encouragement and unlimited support throughout the course of this research program.

I would like to express my gratitude and sincere appreciation to the Network of Centres of Excellence on Intelligent Sensing for Innovative Structures (ISIS-Canada) and the Natural Science and Engineering Research Council of Canada (NSERC) for financing this research work. The help received from the technical staff of the McQuade Heavy Structural Laboratory in the Department of Civil Engineering at the University of Manitoba is also acknowledged.

I would like to thank Mr. Chad Klowak, Mr. Brendan Pachal, Mr. Tylor Goerge, Mr. Vishesh Panjabi for their support in my experimental work. I would also like to appreciate my research group colleagues for their warmth of friendship during my research work.

Finally, I would like to express my deepest homage to my parents, my siblings and my beloved Monisha Ehsan who have always remained beside me with all their heart and affection.

Mohammad Rubiat Islam

TABLE OF CONTENTS

ABSTRACT…… i

ACKNOWLEDGEMENT……. ii

TABLE OF CONTENT…….iii

LIST OF TABLES…….. viii

LIST OF FIGURES …… ix

CHAPTER 1: INTRODUCTION …….. 1

1.1. Introduction……. 1

1.2. Objectives ……... 3

1.3. Scope of the Research……..3

1.4. Research Significance ……..…...3

1.5. Research Methodology ……... 4

1.6. Thesis Organization……5

CHAPTER 2: LITARATURE REVIEW ……... 7

2.1. General ……... 7

2.2. Canadian Highway Bridge Design Code ……... 7

2.3. Functions……8

2.4. Types……... 8

2.5. Traffic Barrier……10

2.6. Traffic Barrier Requirements in CHBDC and AASHTO……10

2.6.1. Performance Level ……..11

2.6.2. Crash Test Requirement……..... 13

2.6.3. Anchorages……..14

2.6.4. Bridge Barrier Design Process…… 16

2.7. Barrier Test……19

2.7.1. Test Levels and Crash Test Requirements in AASHTO…….20

2.7.2. Barrier Test in USA…….22

2.7.2.1. TTI (Test level 4-12, 4-11) Test…….23

2.7.2.2. Pendulum Impact Test and Equivalent Static Test by (CTR at UTA)…...23

2.7.2.3. Barrier Test Results and Discussion……...24

2.7.3. Barrier Testing in Canada……... 25

2.7.4. Static Load Test…….. 26

2.7.4.1. Loading Requirements…….. 26

2.8. Concrete Removal Techniques……..28

2.9. Repair Techniques ……... 31

2.9.1. Splicing (Planting) Technique…… 31

2.9.1.1. Bond Mechanism of Deformed bars……..32

2.9.1.2. Bond Failure Modes…….. 33

2.9.1.3. Bond Behavior of FRP bars…….. 34

2.9.1.4. Factors Affecting Splicing (planting) Technique…….. 35

2.9.2. NSM Technique……. 37

2.9.2.1. Bond Mechanism…….. 38

2.9.2.2. Modes of Failure……39

2.9.2.3. Factors Affecting NSM Technique……40

CHAPTER 3: EXPERIMENTAL PROGRAM ……. 43

3.1. General …… 43

3.2. Experimental Program – Phase I……. 43

3.2.1. PL-2 Barrier Wall Reinforcement Detailing…….. 43

3.2.2. Barrier Wall Prototypes…….. 45

3.2.3. Instrumentation……... 47

3.2.4. Loading Conditions……50

3.2.5. Construction of Barrier Wall Prototype…….. 51

3.2.6. Test Setup……54

3.2.7. Test Matrix and Loading Rates……... 56

3.3. Experimental Program - Phase II……. 58

3.3.1. Repairing Damaged Portion……58

3.3.2. Repairing Using Splicing (Planting) Technique……. 58

3.3.2.1. Repairing Middle Portion Using Splicing (Planting) Technique…….. 58

3.3.2.2. Repairing Edge Portion Using Splicing (Planting) Technique....……...64

3.3.3. Repairing Using NSM Technique……68

3.3.3.1. Repairing Middle Portion Using NSM Technique……68

3.3.3.2. Repairing Edge Portion Using NSM Technique……... 73

CHAPTER 4: TEST RESULTS AND DISCUSSION…… 77

4.1. General …… 77

4.2. Test Results and Discussion of Phase I ……... 77

4.2.1. Ultimate Capacity and Mode of Failure …… 77

4.2.2. Cracking Pattern …… 80

4.2.3. Deflection...…… 83

4.2.3.1. Deflection for Middle Test…….. 83

4.2.3.2. Deflection for Edge Test…….. 86

4.2.3.3. Summary of Deflection…… 88

4.2.4. Strains in Reinforcements ……. 89

4.2.4.1. Strains in Reinforcements for Middle Test …… 89

4.2.4.2. Strains in Reinforcements for Edge Test ……93

4.2.3.3. Summary of Strains ……97

4.2.5. Load Sharing……98

CHAPTER 5: TEST RESULTS, COMPARISINS AND DISCUSSION……. 100

5.1. Test Results of Phase II and Comparisons…….100

5.2. Ultimate Capacity and Mode of Failure…….....100

5.3. Cracking Pattern……106

5.4. Deflections……..... 109

5.4.1. Deflection for M1-P Test…….....110

5.4.2. Deflection for M2-N Test……..112

5.4.3. Deflection for RE-P Test……..... 115

5.4.4. Deflection for LE-N Test……..... 118

5.4.5. Summary of Deflections……... 121

5.5. Strains in Reinforcements…….. 123

5.5.1. Strains in Reinforcements for M1-P Test……. 124

5.5.2. Strains in Reinforcements for M2-N Test…… 128

5.5.3. Strains in Reinforcements for RE-P Test……..... 132

5.5.4. Strains in Reinforcements for LE-N Test……. 135

5.5.5. Summary of Strains in Reinforcements…… 139

CHAPTER 6: SUMMARY, CONCLUSIONS AND FUTURE WORK…….. 142

6.1. Summary…… 142

6.2. Conclusions…… 143

6.2.1. Conclusions from Phase I…… 143

6.2.2. Conclusions from Phase II…… 144

6.3. Future Work……... 146

REFERENCES…….. 146

APPENDIX A: …….. A-1

APPENDIX B: …….. B-1

APPENDIX C: …….. C-1

APPENDIX D: …….. D-1

APPENDIX E: …….. E-1

APPENDIX F: ……... F-1

APPENDIX G: ……...G-1

LIST OF TABLES

Table (2.1): Traffic barrier loads, reproduced from Figure 3.8.8.1, CAN/CSA-S6-06…… 16

Table (2.2): Traffic barrier loads, according to AASHTO……16

Table (2.3): Crash test criteria according to AASHTO…… 22

Table (2.4): TTI test results……...24

Table (2.5): CTR test results……24

Table (3.1): Test matrix…… 56

Table (3.2): Loading rates……. 57

Table (4.1): Ultimate capacity and mode of failure for intact prototypes…… 78

Table (4.2): Maximum deflection of intact prototypes……..88

Table (4.3): Maximum strains in GFRP reinforcements of intact prototypes…….. 97

Table (5.1): Ultimate capacity and mode of failure at middle…….101

Table (5.2): Ultimate capacity and mode of failure at edge……....103

Table (5.3): Maximum deflections of repaired and intact prototypes…….121

Table (5.4): Summary of strains in GFRP reinforcements for repaired and intact prototypes....140

LIST OF FIGURES

Figure (2.1): Bridge barriers, reproduced from CHBDC (CAN/CSA-S6-06 2006) and AASHTO LRFD (2007)……..9

Figure (2.2): Reinforcement detailing of GFRP-RC bridge barrier based on performance level, reproduced from Figure C 16.1 and Figure C16.2 of Commentary on CAN/CSA-S6-06……13

Figure (2.3): Application of design loads to traffic barriers, reproduced from CAN/CSA-S6-06 Figure (12.5.2.4)…….. 15

Figure (2.4): Yield pattern in bridge barrier due to truck collision at the middle and edges of the barrier, reproduced from AASHTO LRFD (2007)……..17

Figure (2.5): Loads requirements of PL-2 barrier wall……27

Figure (2.6) Bond force transfer mechanisms for deformed bars reproduced from ACI 408R-03 (2003)……...32

Figure (2.7): Cracking and damage mechanisms in bond: a) End view showing splitting cracks between bars and concrete cover; b) Side view of member showing shear crack and/or local concrete crushing due to bar pullout; reproduced from ACI 408R-03 2003)……34

Figure (2.8) NSM-FRP strengthened beam (typical)……39

Figure (2.9) Modes of failure of NSM-FRP under pull-out test (reproduced from Soliman et al. 2010)……40

Figure (3.1): Reinforcement detailing of PL-2 barrier wall, reproduced from Figure C 16.1 of Commentary on CAN/CSA-S6-06…….. 44

Figure (3.2): Transverse section of a barrier wall prototype…….46

Figure (3.3): Locations of strain gauges on vertical bars……..47

Figure (3.4): Locations of strain gauges in the barrier wall while testing on the middle portion.48

Figure (3.5): Locations of strain gauges in the barrier wall while testing on the edge……48

Figure (3.6): Locations of LVDT……..49

Figure (3.7): Locations of LVDT's while testing the middle portion of the barrier wall…….49

Figure (3.8): Locations of LVDT's while testing the edge of the barrier wall……. 50

Figure (3.9): Application of transverse load at the middle portion of a barrier wall…… 51

Figure (3.10): Application of transverse load on edges of a barrier wall……. 51

Figure (3.11): Holes layout in the prototype subjected to middle portion testing…… 52

Figure (3.12): Holes layout in the prototype subjected to end portion testing……..52

Figure (3.13): Reinforcement cage of deck slab……... 53

Figure (3.14): Concrete casting……53

Figure (3.15): Finishing concrete of deck slab……. 53

Figure (3.16): Barrier wall reinforcement cage……53

Figure (3.17): Barrier wall formwork……... 53

Figure (3.18): Finishing concrete of barrier wall……..53

Figure (3.19): Curing of barrier wall prototype…… 54

Figure (3.20): Barrier wall prototype…… 54

Figure (3.21): Schematic diagram of test setup…… 55

Figure (3.22): Testing at middle……... 56

Figure (3.23): Testing at edge……... 56

Figure (3.24): Saw cutting of damaged middle portion…… 59

Figure (3.25): Longitudinal view of holes layout at middle……. 60

Figure (3.26): Transverse view of holes layout at middle…… 60

Figure (3.27): Drilling holes……. 61

Figure (3.28): Shapes of vertical bars used in repairing……... 61

Figure (3.29): Mixing epoxy……62

Figure (3.30) Filling gun with epoxy…… 62

Figure (3.31): Injecting epoxy…….. 62

Figure (3.32): Pushing bar inside the hole…… 62

Figure (3.33): New spliced (planted) reinforcement at middle…… 63

Figure (3.34): Lap splice of horizontal bar……... 63

Figure (3.35): Splice repaired middle portion (in yellow color)……...64

Figure (3.36): Longitudinal view of holes layout at the edge…….. 65

Figure (3.37): Transverse view of holes layout at the edge……. 65

Figure (3.38): Edge condition……... 66

Figure (3.39): Edge Concrete removed……66

Figure (3.40): Edge treatment with epoxy…… 67

Figure (3.41): New spliced reinforcement at edge……67

Figure (3.42): Splice repaired edge (in gray color)…….. 67

Figure (3.43): NSM Grooves and holes layout at middle portion in longitudinal direction…….69

Figure (3.44): NSM grooves and holes layout in transverse direction……. 69

Figure (3.45): Cutting NSM grooves…… 70

Figure (3.46): NSM grooves on barrier wall……70

Figure (3.47): NSM grooves at middle portion of barrier wall……70

Figure (3.48): Filling deck slab grooves with epoxy…… 71

Figure (3.49): Placement of transverse bar……... 71

Figure (3.50): vertical bar at the middle portion……...71

Figure (3.51): Filling epoxy in grooves…… 71

Figure (3.52): Placing bar in barrier wall grooves…… 72

Figure (3.53): Putting grout in grooves……72

Figure (3.54): New reinforcement at NSM repaired middle portion…… 72

Figure (3.55): NSM repaired middle portion during curing……. 73

Figure (3.56): Longitudinal view of grooves and holes layout at the edge…….. 74

Figure (3.57): Transverse view of grooves and holes layout at the edge……. 74

Figure (3.58): Edge condition……... 75

Figure (3.59) New NSM reinforcement at edge……76

Figure (3.60): NSM repaired edge (in gray color)…… 76

Figure (4.1): Punching shear failure of M1……...79

Figure (4.2): Punching shear failure of RE……... 80

Figure (4.3): Joint failure of RE……80

Figure (4.4): Cracking pattern of M1 prototype……... 81

Figure (4.5): Critical length (3.2 m) of M2 (shown in arrow)…….. 81

Figure (4.6): Cracking pattern of LE prototype…… 82

Figure (4.7): Critical length (2 m) of RE (shown in arrow)……..82

Figure (4.8): Vertical deflection of overhang deck slab for middle test (typical)…….84

Figure (4.9): Barrier wall horizontal deflection for middle test (typical)…… 85

Figure (4.10): Vertical deflection of overhang deck slab for edge test (typical)…… 86

Figure (4.11): Barrier wall horizontal deflection for edge test (typical)…….. 87

Figure (4.12): Overhang slab transverse bar strains for middle test (typical)……...90

Figure (4.13): Barrier wall horizontal bar strains for middle test (typical)……...91

Figure (4.14): V2 bar strains along the length of the barrier wall for middle test (typical)……..93

Figure (4.15): Overhang transverse bar strains for edge test (typical)……..94

Figure (4.16): Barrier wall horizontal bar strains for edge test (typical)…….. 95

Figure (4.17): V2 bar strains along the length of the barrier wall for edge test (typical)……. 96

Figure (5.1): Punching shear failure of M1-P…….....101

Figure (5.2): Punching shear failure of M2-N…… 102

Figure (5.3): Mode of failure of RE-P…… 104

Figure (5.4): Mode of failure of LE-N……105

Figure (5.5): Cracking pattern of M1-P…….. 106

Figure (5.6): Cracking pattern of M2-N……..... 107

Figure (5.7): Cracking pattern of RE-P…….. 108

Figure (5.8): Cracking pattern of LE-N…….. 108

Figure (5.9): Vertical deflection of overhang slab for M1-P test……... 110

Figure (5.10): Horizontal deflection of barrier wall for M1-P test……111

Figure (5.11): Comparisons of deflections of M1-P with M1…… 112

Figure (5.12): Vertical deflection of overhang slab of for M2-N test…… 113

Figure (5.13): Horizontal deflection of barrier wall for M2-N test…… 114

Figure (5.14): Comparisons of deflections of M2-N with M2……... 115

Figure (5.15): Overhang slab vertical deflection for RE-P test…….. 116

Figure (5.16): Horizontal deflection of barrier wall for RE-P……117

Figure (5.17): Comparisons of deflections of RE-P with RE……118

Figure (5.18): Overhang slab deflection for LE-N test……...119

Figure (5.19): Horizontal deflection of barrier wall for LE-N test……120

Figure (5.20): Comparisons of deflections of LE-N with LE……121

Figure (5.21): Overhang transverse bars strain for M1-P test…… 124

Figure (5.22): Barrier wall horizontal bar strains for M1-P test……125

Figure (5.23): V2 bar strains along the length of the barrier wall for M1-P test……126

Figure (5.24): Comparison of strains of M1-P with M1……127

Figure (5.25): Overhang transverse bar strains for M2-N…….. 128

Figure (5.26): Barrier wall horizontal bar strains of M2-N…… 129

Figure (5.27): V2 bar strains along the length of barrier wall for M2-N test……. 130

Figure (5.28): Comparison of strains of M2-N with M2…… 131

Figure (5.29): Overhang transverse bar strain for RE-P test…….. 132

Figure (5.30): Barrier wall horizontal bar strains for RE-P test……. 133

Figure (5.31): V2 bar strains of the barrier wall for RE-P test……... 134

Figure (5.32): Comparison of strains of repaired RE-P with intact RE……. 135

Figure (5.33): Overhang transverse bar strains for LE-N test…… 136

Figure (5.34): Horizontal bar Strains for LE-N test……... 137

Figure (5.35): V2 bar strains along the length of the barrier wall for LE-N test…… 138

Figure (5.36): Comparison of strains of repaired LE-N with intact LE……. 139

Chapter 1

Introduction

1.1. Introduction

One of the main safety features in highway bridges is barrier walls. The purpose of a concrete bridge barrier is to redirect vehicle in a controlled manner in the event of a collision. The vehicle shall not over turn or rebound across traffic lanes. The barrier shall have sufficient strength to survive the initial impact of the collision and to remain effective in redirecting the vehicle. Typically this barrier wall is reinforced with steel bars. However, the use of steel has been always associated with corrosion problems especially in harsh environmental conditions. Researchers such as Nanni (1993), Benmokrane et al. (1996), and Cosenza et al. (1997) have established glass fiber reinforced polymer (GFRP) bars as an alternative to steel bars. Nowadays GFRP bars are being widely used in situations where corrosion and durability are of major concern, and they are performing well (Mufti et al. 2007). Bridge barrier and its connection totally reinforced with GFRP bars were first investigated by El-Salakawy et al. (2004). Based on that research, the Canadian Highway Bridge Design Code (CHBDC) CAN/CSA-S6-06 provides detailing of GFRP-reinforced concrete barrier wall; and now construction industries are using it widely.

Furthermore, based on performance level, the CHBDC (CAN/CSA-S6-06) provides three different types of barrier walls, namely PL-1, PL-2 and PL-3. In low traffic volume roads PL-1 barrier walls are used, while PL-2 barrier walls are used in moderate to high traffic volume highways, and PL-3 barrier walls are used in high traffic volume highways with high percentage of trucks. The reinforcement configurations of the three types are very similar in terms of shape

and spacing. Among those types, PL-2 is the most used type because of its applicability in high to moderate traffic volume highways. Very limited research has been conducted to investigate the structural performance of GFRP-reinforced concrete bridge barriers such as Ahmed et al. (2011).

Though GFRP reinforced structures are less susceptible to environmental adverse effects by nature (Mufti et al. 2007), they are not immune to damage situations caused by accidents of vehicles. There is a growing demand from construction industries to provide proper guidelines to repair these GFRP-reinforced concrete (RC) structures efficiently. A study has been taken place addressing these repair issues of GFRP-RC bridge decks (El-Salakawy et al. 2010). However, efficiency of rehabilitation techniques in repairing damaged concrete bridge barriers reinforced with internal GFRP bars lacks test experiments. To determine effective repair techniques for damaged GFRP-RC barriers, there are some issues that need to be determined. First, identify extent and type of damage that can occur on a bridge barrier in case of an accident at different critical locations. Second, realize ways of removing damaged portions. Third, investigate effectiveness of available repairing technique such as near surface mounted (NSM) and splicing or planting (El-Salakawy et al. 2010).

To address all these issues, an extensive laboratory investigation was carried out. It was divided into two phases. First phase included construction and testing of three full-scale 6.0-m long GFRP-RC PL- 2 barrier walls under monotonic load simulating vehicle crash test up to failure. Second phase included repairing of these damaged barrier walls using splicing (planting) and NSM techniques, and re-testing the repaired barrier walls using same load conditions to evaluate the efficiency of the repair techniques.

1.2. Objectives

The objectives of this research work are to:

- Assess the structural performance and damage of PL-2 barrier walls subjected to equivalent static load simulating the vehicle crash test.
- Rehabilitate the damaged sections by NSM and Splicing (Planting) techniques.
- Evaluate the used two repair techniques by subjecting the rehabilitated bridge barrier walls to same loading conditions mentioned above and make recommendations, if necessary, to improve efficiency up to code requirements level.

1.3. Scope of the Research

In this research, PL-2 GFRP-RC bridge barrier was selected for repairing because of its application in moderate to high volume traffic highways throughout Canada. To simulate real condition, three full-scale 6-m long PL-2 barrier wall segments monolithically cast with overhang bridge deck slabs were constructed as test prototypes. Sand-coated GFRP straight and bent bars were used to reinforce the test prototypes. For testing, monotonic load simulating vehicle crash test was applied at middle and edge of the test prototypes up to failure. Also, two repair techniques, Near Surface Mounted (NSM) technique and Splicing (Planting) technique, were used in repairing the damaged prototypes.

1.4. Research Significance

Even though GFRP-RC bridge barriers are not susceptible to corrosion (Mufti et al. 2007), due to vehicular accidents, these barriers can get damaged. In such cases, repairing is required. To date, no research data or design recommendations exist on the repair of such damaged GFRP-RC

bridge barriers. Therefore, this present research is aimed to provide the much needed recommendations and guidelines to repair damaged GFRP-RC bridge barrier effectively.

1.5. Research Methodology

The entire research project is divided into two phases; Phase I and Phase II. In Phase I, three full-scale 6.0-m long GFRP-RC PL-2 bridge barriers are constructed and tested to evaluate the structural behaviour of these barrier walls. Tasks related to this phase are as follows:

- Making appropriate formwork for test prototypes.
- Placement of GFRP bars in bridge deck slab as per design and in PL-2 barrier wall as per CHBDC (CAN/CSA-S6-06).
- Installing strain gauges on bars in different critical locations of prototypes.
- Casting of three concrete bridge barrier prototypes.
- Providing adequate curing to develop concrete strength.
- Application of monotonic load on the bridge barrier according to CAN/CSA-S6-06 for PL-2.
- Recording strain gauges values and LVDT's measurements using Data Acquisition System (DAQ)
- Mapping of cracking pattern.
- Recording ultimate capacity and mode of failure.

In Phase II, damaged barrier walls are repaired using either splicing (planting) technique or NSM technique. Then, these repaired barrier walls are tested to evaluate the efficiency of the used repair techniques. Tasks related to this phase are as follows:

- Identification of damaged portions of barrier walls both at middle and edges.
- Saw cut the damaged portions.
- Two repair techniques, splicing (planting) and NSM technique, are used.
- Cut grooves for NSM technique and drill holes for Splicing technique.
- Insert new bars into the grooves and holes and use epoxy as bonding agent.
- Tie up new bars to make reinforcement cage.
- Casting new concrete to replace the damaged portions of three bridge barrier prototypes.
- Application of monotonic load on the bridge barrier according to CAN/CSA-S6-06 for PL-2.
- Recording strain gauges values and LVDT's measurements using Data Acquisition System (DAQ)
- Mapping of cracking pattern.
- Recording ultimate capacity and mode of failure.
- Compare the results of repaired barrier walls with their corresponding intact barrier walls.

1.6. Thesis Organization

This thesis consists of six chapters. The contents of each chapter are as follows:

- Chapter one presents introduction explaining the relevance of the research work, research objectives, scope of work, and research methodology.
- Chapter two consists of literature review on different aspects of GFRP-RC bridge barrier such as reinforcement detailing, dimensions, anchorage, loading requirements, test requirements, existing repair techniques of damaged RC structures.

- Chapter three provides details of the experimental program; size and reinforcements detailing of test prototypes, fabrication of test prototypes, instrumentations, test setup, test condition, repair techniques of damaged prototypes.
- Chapter four provides analysis and discussion of experimental test results in terms of ultimate capacity and mode of failure, cracking pattern, deflection and strains in reinforcements of intact prototypes.
- Chapter five provides test results of repaired prototypes, and comparisons of repaired prototypes in terms of ultimate capacity and mode of failure, cracking pattern, deflection and strains in reinforcements with their intact counterparts to evaluate the efficiency of the used repair techniques.
- Chapter six presents summary of this research work, conclusions derived from this research work and recommendations for future research.

Chapter 2

Literature Review

2.1. General

In order to achieve the objectives mentioned in Chapter 1, it is necessary to review relevant previous work to identify main factors affecting the testing procedure and behaviour of such barriers. As this present research deals with repairing of damaged GFRP-RC PL-2 bridge barriers, this chapter will explore literature including current code provisions of bridge barrier, testing requirements of bridge barriers and repairing techniques of damaged barriers.

2.2. Canadian Highway Bridge Design Code

Canadian Highway Bridge Design Code (CHBDC) (CAN/CSA-S6-06 2006), by Canadian Standards Association (CSA), provides dimensions and reinforcements detailing of steel and GFRP reinforced concrete bridge barriers. These detailing of bridge barriers is outlined in Section 12 of the CHBDC. In addition, each province or territory may have supplementary specifications and standards establishing detailed requirements, consistent with current nationwide practices, which apply to common highway bridge barriers. Besides the national and provincial codes, there are also references made to relevant literature from other jurisdictions. For example, concerning crash test requirements, the CHBDC refers to the American Association of State Highway and Transportation Officials (AASHTO)'s Guide Specifications of Bridge Railings (AASHTO LRFD 2007). This guide made further reference to the National Cooperative Highway Research Program (NCHRP), Report 350: Recommended Procedures for the Safety Performance Evaluation of Highway Features (NCHRP Report 350 1993).

2.3. Functions

The main functions of a bridge barrier are listed below:

- The Canadian Highway Bridge Design Code, CHBDC, (CAN/CSA-S6-06 2006) identifies the main function of barrier as to delineate the superstructure edge and to reduce the consequences of vehicles leaving the roadway.
- Barrier redirects vehicle in a controlled manner in the event of a collision.
- The vehicle shall not over turn or rebound across traffic lanes.
- According to AASHTO LRFD (2007) barrier shall have sufficient strength to survive the initial impact of the collision and to remain effective in redirecting the vehicle.

2.4. Types

According to CHBDC, (CAN/CSA-S6-06 2006) bridge barriers can be classified into the following four categories:

- Traffic barrier
- Pedestrian barrier
- Bicycle barrier
- Combination barrier

These four types of bridge barriers are shown in Figure (2.1).

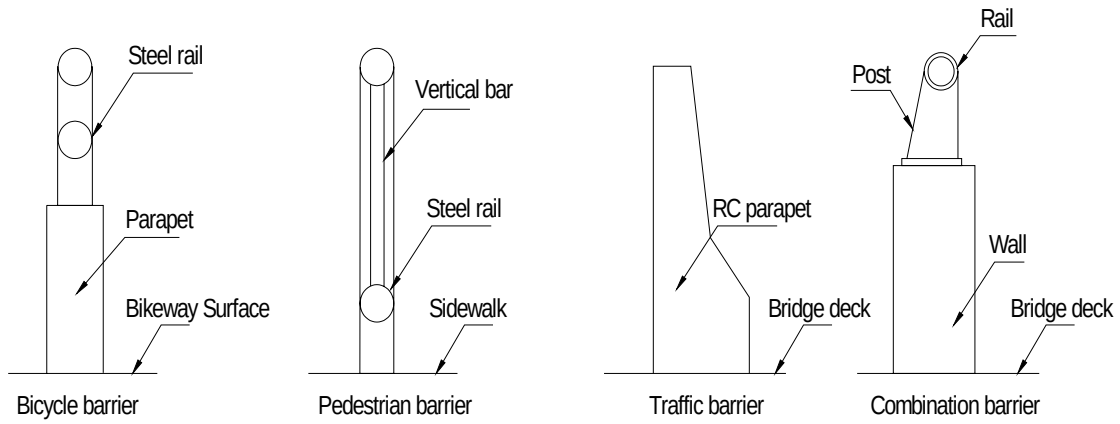

Figure (2.1): Bridge barriers, reproduced from CHBDC (CAN/CSA-S6-06 2006) and AASHTO LRFD (2007)

In evaluating bridge barriers, besides the basic strength requirements, there are general factors that should be considered. These factors are durability, ease of repair, snow accumulation on and snow removal from deck, visibility through or over barrier, deck drainage, future wearing surfaces, and aesthetics. In addition, damaged barriers need to be repaired quickly with minimal disruption to traffic. Also, traffic barriers should be designed with features such as anchorages that are unlikely to be damaged or cause damage to the bridge deck during an accident and effective repair technique that allows damaged sections to be repaired quickly.

According to AASHTO, applications of various types of barrier are as follows:

- Traffic railing is used when a bridge is for the exclusive use of highway traffic;
- A combination barrier in conjunction with a raised curve and sidewalk is used only on low speed highways;
- On high speed highways, the pedestrian or bicycle path should have both an outboard pedestrian or bicycle railing and an inboard combination railing; and

- Separate pedestrian bridges should be considered where the amount of pedestrian traffic or other risk factor so indicate.

This present study deals with traffic barrier; therefore, subsequent portion of this chapter will discuss various aspects of traffic barrier only.

2.5. Traffic Barrier

The primary purpose of traffic railings shall be to contain and redirect vehicles using the structures. All new traffic barrier system shall be shown to be structurally and geometrically crashworthy. According to AASHTO, consideration should be given to:

- Protection of the occupants of the vehicle in collision with the railing,
- Protection of other vehicle near the collision,
- Protection of persons and property on roadways and other areas underneath the structure,
- Possible future rail upgrading,
- Railing cost effectiveness, and
- Appearance and freedom of view from passing vehicles.

2.6. Traffic Barrier Requirements in CHBDC and AASHTO

Traffic barriers are to be provided on both sides of highway bridges to delineate the superstructure edge and thus reducing the consequences of vehicles leaving the roadway upon the occurrence of an accident (CAN/CSA-S6-06 2006). Crash tests are used to determine barrier adequacy in reducing the consequences of vehicles leaving the roadway. The adequacy of a traffic barrier in reducing the consequences of a vehicle leaving the roadway is based on the level

of protection provided to the occupants of the vehicle, to other vehicles on the roadway and to people and property beneath the bridge. This protection is provided by various ways: by retaining the vehicle and its cargo on the bridge, by smoothly redirecting the vehicle away from the barrier, and by limiting the rebound of the vehicle back into traffic.

2.6.1. Performance Level

The requirement for traffic barrier is dependent on the site as well as on the expected frequency and consequences of vehicle accidents at that site. This procedure assumes that the frequencies and consequences of vehicle accidents at bridge sites are a function of the percentage of trucks, design speed, highway type, curvatures, grades, and superstructure height. The ranking system used in CHBDC (CAN/CSA-S6-06 2006) to determine the bridge site condition is categorized into three levels:

Performance Level 1 (PL-1): The performance level for traffic barriers on bridges where the expected frequency and consequences of vehicles leaving the roadway are similar to that expected on low traffic volume roads.

Performance Level 2 (PL-2): The performance level for traffic barriers on bridges where the expected frequency and consequences of vehicles leaving the roadway are similar to that expected on high to moderate traffic volume highways.

Performance Level 3 (PL-3): The performance level for traffic barriers on bridges where the expected frequency and consequences of vehicles leaving the roadway are similar to that expected on high traffic volume highways with high percentage of trucks.

Based on the performance level (PL), the CHBDC (CAN/CSA-S6-06 2006) specifies the longitudinal, transverse, and vertical load a barrier satisfying this PL would need to withstand. There is also a minimum barrier height requirement based on the PL and the minimum barrier heights for PL 1, 2, and 3 traffic barriers are 0.68 m, 0.80 m, and 1.05 m respectively. These traffic barrier height requirements are intended to prevent impacting vehicles from vaulting or rolling over a barrier. Typically the higher the center of gravity of the impacting vehicle, the greater the required traffic barrier height is needed to contain it. Furthermore, based on performance level (PL), CHBDC (CAN/CSA-S6-06) gives dimensions and reinforcement detailing of GFRP-RC bridge barrier. Figure (2.2) shows the dimensions and reinforcement detailing of PL-2 and PL-3 concrete bridge barriers totally reinforced with GFRP bars.

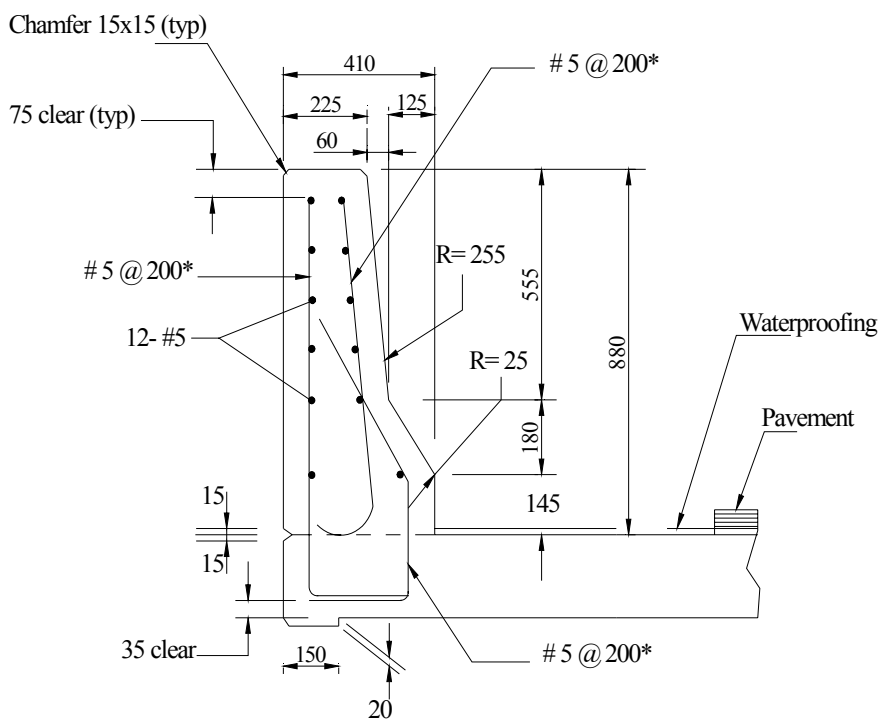

a) Reinforcement detailing of PL-2 GFRP-RC bridge barrier

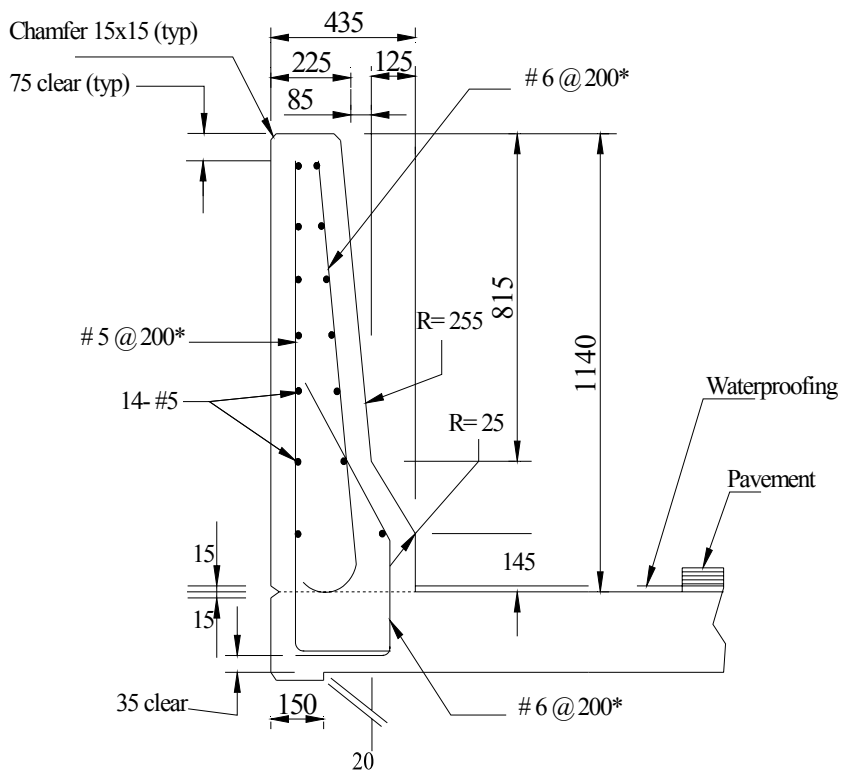

b) Reinforcement detailing of PL-3 GFRP-RC bridge barrier

* Spacing of these bars is to be reduced to 100 mm for the following lengths of barrier wall:

- 1m on each side of a joint in the wall;
- 1m on each side of a luminaire embedded in the wall; and
- 1m from the vertical edges of the wall.

Figure (2.2): Reinforcement detailing of GFRP-RC bridge barrier based on performance level, reproduced from Figure C 16.1 and Figure C16.2 of Commentary on CAN/CSA-S6-06

2.6.2 Crash Test Requirement

In Section 12.5.2.3 of the CHBDC (CAN/CSA-S6-06 2006), it is specified that, with the defined performance level, the crash test requirements should be in accordance with the crash test requirements of AASHTO Guide Specifications for Bridge Railing (AASHTO LRFD 2007). Those crash test requirements shall be satisfied along the entire length of a traffic barrier,

including at any changes in barrier type, shape, alignment, or strength that may affect the barrier performance. Alternative performance levels shall meet the crash test requirements of the optimum performance level or of a more severe performance level as considered. The specifics of the crash test are outlined in the National Cooperative Highway Research Program (NCHRP) Report 350: Recommended Procedures for the Safety Performance Evaluation of Highway Features (NCHRP Report 350 1993). The crash test requirements for barrier Test Levels 2, 4, and 5 of NCHRP Report 350 shall be taken as meeting the crash test requirements for Performance Level 1, 2, and 3, respectively. According to Section 12.5.2.3.4 in CHBDC (CAN/CSA-S6-06 2006), any changes in details affecting the geometry, strength, or behaviour of the traffic barrier or traffic barrier transition that meets the aforementioned requirements can be demonstrated to not adversely affect barrier-vehicle interaction.

2.6.3. Anchorages

The performance of the traffic barrier anchorage during crash testing is the basis for its capability. The anchorage is considered to be acceptable if no significant damage occurs in the anchorage or deck during crash testing. If crash test results for the anchorages are not available, the anchorage and deck shall be designed to resist the maximum bending, shear and punching loads that can be transmitted to them by the traffic barrier. The loads should be applied as in Figure (2.3).

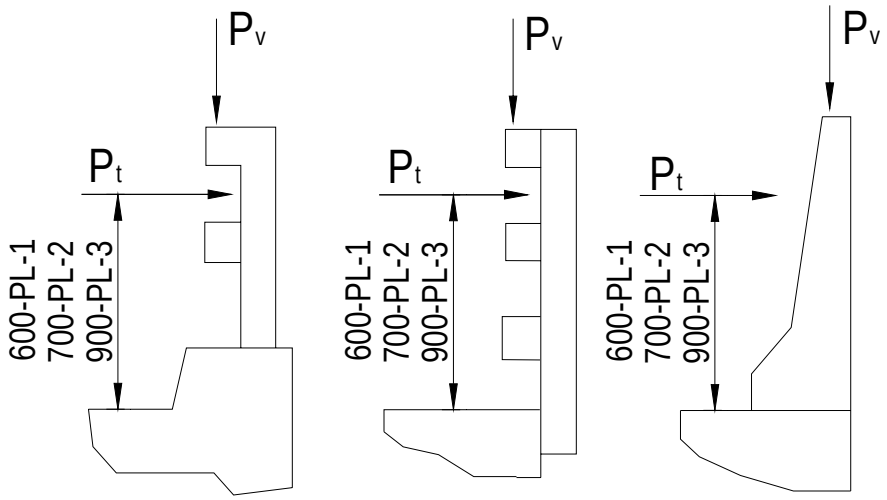

Notes:

(a) Traffic barrier types are illustrative only and other types may be used

(b) Transverse load Pt shall be applied over a barrier length of 1200 mm for PL-1 barriers, 1050 mm for PL-2 barriers and 2400 mm for PL-3 barriers

(c) Longitudinal load Pl shall be applied at the same locations and over the same barrier lengths as Pt. For post and railing barriers, the longitudinal load shall not be distributed to more than 3 posts.

(d) Vertical load Pv shall be applied over a barrier length of 5500 mm for PL-1 and PL-2 barriers and 12000 mm for PL-3 barriers

(e) These loads shall be used for the design of traffic barrier anchorages and decks only.

Figure (2.3): Application of design loads to traffic barriers, reproduced from CAN/CSA-S6-06 Figure (12.5.2.4)

However, the loads have to be greater than those resulting from the loads defined in Section-3.8.8 of the CHBDC (Barrier Loads). The transverse, longitudinal, and vertical loads should be applied simultaneously and are specified as shown in Table (2.1).

Table (2.1): Traffic barrier loads, reproduced from Figure 3.8.8.1, CAN/CSA-S6-06

Direction	PL-1			PL-2			PL-3		
	Force (kN)	Length (mm)	Height (mm)	Force (kN)	Length (mm)	Height (mm)	Force (kN)	Length (mm)	Height (mm)
Transverse	50	1200	600	100	1050	700	210	2400	900
Longitudinal	20	1200		30	1050		70	2400	
Vertical	10	5500		30	5500		90	12000	

According to AASHTO LRFD Bridge Design Specifications (AASHTO LRFD 2007), design forces for traffic railings, from Table A13.2-1, are given in Table (2.2).

Table (2.2): Traffic barrier loads, according to AASHTO (AASHTO LRFD 2007)

Direction	Test Levels 2 (PL-1)			Test Levels 4 (PL-2)			Test Levels 5 (PL-3)		
	Force (kN)	Length (mm)	Height (mm)	Force (kN)	Length (mm)	Height (mm)	Force (kN)	Length (mm)	Height (mm)
Transverse	120	1220	508	240	1070	813	516	2440	1016
Longitudinal	40	1220		80	1070		173	2440	
Vertical	20	5500		80	5500		222	12200	

2.6.4. Bridge Barrier Design Process

Both CHBDC (CAN/CSA-S6-06 2006) and AASHTO LRFD (2007) specified that bridge barrier should be tested by vehicle crash test to evaluate its structural performance and effectiveness in redirecting vehicle in collision. However, to start the design of reinforcement and anchorage of barrier wall to bridge deck overhang, both codes specified monotonic loads equivalent to vehicle impact loads, which act on barrier wall in case of an accident. For example, in case of PL-2 barrier wall, CHBDC (CAN/CSA-S6-06 2006) specifies transverse, longitudinal and vertical loads of 100, 30 and 30 kN, respectively, that can be applied simultaneously over a barrier length of 1050 mm. However, only transverse load is considered in designing both barrier wall and its anchorage to deck slab, as it creates the critical load carrying capacity. Similarly, in AASHTO (AASHTO LRFD 2007) this transverse impact load is 240 kN. Furthermore, for design purposes,

this transverse load should be multiplied by a live load factor of 1.7 (CAN/CSA-S6-06 2006) or 1.6 (AASHTO LRFD 2007). Therefore, the design transverse impact load for PL-2 barrier wall is either 170 kN (CAN/CSA-S6-06 2006) or 384 kN (AASHTO LRFD 2007). This equivalent design load is then used in yield line analysis, adopted by AASHTO, to calculate horizontal and vertical reinforcement amount in the barrier walls reinforced with steel bars.

In yield line analysis, yield lines pattern on barrier wall at failure is assumed. This assumed yield line pattern caused by a truck collision that produces a force, Ft, which is distributed over a length Lt, is shown below in Figure (2.4). Here, L_c means critical length over which most of the cracks distribute and H means height of the barrier wall.

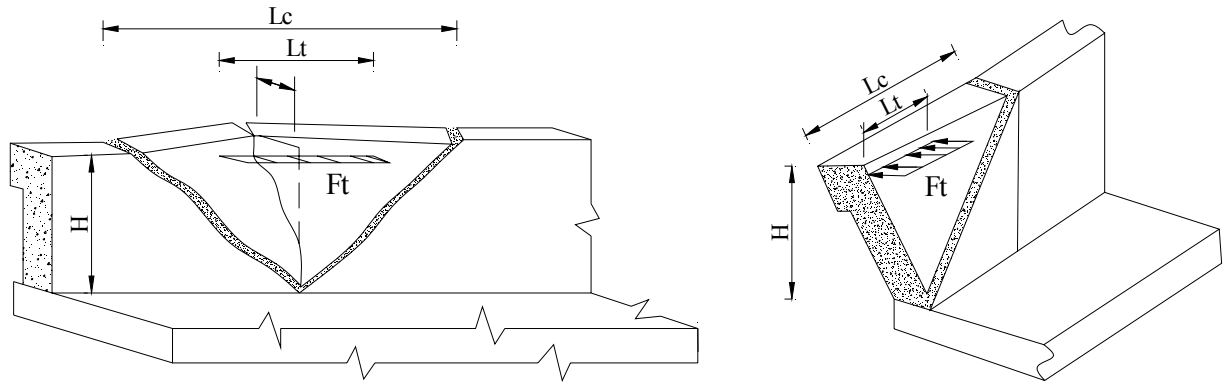

Figure (2.4): Yield pattern in bridge barrier due to truck collision at the middle and edges of the barrier, reproduced from AASHTO LRFD (2007)

Along these yield lines it is assumed that steel reinforcement gets yielded to calculate moment capacity at those locations. Usually this design process is performed in the following steps. First, maximum allowable spacing of reinforcement (300 mm in both CHBDC and AASHTO) is chosen for both vertical and horizontal reinforcement; second, using this reinforcement ratio,

ultimate moment capacity about the vertical and horizontal axis of the barrier wall is calculated; third, these moment capacities and barrier wall dimension are then used in yield line equations to calculate resistance capacity of the barrier wall. If resistance capacity is not higher than design impact load, new spacing less than the initial one is selected and iterates these three steps until the required strength is achieved.

In case of GFRP-RC bridge barrier, codes do not provide any analysis method similar to yield line analysis to calculate reinforcement amount as well as ultimate capacity of such barriers. However, recent research (El-Salakawy et al. 2004 and Sennah et al. 2011) suggests using the same yield line approach for GFRP-RC bridge barrier by replacing yielding with rupture since GFRP bars do not yield.

Now, for PL-2 GFRP-RC bridge barrier, the CHBDC (CAN/CSA-S6-06 2006) provides the spacing of 200 mm for vertical and horizontal reinforcement, which results in yield line capacity of 782 kN (El-Salakawy et al. 2004) much higher than design impact load of 170 kN. This difference in capacity is desirable because the higher capacity of barrier wall ensures that it will be serviceable even after experiencing vehicle collision.

Once this preliminary design process is completed, barrier wall and its anchorage are tested under monotonic static load up to failure to evaluate barrier wall ultimate capacity as well as to check anchorage performance. Authors of this present research found that static capacity of PL-2 GFRP reinforced barrier wall was 382 kN, which was higher than design impact load as expected, and mode of failure was punching shear failure. It was reported that 6 m long tests specimen carried load in two-way action in contrary to Ahmed et al. (2011) 2.6 m long specimen which resulted in one-way un-realistic mode of failure. It was also found out that static test of

PL-2 GFRP-RC barrier wall exhibited lower capacity than yield line capacity because the failure pattern in GFRP-RC barrier was different than yield line prediction, Finally, newly designed barrier wall must be subjected to vehicle crash test as specified by the codes to comply with certain criteria for structural adequacy, occupant risk, and vehicle trajectory after collision. (CAN/CSA-S6-06)

Sennah et al. (2011) performed the vehicle crash test of newly designed PL-3 barrier wall reinforced with GFRP bars of different configuration after following the design process mentioned above. In their specimen, they used GFRP ribbed bars at 300 mm spacing as vertical and horizontal bars of barrier wall, and used GFRP headed bars as anchorage between deck slab and barrier wall. It was reported that newly designed PL-3 GFRP-RC bridge barrier performed well against vehicle crash test.

2.7. Barrier Test

To determine mode of failure and ultimate capacity of barrier, several tests are available. They are Crash test, Impact Pendulum test and Static (Monotonic) load test. These three tests are discussed briefly here:

In vehicle crash test, a surrogate vehicle is collided with the barrier wall at a certain speed and at a particular angle as recommended by AASHTO LRFD (2007) depending upon performance level. In this collision, the barrier wall experiences transverse load due to front side collision, longitudinal load due to dragging of vehicle and vertical load due to vehicle override. Though the time of collision is very small, it imparts impact energy on the barrier wall. This impact energy in turns causes damages to the barrier wall. (Alberson et al. 2004, Sennah et al. 2011)

In pendulum impact test, a solid mass either pear shaped iron ball (El-Salakawy et al. 2004) or rectangular steel stock (Mitchell et al. 2006) acting as pendulum is used to impact on the barrier wall. In this test, the mass is selected and positioned such that it can produce same amount of impact force that is produced in case of vehicle crash test. Typically, acceleration history (acceleration vs. time graph) of both pendulum impact test and vehicle crash test is matched in terms of peak acceleration and duration of peak acceleration. (Mitchell et al. 2006). Therefore, both vehicle crash test and pendulum impact test produce similar results in terms of damaged and cracking pattern. (Mitchell et al. 2006, El-Salakawy et al. 2004)

In static (monotonic) load test, barrier wall is subjected to transverse load monotonically, distributed over particular length and at particular height recommended by codes (CAN/CSA-S6-06, 2006 or AASHTO LRFD, 2007), up to failure. Unlike vehicle crash test and pendulum impact test, static test does not impact on the barrier wall, rather it applies load monotonically (Ahmed et al. 2011).

Subsequent sections will briefly discuss code requirements regarding barrier test and previous studies associated with crash test, pendulum impact test and static load test.

2.7.1. Test Levels and Crash Test Requirements in AASHTO

There are six test levels described in AASHTO. They are as follows:

Test Level 1 (TL-1)

- Low posted speeds and low volume of traffic
- Mainly in local roads

Test Level 2 (TL-2)

- Small number of heavy vehicles is expected and posted speeds are reduced
- Local and collector roads

Test Level 3 (TL-3)

- Low mixtures of heavy vehicles
- Wide range of high speed arterial highways

Test Level 4 (TL-4)

- Mixture of trucks and heavy vehicles
- High speed highways, freeways, expressways and interstate highways

Test Level 5 (TL-5)

- Large trucks make up a significant portion of daily traffic
- High speed highways, freeways, expressways and interstate highways

Test Level 6 (TL-6)

- Tanker type trucks or similar high center of gravity vehicles are anticipated.

The testing criteria for the chosen test level shall correspond to vehicle weights and speeds and angles of impact outlined in the Table (2.3).

Table (2.3): Crash test criteria according to AASHTO (AASHTO LRFD 2007)

Vehicle Characteristics	Small Automobiles		Pickup Truck	Single-Unit Van Truck	Van-Type Tractor-Trailer		Tractor-Tanker Trailer
W (N)	7000	8000	20000	80000	220000	355000	355000
B (mm)	1700	1700	2000	230	2450	2450	2450
G (mm)	550	550	700	1250	1630	1850	2050
Crash angle, θ	20^0	20^0	25^0	15^0	15^0	15^0	15^0
Test Level	Test Speeds (km/hr.)						
TL-1	50	50	50	N/A	N/A	N/A	N/A
TL-2	70	70	70	N/A	N/A	N/A	N/A
TL-3	100	100	100	N/A	N/A	N/A	N/A
TL-4	100	100	100	80	N/A	N/A	N/A
TL-5	100	100	100	N/A	N/A	80	N/A
TL-6	100	100	100	N/A	N/A	N/A	80

2.7.2. Barrier Test in USA

- A series of three crash tests complying with National Co-operative and Highway Research Program (NCHRP) Report 350, Test Level 4, were performed at the Texas A&M University sponsored by Texas Transportation Institute (TTI) followed by a series of static testing. (Alberson et al. 2004)
- The Center for Transportation Research (CTR) at the University of Texas at Austin, sponsored by Texas Transportation Institute (TTI), performed the pendulum test and equivalent static tests for the T203 and T501 barriers with mechanical anchors. (Mitchell et al. 2006)

2.7.2.1. TTI (Test level 4-12, 4-11) Test

Crash Test

- In test level 4-12 single-unit van-truck, traveling at 50.6 mi/h (81.4 km/h), impacted the Florida bridge rail 5.6 ft (1.7 m) upstream of the first joint at an impact angle of 14.3 degrees.
- In test level 4-11 the 4544-lb (2063 kg) pickup truck, traveling at a speed of 61.1 mi/h (98.3 km/h), impacted the Florida Jersey safety shaped bridge rail 4.1 ft (1.25 m) upstream of the joint at an impact angle of 26.4 degrees.

Static Load Test

- The static load tests were performed with a hydraulic ram attached to a braced load frame, pushing on a load cell, and placed against a spreader beam, W12×50 (W310×74), 42 inches (1067 mm) long.

2.7.2.2. Pendulum Impact Test and Equivalent Static Test by (CTR at UTA)

- Investigators for this project developed an impact pendulum test setup to represent a surrogate vehicle for Test Level 3 of *NCHRP Report 350*.
- Tests were conducted on stand-alone cast-in-place and retrofit T203 and T501 barrier specimens.
- A quasi-static test was also conducted
- Finite element models of the cast-in-place and retrofit T203 and T501 barrier specimens were developed using LS-DYNA, and they were validated using the pendulum impact tests. Using those models, vehicular crash simulations were

conducted to *NCHRP Report 350* Test Level-3 and Test Level-4 standards to predict the performance and robustness of the retrofit T203 and T501 barrier designs when subjected to large impact forces.

2.7.2.3. Barrier Test Results and Discussion

Results of barrier tests mentioned above are tabulated in Table (2.4) and Table (2.5)

Table (2.4): TTI test results

TTI test Level 4 results		
Location of test	Yield line capacity (kN)	Static test capacity (kN)
Middle	276	325
Left end	185	201
Right end		156

Table (2.5): CTR test results

CTR test result		
Barrier type	Dynamic capacity (kN)	Static test capacity (kN)
T203	271	267
T501	287	258

It can be concluded from the test results that the static analysis using yield line theory provides good estimates of failure loads. Dynamic crash testing may not be necessary in the future for certifying the actual barrier capacities. In addition, dynamic effects such as strain rates do not play a role in the relatively slow loading of the barrier. A concrete barrier does not require large displacements to achieve its maximum capacity; therefore inertia effects are not critical. Therefore, static testing is considered an accurate and reproducible way of assessing barrier behaviour and ultimate capacity (Alberson et al. 2004).

2.7.3. Barrier Testing in Canada

In Canada, concrete bridge barrier and its connection to the bridge deck slab, totally reinforced with GFRP bars, were first investigated by El-Salakawy et al. (2003 & 2004). In that investigation, 10 m long PL-2 and PL-3 barrier walls using GFRP bars were constructed, and were tested by subjecting the barrier walls under pendulum impact load to simulate vehicle crash test. It was concluded that, at failure, GFRP-reinforced barriers behaved in a similar way to their counterparts reinforced with steel. It was also concluded that the affected length, defined as the length over which cracks spread due to the application of impact load, is 2.9 to 3.3 m at the top of the wall, diminishing to 0.9 to 1.2 m at the base of the wall for PL-2 barrier. These results are in good agreement with the yield line analysis given by AASTHO, which obtained this affected (or critical) length for PL-2 barrier to be approximately 2.9 m at the middle section and 1.5 m at the edge.

Based on that research, the proposed reinforcement configurations for GFRP-reinforced concrete barriers were adopted by the Canadian code, CAN/CSA-S6-06. Since then very limited studies were conducted to investigate the different structural performance aspects of GFRP reinforced bridge barrier such as Ahmed et al. (2011). In that study, 2.6 m long GFRP reinforced concrete bridge barrier wall prototypes were tested under monotonic loading up to failure. Tested barrier walls exhibited one-way un-realistic mode of failure. It was also reported that the load carrying capacity of the investigated barrier walls were not achieved and the failure was due to concrete splitting in the slab. Vehicle crash testing of a GFRP reinforced PL-3 concrete bridge barrier, utilizing new reinforcements orientation and GFRP threaded bars as vertical reinforcement, was

conducted by Sennah et al. (2011). It was reported that the barrier wall contained and redirected vehicle without penetration, and overriding or under-riding.

2.7.4. Static Load Test

Though both CAN/CSA-S6-06 and AASHTO LFRD (2007) require that any new type of barrier should be tested using vehicle crash test, because of its high cost and availability of alternate way of evaluating barrier, researchers at present are using either impact pendulum test or static load test (Deitz et al. 2004, El-Salakawy et al. 2004, Matta et al. 2009, Alberson et al. 2004). Again based on the same argument, now trend is to use static load test to simulate vehicle impact instead of pendulum impact test (Deitz et al. 2004, Mitchell et al. 2006, Ahmed et al. 2011, Jeon et al. 2011). This present research deals with the performance evaluation of both intact and repaired barrier walls in terms of ultimate strength, cracking pattern, deflections and strains in reinforcements at failure which can be measured by static load test because the load can be applied in a controlled manner up to the failure of the barrier, therefore, static load test will be used in this present research. (Jeon et al. 2011)

2.7.4.1 Loading Requirements

According to the CHBDC, a barrier satisfying Performance Level 2 (PL-2) needs to meet the specified loading requirement shown in Figure (2.5).

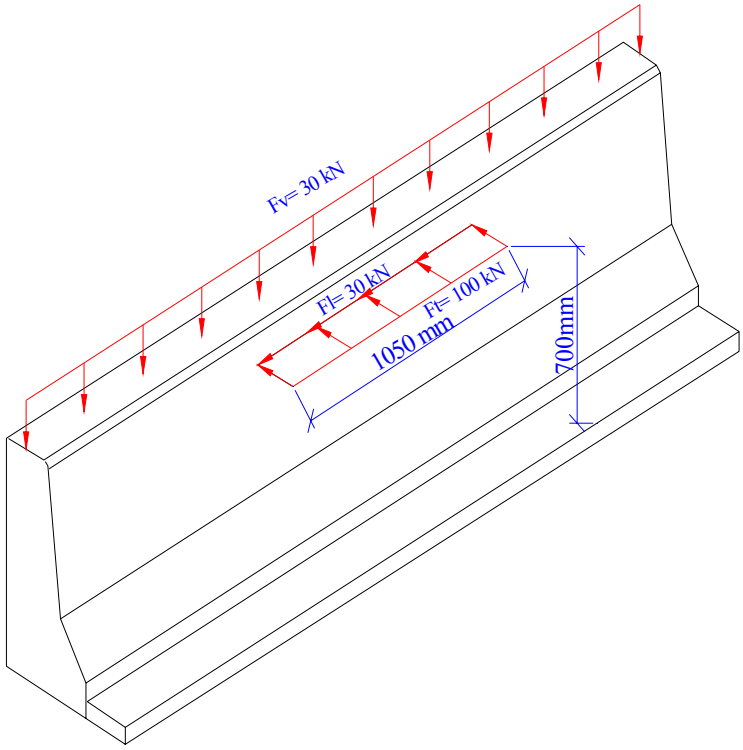

Figure (2.5): Loads requirements of PL-2 barrier wall

The effect of the vertical and longitudinal loads in regard to the failure mode and capacity of the barrier wall can be deemed to be negligible. Therefore, in the experiment, the barrier will be subjected to a 100 kN transverse load only that is applied uniformly over a length of 1050 mm at 700 mm above the base of the barrier. The code states that the transverse load can be applied at any location along the barrier. Based on experiments conducted by El-Salakawy et al. (2004) and Alberson et al. (2004), the critical sections along the barrier wall are at middle and at both edges. In this present research, load will be applied at the middle and the edges of the barrier wall.

2.8. Concrete Removal Techniques

There are numerous methods available to remove damaged concrete such as Blasting, Cutting, Impacting, Milling, Hydro-demolition, Pre-splitting, Abrasive Blasting, Jack Hammering. Some of these methods are discussed briefly in the following portion.

- **Hydro-demolition**

  Hydro-demolition (also known as hydro blasting, hydro-milling, water-blasting, and water-jetting) is a concrete removal technique which utilizes high-pressure water to remove deteriorated and sound concrete. A water jet with pressure ranging between 70 and 340 MPa is used for concrete removal (ACI 555R-01 2001). However, Deitz et al. (2000) reported that water jet removed the sand-coating and surface resin layers, which reduced the bond performance and left the fibres vulnerable to alkali attack and thus recommended not to use this technique to remove concrete from GFRP-RC structures.

- **Blasting**

  An explosive blasting technique referred to as mini-blasting (Lauritzen and Petersen 1991) is used for partial demolition of concrete structural members. In this technique, blasting mats are used to minimize flyrock, and textile fiber mats are used to lower dust and noise levels. (Lauritzen and Petersen 1991)

- **Demolition using Expansive agent**

  In this technique holes are made on the concrete surface and then these holes are filled with expensive mortar. After the curing period, mortar tends to expand and causes damage to concrete. However, El-Salakawy et al. (2010) concluded that this technique is time consuming and may not suitable for large areas.

- **Jack hammering**

Pneumatic breaker (frequently known as a jack-hammer but properly known as a paving breaker) is currently the most prevalent method for concrete removal in bridge rehabilitation work. The breaker is hand held and powered by compressed air to deliver a series of high frequency blows which fracture the concrete in a small, easily controlled area. The production of pneumatic breakers depends on two factors; the size of the breaker and the skill of the operator (SHRP-S-336 1992). However, removal of concrete of GFRP-RC structures resulted in damage of GFRP bars and may not be suitable for such structures. (El-Salakawy et al. 2010)

- **Cutting**

Concrete saws use industrial-diamond-coated circular blades to cut concrete and reinforcement. These blades range in size from 100 mm - 1.2 m. Water is sprayed onto the blade and into the cut to cool the blade and reduce friction between the blade and cut sidewall. Sawing is a low-cost, versatile technique for performing a number of tasks including: cutting the perimeter of an area where pneumatic breakers are to be used for removing concrete; cutting to full depth in slabs and decks so that sections may be removed; and cutting joints in new concrete. (ACI 555R-01 2001)

- **Impacting methods**

Impacting methods generally employ the repeated striking of a concrete surface with a mass to fracture and spall the concrete. Impact methods are sometimes used in a manner similar to cutting methods to disjoint the concrete for removal as a unit(s) by breaking out concrete along the removal perimeter of thin members such as slabs, pavements, decks, and walls.

Impacting methods include the boom-mounted and hand-held breakers and spring-action hammers (EM 1110-2-2002, 1995)

- **Pre-splitting**

Pre-splitting methods employ wedging forces in a designed pattern of boreholes to produce a controlled cracking of the concrete to facilitate removal of concrete by other means. The pattern, spacing, and depth of the boreholes affect the direction and extent of the pre-splitting planes. Pre-splitting methods include chemical-expansive agents and hydraulic splitters. (EM 1110-2-2002, 1995)

- **Crushing methods**

Crushing methods employ hydraulically powered jaws to crush and remove the concrete. There are two types of crushers; Boom-mounted crusher and Portable mechanical crusher. This method can be used for removing concrete from decks, walls, columns, and other concrete members. The major limitations are that the removal boundary must be saw cut to reduce over breakage, crushing must be started from a free edge or hole made by hand-held breakers or other means, and the exposed reinforcing is damaged beyond reuse. (EM 1110-2-2002, 1995)

In case of GFRP reinforced concrete, effective concrete removal techniques have been investigated by El-Salakawy et al. (2010). It has been found in this investigation that Jackhammer seemed to be the most effective concrete removal technique but it resulted in moderate to severe damage to the FRP reinforcement, therefore it is recommended that FRP bars in the demolished area should not be accounted for to carry any load and should be fully

replaced. Based on this recommendation it has been decided in this present research that full depth removal of damage concrete will be done by saw-cutting.

2.9. Repair Techniques

Effective repair technique for GFRP-RC bridge deck slabs has been investigated by El-Salakawy et al. (2010). In that investigation, two techniques have been found effective for repairing this kind of GFRP reinforced concrete structure. One technique is the splicing (planting) and other technique is the near-surface mounted (NSM) technique. Both of these techniques are discussed briefly in the following portions.

2.9.1. Splicing (Planting) Technique

Splicing (planting) technique consists of drilling holes in the existing concrete, partially filling the holes with adhesive, then inserting (planting) the new FRP bar (according to the instructions of the manufacturer of the adhesive). This splicing (planting) technique is affected by some general factors; according to El-Salakawy et al. (2010), these general factors are:

- Embedment length
- Bonding agent
- Splicing Spacing
- Hole diameter and
- Concrete cover

To understand the effect of these factors listed above, bond mechanism between FRP bar and concrete, bond failure and bond behaviour of FRP bar are discussed below.

2.9.1.1. Bond Mechanism of Deformed bars

Bond strength between the concrete and its reinforcement influences strength and stability of reinforced concrete structures. Typically concrete resists compressive forces, whereas the reinforcement resists the tensile forces. This indicates that there must be a force transfer or bond stress between these two materials. If there is no force, the reinforcement would pull out of the concrete, and the structure would collapse due to tensile loading. In reinforced concrete, the transfer of forces between a deformed reinforcing bar and concrete occurs by three mechanisms: (1) chemical adhesion between the bar and the concrete, (2) frictional forces arising from the roughness of the interface, forces transverse to the bar surface, relative slip between the bar and surrounding concrete, and (3) mechanical anchorage or bearing arising from the textures or profile of the rebar surface (ACI 408R-03, 2003). The forces on the rebar are balanced by compressive and shear stresses on the concrete contact surfaces. These forces are resolved into tensile stresses that can result in cracking planes that are perpendicular to the reinforcement (radial splitting force) and parallel to the reinforcement (effective bond force). Figure (2.6) shows the force transfer mechanism.

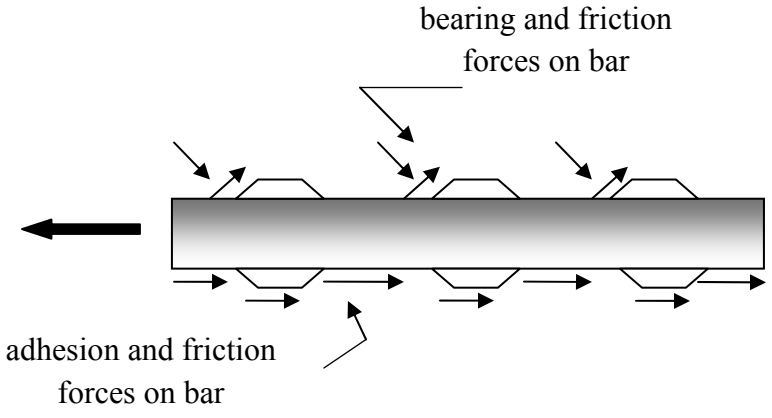

Figure (2.6) Bond force transfer mechanisms for deformed bars reproduced from ACI 408R-03

To prevent bond failure, the rebar must be embedded deep enough into the concrete and should have enough confinement provided by the concrete cover and/or transverse reinforcement. Under these conditions, the radial and tangential stresses developed along the bar will be less than the capacity of the concrete and the reinforcing bar will achieve its design tensile strength and not undergo bond failure. If inadequate anchorage length or confinement is provided, radial and tangential stresses developed may be greater than the concretes capacity and can lead to bond failure.

2.9.1.2. Bond Failure Modes

Bond failures are divided into either splitting or pullout failure:

- **Splitting Failure:** This failure mode occurs when the concrete surrounding the reinforcing bar develops transverse splitting cracks (Figure 2.7 a). Splitting failure results in cracking along the planes those are both perpendicular and parallel to the reinforcement. As the reinforcing bars are loaded they exert radial pressure on the surrounding concrete. If the surrounding concrete and/or the transverse reinforcement are not adequate enough to resist this pressure, a splitting crack initiates at the concrete-rebar interface and propagates towards the surface, leading to the failure of the concrete by concrete cover splitting.
- **Pullout Failure:** This failure mode occurs when the rebar pulls out of the concrete when the cover, bar spacing or transverse reinforcement is sufficient to prevent or delay a splitting failure. Pullout failure occurs when the radial forces from the loaded reinforcing bar are lower than what the surrounding concrete and/or transverse reinforcement can resist, and the tangential forces are higher than what the concrete can resist. Pullout

failure results in a shearing along a surface at the top of the ribs around the bars (Figure 2.7 b).

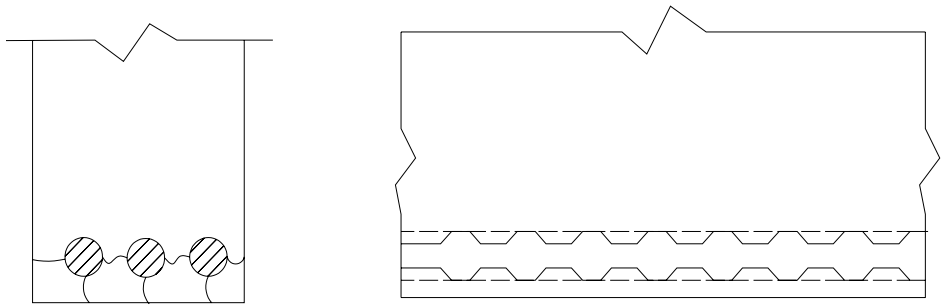

Figure (2.7): Cracking and damage mechanisms in bond: a) End view showing splitting cracks between bars and concrete cover; b) Side view of member showing shear crack and/or local concrete crushing due to bar pullout; reproduced from ACI 408R-03 (2003)

2.9.1.3. Bond Behaviour of FRP Bars

The bond behaviour of FRP bars and concrete is not the same as that of steel bars because of the distinct differences in the force transfer and failure mechanisms of steel and FRP bars. Their different behaviour is attributed to the differences in material properties and their interaction mechanisms with concrete (Chaallal and Benmokrane 1993). Steel is an isotropic, homogeneous, and elasto-plastic material, whereas FRP is an anisotropic, non-homogenous and linear elastic material. The anisotropic nature of the FRP rebar is due to the fact that its shear and transverse properties are influenced by the resins, whereas the longitudinal properties are influenced by the fibres (Cosenza et al. 1997). Material anisotropy leads to different physical and mechanical properties in both longitudinal and transverse directions; therefore, it is necessary for the anisotropic behaviour of FRP bars to be considered in the development of design equations, and in the understanding of failure mechanisms (GangaRao et al. 2001). The

surface texture of FRP rebar is created by epoxy, fibres or sand coating and causes the bars to be non-homogeneous. The non-uniform composition of FRP bars results in a reduction in their bond performance. As a result, it has been observed that for FRP bars the main force transfer mechanisms between the FRP rebar and concrete are through adhesion and friction (Daniali, 1992; Ehsani et al., 1993; Larralde and Silva-Rodriguez, 1993; Benmokrane et al., 1996). A recent study by Alves et al. (2011) investigated the bond durability of GFRP bars embedded in concrete. It was concluded that smaller diameter GFRP bars showed higher bond stress than that of larger diameter bars. It was also reported that fatigue loading on GFRP-RC structures caused significant deterioration in the bond strength. Furthermore, that study investigated the effect of freeze-thaw cycles on bond behaviour and it was reported that freeze-thaw cycles along with sustained load increased the bond strength of GFRP bars.

2.9.1.4. Factors Affecting Splicing (Planting) Technique

Factors affecting splicing technique are discussed briefly in the following portion.

- **Embedment length**

  Embedment length refers to the length that is necessary to develop the tensile strength of spliced FRP bar. In contrast, inadequate embedment length can result in bar slippage out of the concrete before achieving ultimate tensile strength of spliced bar. Normally an embedment length of 30d can achieve the full tensile capacity GFRP bars under direct axial tension loads, where d is the diameter of the spliced bar. However, in case of the anchorage zone, due to high flexural stress, anchorage length needs to be more than 30d. (El-Salakawy et al. 2010)

- **Bonding agent**

Spliced FRP bars get bonded with the surrounding concrete through bonding agent. There are mainly two types of bonding agent, namely grout and epoxy. Typically epoxy has higher tensile strength than that of grout. (El-Salakawy et al. 2010) Influence of these two types of bonding agent in splicing technique was studied by El-Salakawy et al. (2010). It was concluded that epoxy as a bonding agent exhibited higher performance in achieving ultimate capacity of repaired section than grout.

- **Splice hole spacing**

Hole spacing means the center to center distance between the existing bar and the planted bar. As per ACI 355.2-01 (2001) this hole spacing should be between two to three times the bar diameter (d). In El-Salakawy et al. (2010) study, it was concluded that increasing the spacing between the planted and original bars increased the ultimate capacity of the repaired section.

- **Hole diameter**

Typically, hole diameter in case of splicing technique is governed by the technical specification of the bonding agent. Usually, hole diameter is 2 to 3mm larger than the spliced bar. (El-Salakawy et al. 2010) This empty space between spliced bar and surrounding concrete is filled by bonding agent to make bond between bar and concrete.

- **Concrete cover**

The splitting and pullout modes of failure depend on the amount of concrete cover (Darwin et al., 1996). For small cover and bar spacing's, it is likely that splitting tensile failure will occur, where as for large cover and bar spacing, it is possible to obtain a pullout failure mode

resulting in higher bond strength (ACI 408R-03). In case of spliced FRP bar, larger concrete cover results in higher ultimate capacity of the repaired section than that of smaller concrete cover. (El-Salakawy et al. 2010)

2.9.2. NSM Technique

The near surface mounted (NSM) technique originated in Europe in the 1950's to increase the strength of RC structures. Steel bars were inserted in grooves cut into the concrete cover of RC flexural members and a cement grout was used to bond the bars to concrete (De Lorenzis and Nanni 2002). However, conventional black steel NSM reinforcement created difficulties due to corrosion experienced by these relatively unprotected bars. Hence, black steel was replaced by stainless steel and more recently by fibre reinforced polymer (FRP) bars. In present days, NSM technique using FRP bars is widely used for flexural strengthening in the negative moment region of slabs and girders (Hassan and Rizkalla, 2004). Researchers such as Blaschko and Zilch (1999), De Lorenzis and Nanni (2002), Hassan and Rizkalla (2002) and Soliman et al. (2011) investigated various aspects of NSM techniques using FRP bars and proved this technique as an effective way for flexural strengthening of existing structures. Furthermore, usage of NSM technique in repairing damaged concrete bridge deck slab was first investigated by El-Salakawy et al. (2010). It was reported that NSM technique could be used for repairing damaged FRP-RC structures.

In NSM technique, longitudinal grooves are first cut into the concrete cover of beams or slabs, then the reinforcing bars are inserted into these grooves and bonded with an appropriate bonding agent; typically an epoxy paste or a cement grout. This NSM technique in repairing damaged

FRP-RC structures is influenced by various factors; according to El-Salakawy et al. (2010) these factors are as follows:

- Location of NSM-FRP bar
- NSM groove size
- Embedment length
- Bonding agent

Before discussing these factors, bond mechanism and failure mode of NSM-FRP need to be discussed for clear understanding of these factors. Subsequent portion will discuss the bond mechanism and mode of failure first and then discuss these factors briefly.

2.9.2.1. Bond Mechanism

In NSM technique, FRP bar is covered with adhesive that provides bonding between FRP bar and existing concrete. Therefore, bonding in NSM exists in two interfaces; FRP-epoxy interface and epoxy-concrete interface. The bond mechanism of NSM-FRP bar was investigated by Hassan and Rizkalla (2004). It was reported that there were two main stages of bond mechanism. They are as follows:

Stage I: In this stage initial bond is developed due to chemical adhesion. No slip occurs at this stage.

Stage II: In this stage breaking out of chemical adhesion takes place and bond forces are transferred by the mechanical friction provided by the lugs of the bars. Also, in concrete and epoxy bond stresses developed, which cause transverse micro cracks at the tips of the lugs; consequently, allows the bar to slip. Finally, de-bonding failure occur through a

significant increase of the bearing forces accompanied by numerous internal cracks around the deformed FRP bars. This de-bonding could occur either at the FRP-epoxy interface or at the concrete-epoxy interface. Typical cross section of NSM-FRP strengthened beam is shown in Figure (2.8).

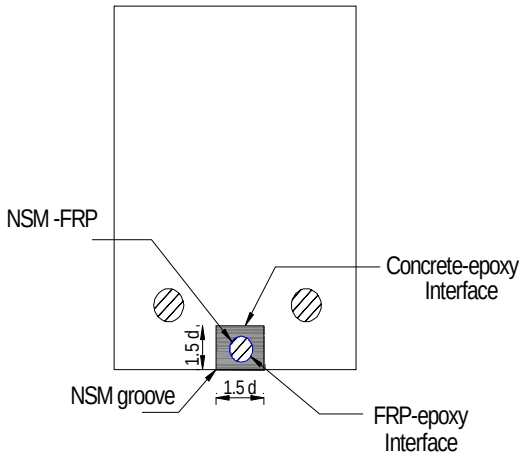

Figure (2.8) NSM-FRP strengthened beam (typical)

2.9.2.2. Modes of Failure

Hassan and Rizkalla (2004) identified two different types of modes of failure associated with NSM-FRP bar. The first mode of failure is due to splitting of the epoxy cover as a result of high tensile stresses at the FRP-epoxy interface, and is termed “epoxy split failure”. Soliman et al. (2010) also reported this type of mode of failure and termed this failure as “epoxy cracking (splitting)”. However, increasing the thickness of the epoxy cover reduces the induced tensile stresses significantly. Furthermore, using adhesives of high tensile strength delay epoxy split failure. This failure usually forms with longitudinal cracking through the epoxy cover. The second type of mode of failure is due to cracking of the concrete surrounding the epoxy adhesive and is termed “concrete split failure”. Soliman et al. (2011) also reported this mode of failure and

termed this failure as “concrete tension failure (semi-cone failure)”. This mode of failure takes place when the tensile stresses at the concrete-epoxy interface reach the tensile strength of the concrete. In addition, Soliman et al. (2010) reported another type of mode of failure that is rupture of NSM-FRP bar. It takes place when both epoxy and surrounding concrete has higher tensile strength and also the embedment length is long enough so that NSM-FRP bar can develop its ultimate tensile strength. These three modes of failure are shown in Figure (2.9).

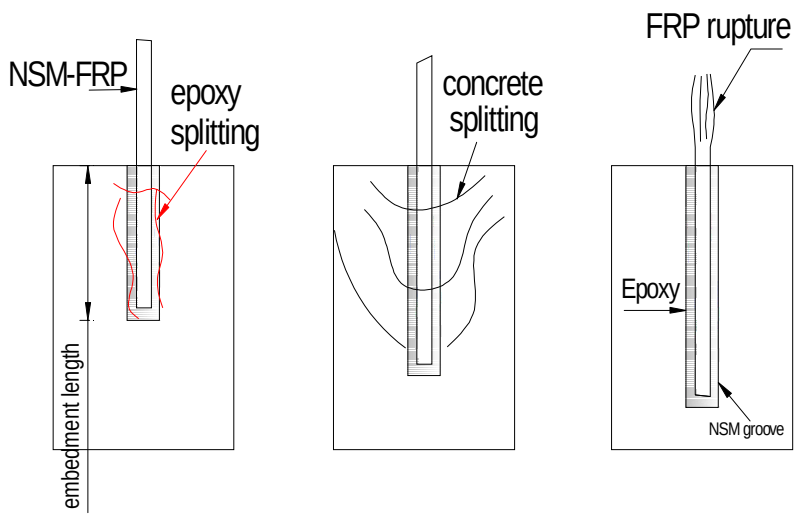

Figure (2.9) Modes of failure of NSM-FRP under pull-out test (reproduced from Soliman et al. 2011)

2.9.2.3. Factors Affecting NSM Technique

Factors affecting NSM technique are discussed briefly in the following portion.

- **Location of NSM-FRP bar**

NSM-FRP bar can either be placed in line with the original bar or somewhat offset to the original bar. El-Salakawy et al. (2010) reported that the location of the NSM-GFRP bar with

respect to the original reinforcement bars has insignificant effect on the ultimate capacity of repaired FRP-RC slab.

- **NSM groove size**

Two grove sizes for NSM techniques used by Hassan and Rizkalla (2004) were 1.5 d and 2 d, where d is the diameter of the bar. It was also reported that widening the groove minimized the induced tensile stresses at the concrete-epoxy interface and increased the de-bonding loads of NSM bars. Also, large epoxy cover and high tensile strength of the epoxy adhesive provided high resistance to epoxy split failure and shifted the failure to occur at the concrete-epoxy interface. (Hassan and Rizkalla 2004). El-Salakawy et al. (2010) used 1.5 d groove size (both width and depth) in their study and reported that it performed well.

- **NSM groove spacing**

The influence of clear groove spacing on interfacial stresses was investigated by Hassan and Rizaklla (2004). It was reported that the tensile stress at the concrete-epoxy interface was greatly influenced by the clear spacing between the grooves of NSM FRP bars. Increasing the clear groove spacing reduced the tensile stress considerably up to a clear groove spacing of 2.0 d; also clear spacing between the grooves of NSM bars has a negligible effect on the induced tensile stresses at the FRP-epoxy interface. Furthermore, they suggested that the minimum clear spacing between the grooves of NSM FRP bars should not be less that twice the diameter of the bars regardless of the groove width. Using clear groove spacing to bar diameter ratio less than 2d results in overlapping of the tensile stresses at the concrete-epoxy interface and accelerates de-bonding failure. In case of cement adhesive, Soliman et al. (2011) reported decrease in the failure load; this was due to greater shrinkage of cement in

bigger groove size. Therefore, it was recommended not to use groove size greater than 1.5 times the bar diameter when cement adhesive is used.

- **Embedment length**

Embedment length is required to develop bond stress and tensile strength of FRP bar. Increasing the embedment length results in increase in failure load and decrease in bond stress due to longer load distribution (Hassan and Rizkalla, 2004). Moreover, longer bonded length can cause bar rapture failure (Soliman et al. 2011). Normally 30d embedment length is recommended for NSM technique. However, length longer than 30db is recommended for NSM bars when the anchorage zone is subjected to flexural cracks. (El-Salakawy et al. 2010)

- **Bonding agent**

Two different types of bonding agent are available; Cement grout and Epoxy. This bonding agent influences the mode of failure. The main mode of failure in case of epoxy adhesive is concrete tension failure (semi-cone failure) accompanied with or without epoxy cracking (splitting). In case of cement adhesive mode of failure is splitting at the concrete-cement interface (Soliman et al. 2011). Furthermore, El-Salakawy et al. (2010) reported that NSM-FRP bar installed with epoxy performed well in terms of ultimate capacity than that of grout.

Chapter 3

Experimental Program

3.1. General

To investigate the structural behaviour of a GFRP-RC bridge barrier and to find out repair techniques for the damaged barrier, an experimental program was conducted in the W. R. McQuade heavy structures laboratory at the University of Manitoba. The entire experimental program was divided into two phases. In phase I, three full scale GFRP-RC bridge barrier wall prototypes were cast and tested under static monotonic load up to failure simulating vehicle crash test. In phase II, damaged barrier walls were repaired using two techniques; Near Surface Mounted (NSM) and Splicing (Planting), and re-tested under identical load to that of Phase I. This chapter presents the construction of barrier prototypes, instrumentation, test setup and procedure, and repairing processes of damaged barrier wall prototypes in detail.

3.2. Experimental Program - Phase I

In phase I, three full-scale 6.0-m long GFRP-RC PL-2 bridge barrier wall prototypes were constructed. The barriers were tested at two locations, middle and edge. As such, each test was repeated twice; one prototype was tested at the two edges and two prototypes were tested at the middle.

3.2.1. PL-2 Barrier Wall Reinforcement Detailing

PL-2 barrier is selected in this present research for its wide use in highway bridges throughout Canada. However, results from this research are valid and can be extended to all other types (PL-1 and PL-3) of barriers because all these barriers have similar vertical and horizontal

reinforcements arrangement; similar spacing of reinforcement and similar connection with overhang deck slab. The differences are mainly in the concrete dimensions (height and width). The Canadian Code, CHBDC (CAN/CSA-S6-06), provides detailing of reinforcement for both barrier wall and connection for PL-2 barrier wall. Figure 3.1 shows the reinforcement detailing of PL-2 barrier wall.

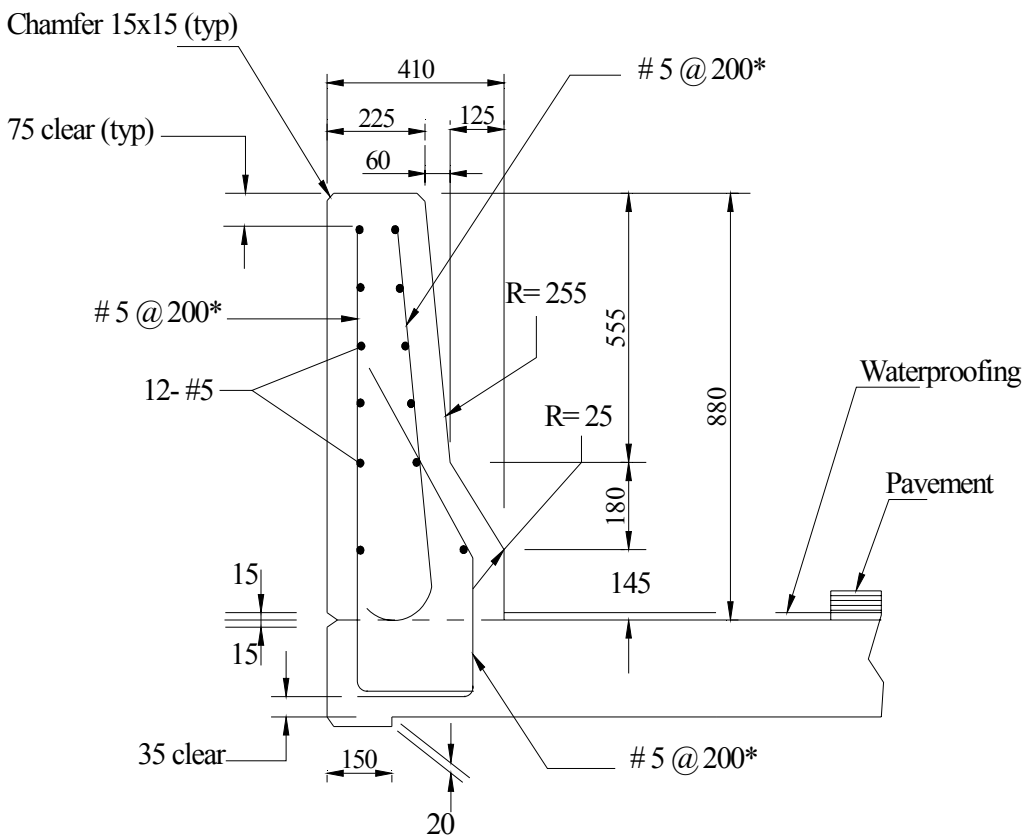

*Spacing of these bars is to be reduced to 100 mm for the following lengths of barrier wall:

(a) m on each side of a joint in the wall;

(b) m on each side of a luminaire embedded in the wall; and

(c) m from the vertical edges of the wall.

Figure (3.1): Reinforcement detailing of PL-2 barrier wall, reproduced from Figure C 16.1 of Commentary on CAN/CSA-S6-06

3.2.2. Barrier Wall Prototypes

For design purposes, bridge deck slabs with overhangs consist of two parts. One is the cantilever slab (overhang) and the other is the slab bounded by the supporting bridge girders (CAN/CSA S6-06 2006). For the overhang part, as a determinate part of the structure, there is only one method of analysis using the applied dead and live wheel loads. For the remaining part of the slab, both flexural and empirical design methods can be used as specified in CHBDC (CAN/CSA S6-06 2006). According to Clause 8.18.2 of CHBDC (CAN/CSA S6-06 2006), minimum thickness of the deck slab is 175 mm, therefore, a 200-mm slab thickness was chosen in this research. Also, Clause 16.4.4 of CHBDC (CAN/CSA S6-06) specifies minimum clear cover to be 35 ± 10 mm. As such, a 38-mm clear cover was used.

The full-scale barrier wall was cast on the overhang deck slab which was supported on 800 × 450 mm concrete beam. This concrete beam has two rows of 50-mm holes to tie the test prototype to the laboratory strong floor using 25-mm and 38-mm diameter dywidag bars and steel bearing plates (100×100×25 mm). As discussed in Section 2.7.3 of this thesis (El-Salakawy et al. 2003 & 2004), the affected (or critical) length of the barrier wall is assumed to be 3.0 m for the middle test and 1.5 m for the edge test. In addition, the barrier prototypes were tested to failure on two edges and on the middle part, repaired, then retested. Therefore, for the repair stage, an adequate length should be provided so that spliced and NSM bars can be embedded into the adjacent intact concrete. This length is assumed to be 1.5 m (double the required embedment length) on each side. Consequently, 6.0-m barrier wall length was selected.

The reinforcement configuration of PL-2 barrier wall was taken from the CHBDC (CAN-CSA-S6-06 2006). The design of the overhang deck slab is given in Appendix A. The obtained

reinforcement was No. 19 spaced at 100 mm in the transverse direction and No. 16 spaced at 200 mm in the longitudinal direction.

The supporting beam is designed against torsion caused by the dead load of the overhang deck slab and the barrier wall, and the applied static load (Appendix A). The obtained reinforcement included No. 15M 2-legg steel stirrups spaced at 100 mm and a total of eight No. 20M longitudinal bars. Figure 3.2 shows the dimensions and reinforcement detailing of the barrier wall prototype.

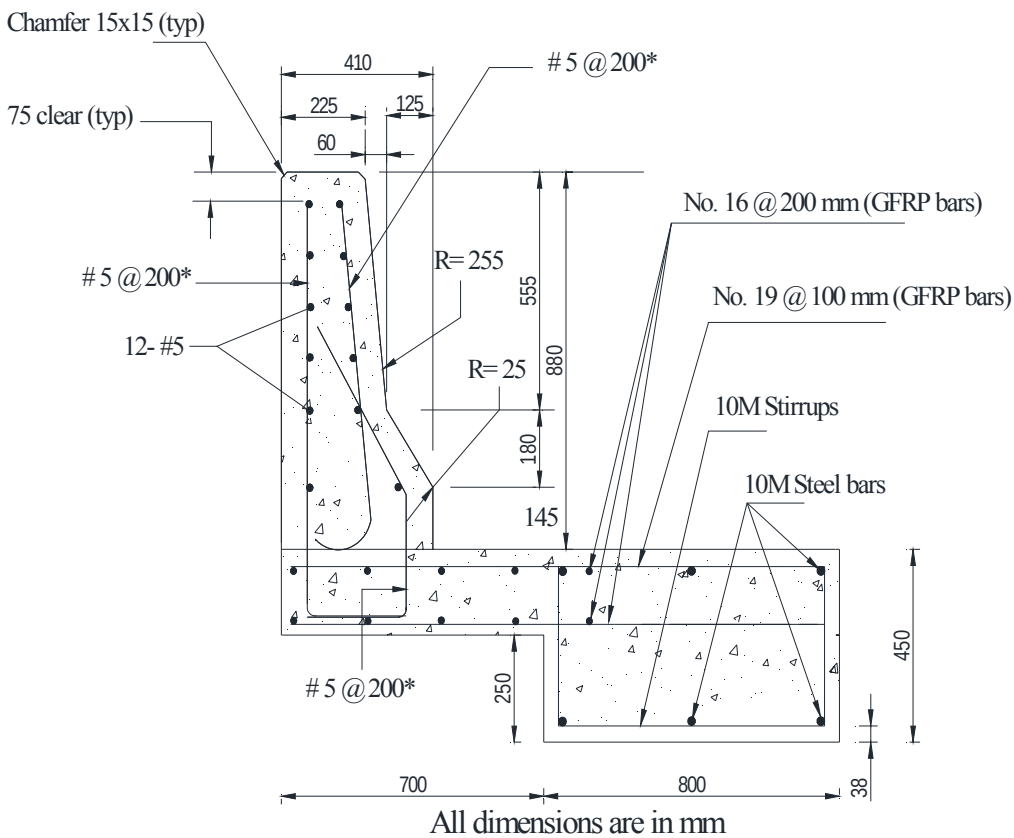

* Spacing of these bars is to be reduced to 100 mm on both edges.

Figure (3.2): Transverse section of a barrier wall prototype

3.2.3. Instrumentation

To measure strain on GFRP reinforcing bars, 6-mm electrical resistance strain gauges were used in this investigation. Locations of strain gauges on the vertical bent bars of the barrier wall are shown in Figure (3.3). Horizontal strain gauges were also put on the second bar from the top of the barrier wall as maximum moment would occur in that place. Transverse strain gauges were installed at the connection between the barrier wall and the deck slab. Locations of vertical, horizontal and transverse strain gauges while applying load on the middle portion and on the two edges of the barrier wall are given in Figure 3.4 and 3.5, respectively.

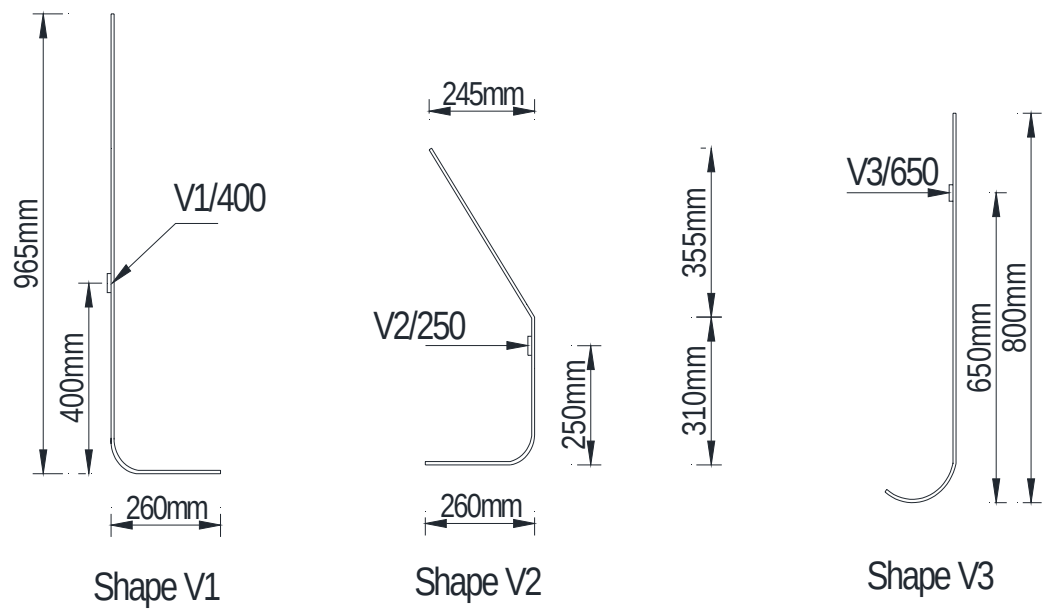

Figure (3.3): Locations of strain gauges on vertical bars

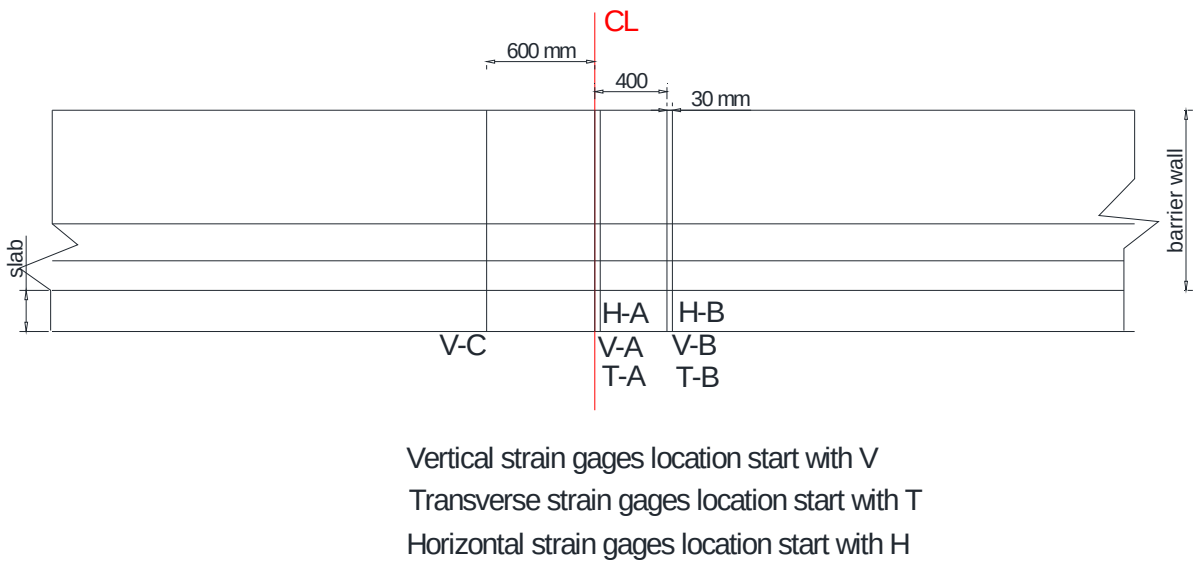

Figure (3.4): Locations of strain gauges in the barrier wall while testing on the middle portion

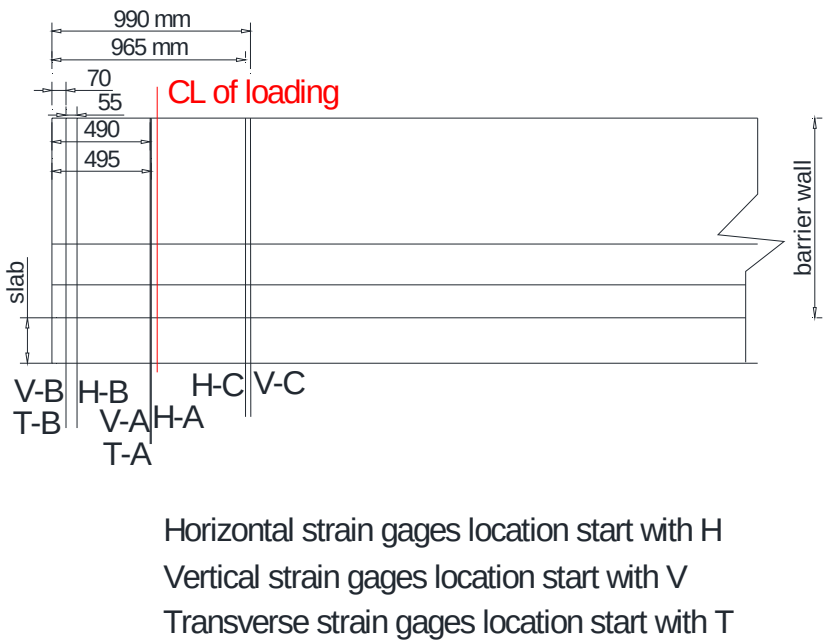

Figure (3.5): Locations of strain gauges in the barrier wall while testing on the edge

To measure both horizontal and vertical deflection of the barrier wall, linear variable differential transducer (LVDT) were used. LVDT's were attached horizontally at the top edge of the barrier

wall and at the barrier wall-slab joint. LVDT's were also placed vertically to measure the vertical displacement of the overhanging slab. Figure 3.6 to 3.8 shows locations of LVDT's on the barrier wall prototype.

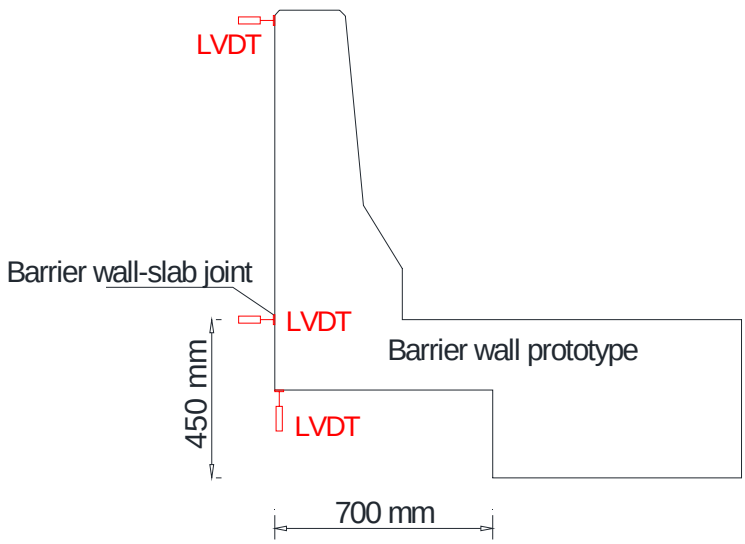

Figure (3.6): Locations of LVDT

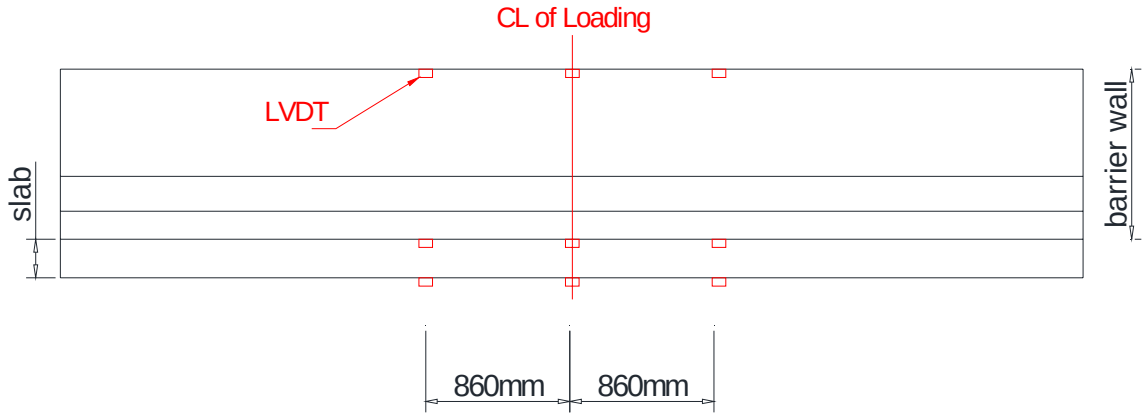

Figure (3.7): Locations of LVDT's while testing the middle portion of the barrier wall

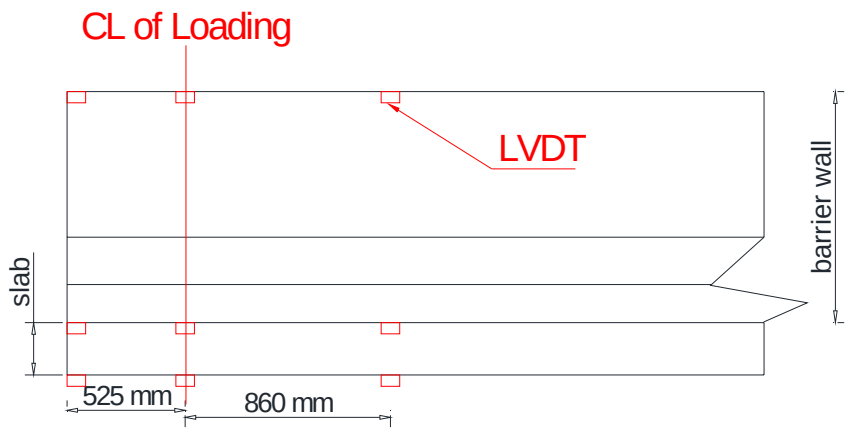

Figure (3.8): Locations of LVDT's while testing the edge of the barrier wall

3.2.4. Loading Conditions

According to the CHBDC, a barrier satisfying Performance Level 2 must withstand the loading summarized in Table (2.1) of this thesis.

The effect of the vertical and longitudinal loads in regard to the failure mode and capacity of the parapet can be deemed to be negligible. Hence, in the experiment, the barrier will be subjected to transverse load only that is applied uniformly over a length of 1050 mm at 700 mm above the base of the barrier. The code states that the transverse load can be applied at any location along the barrier. Based on literature, the worst loading case exists when the load is applied at the end of the barrier due to the discontinuity of the edge (Alberson et al. 2004, El-Salakawy et al. 2004). In this experiment load was applied at the two possible locations of accidents, middle portion and end portion, of the barrier wall. Figure 3.9 and 3.10 show loading conditions at the middle and at edges, respectively.

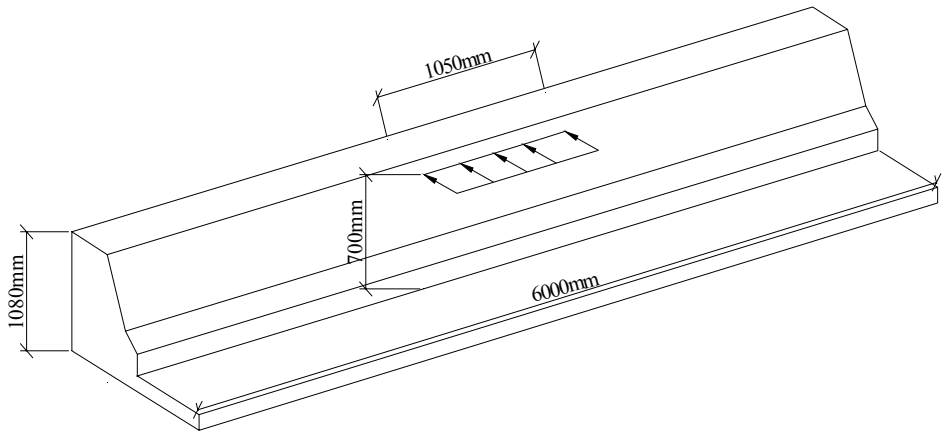

Figure (3.9): Application of transverse load at the middle portion of a barrier wall

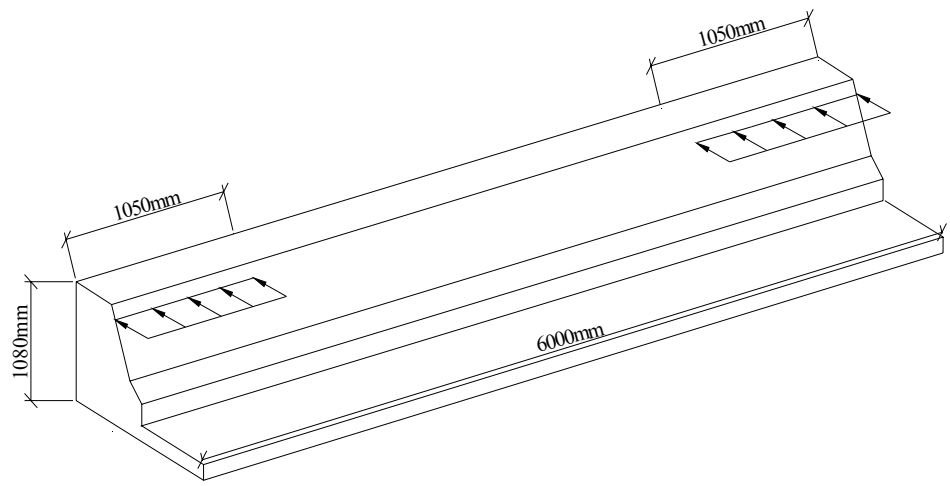

Figure (3.10): Application of transverse load on edges of a barrier wall

3.2.5. Construction of Barrier Wall Prototype

Barrier wall prototypes were cast in two stages simulating real life situation. Supporting beam and the overhang deck slab were cast first and then after 3 days barrier wall was casted. The 50-mm diameter holes were formed in the beam by installing 50-mm diameter PVC pipes through

the beam depth before casting the concrete. Locations of the holes in the beam while testing the middle portion and the two edges of the barrier wall are given in Figure 3.11 and 3.12, respectively.

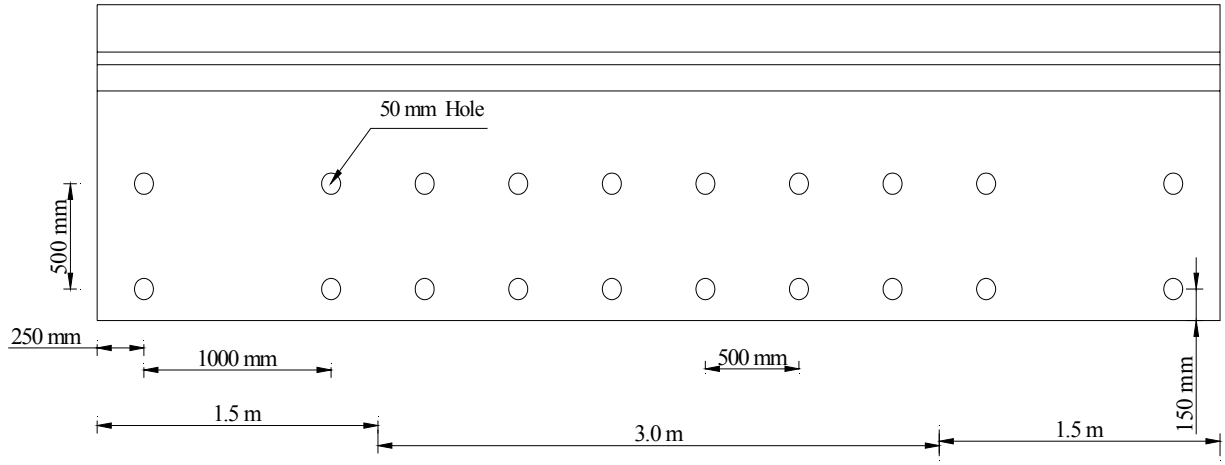

Figure (3.11): Holes layout in the prototype subjected to middle portion testing

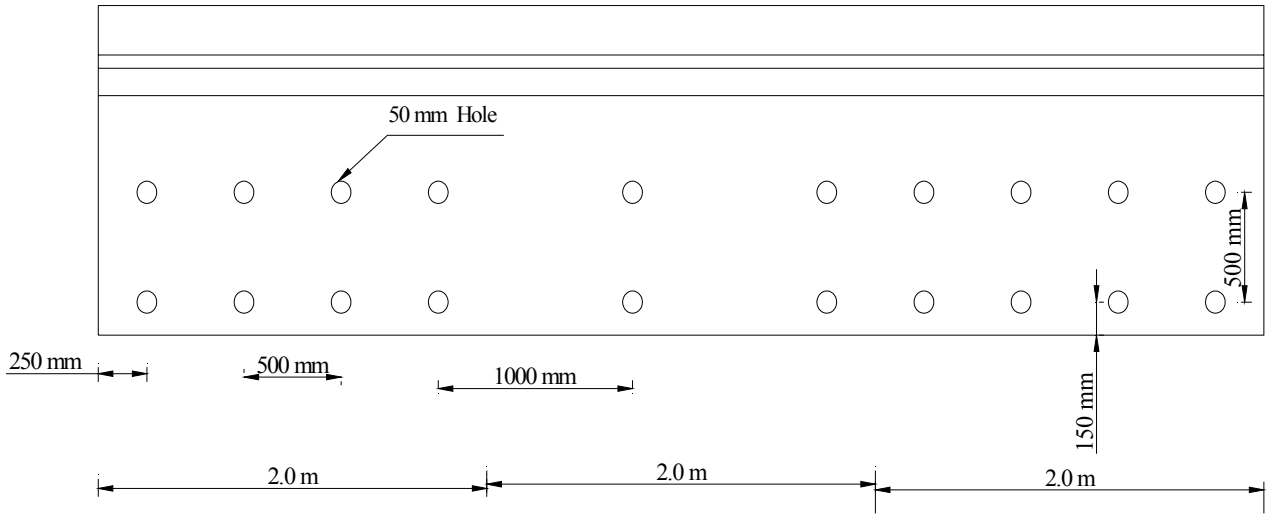

Figure (3.12): Holes layout in the prototype subjected to end portion testing

The construction process of barrier wall prototypes is shown in Figure 3.13 to 3.20.

Figure (3.13): Reinforcement cage of deck slab

Figure (3.14): Concrete casting

Figure (3.15): Finishing concrete of deck slab

Figure (3.16): Barrier wall reinforcement cage

Figure (3.17): Barrier wall formwork

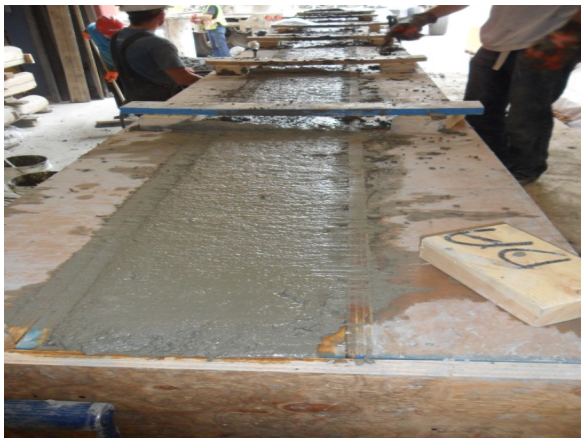

Figure (3.18): Finishing concrete of barrier wall

Figure (3.19): Curing of barrier wall prototype

Figure (3.20): Barrier wall prototype

In this research, normal strength concrete was used for barrier walls as well as bridge deck slabs as per specification 1030 (I) (Standard Construction Specification, March 2010) provided by Manitoba Infrastructure and Transportation (MIT). Target concrete compressive strength was 40 MPa. Furthermore, curing of concrete was done following the same specification provided by MIT. In this curing process, concrete surface was covered with a single layer of clean, soaking wet burlaps as soon as the surface would not be marred by so doing. Then these burlaps were covered by polyethylene and kept saturated by applying water every day for up to 7 days.

3.2.6. Test Setup

To test the prototype under monotonic load, a test frame with 1000 kN actuator was constructed. Figure 3.21 shows the schematic diagram of the test setup. For testing on the middle portion, two barrier wall prototypes were tightened to the laboratory strong floor by twenty 25-mm diameter Dywidag bars (anchors) and nuts. A tensile force of 130 kN was applied on each anchor to assure that no rigid body displacement occurs during testing. A total of forty, 25-mm thick square steel plates (100 × 100 mm) were used as bearing plates between the nuts and the concrete beam

surface. Figure 3.22 shows the restraining condition for testing on the middle portion. For testing on the edges eight 38-mm diameter Dywidag bars close to the end were stressed down with tensile force of 325 kN on each bar and four 25-mm diameter Dywidag bars near the middle of the prototype were stressed down with tensile force of 130 kN on each bar. The other side of the prototype was remained unstressed in this case. Figure 3.23 shows the restraining condition for testing on the edge. A clear space of 250 mm was used between the bottom surface of the barrier (overhang) and the laboratory strong floor to allow for deflection and rotation of the barrier wall and slab during testing. Load was applied on the barrier wall at a vertical distance of 700 mm from the slab top surface.

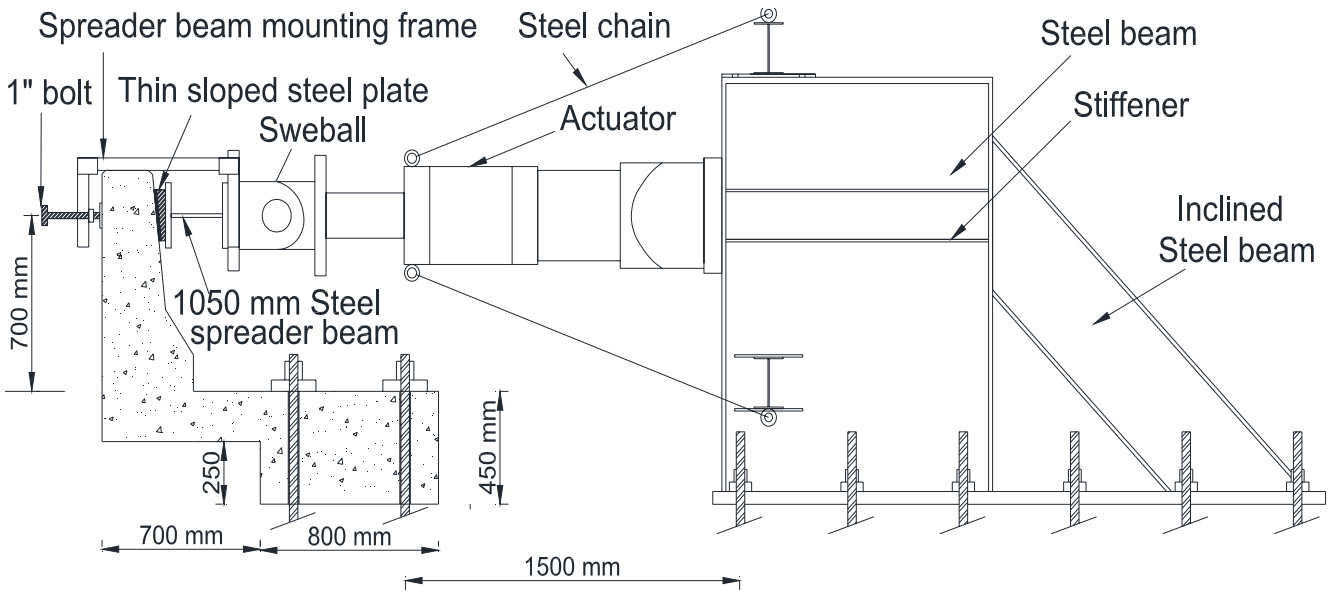

Figure (3.21): Schematic diagram of test setup

Figure (3.22): Testing at middle

Figure (3.23): Testing at edge

3.2.7. Test Matrix and Loading Rates

In phase I, two intact barrier walls were tested at middle, and the third one was tested at both edges. In phase II, two repaired barrier wall were tested at the middle and the third repaired one was tested at both edges. Test matrix for both the phases is shown in Table (3.1).

Table (3.1): Test matrix

Barrier Prototype No.	Test Location	Test Designation		Repair Technique
		Phase I (Intact)	Phase II (Repaired)	
1	Middle	M1	M1-P	Planting
2	Middle	M2	M2-N	NSM
3	Left Edge	LE	LE-N	NSM
	Right Edge	RE	RE-P	Planting

As per CAN/CSA-S6-06, static load was applied on the barrier wall at 700 mm above the top of the slab surface. Load was applied over 1050 mm length. All the tests were done using

displacement control mode of the actuator. Loading rates testing middle portion and edges are shown in Table (3.2).

Table (3.2): Loading rates

Test Designation	Load range (kN)	Rates (mm/min)
M1 M2 M1-P M2-N	0-200	1
	200-325	2
	325 to failure	3
LE LE-N RE RE-P	0-200	1
	200 to failure	2

3.3. Experimental Program - Phase II

In phase II, damaged portion of tested barrier wall prototypes were cut off; holes or grooves were drilled or cut; bars were planted inside the holes or grooves using epoxy; new reinforcements were added; new concrete was cast; and finally repaired prototypes were tested using monotonic load up to failure using the same load conditions and instrumentations of intact barrier walls.

3.3.1. Repairing Damaged Portion

Two different methods of repairing were utilized to repair the damaged barrier wall; NSM and splicing (planting) technique. Based on previous work (El-Salakawy et al. 2010), the four parameters associated with these two repair techniques were set as follows:

Bar hole-diameter: 3-mm larger than bar diameter.

Spacing of the bars (centre-to-centre): 3 times bar diameter, when possible (50 and 57 mm for top and bottom reinforcement, respectively).

Bonding agent: Epoxy.

Embedment length: $40\,d_b$, when possible (760 and 640 mm for top and bottom reinforcement, respectively)

3.3.2. Repairing Using Splicing (Planting) Technique

Splicing technique was used to repair both middle portion and edge of barrier wall prototypes. Repairing processes of both middle portion and edge portion are discussed below.

3.3.2.1. Repairing Middle Portion Using Splicing (Planting) Technique

In repairing damaged middle portion using splicing technique, the following procedure was used:

- A 3.2-m long damaged middle portion of the barrier wall including the underneath overhang slab was cut off using concrete saw. Figure 3.24 shows the saw cut of barrier wall.

Figure (3.24): Saw cutting of damaged middle portion

- After removing the damaged portion, using concrete drill machine, holes were drilled both on the barrier wall and the overhang deck slab. Figure 3.25 and 3.26 show the holes layout, and Figure 3.27 shows drilling of holes.
- After drilling, all holes were cleaned off using air blower to make them clean for bar plantations. Interface concrete surface was chipped off using jack hammer to make it rough for better bonding between new and old concrete.

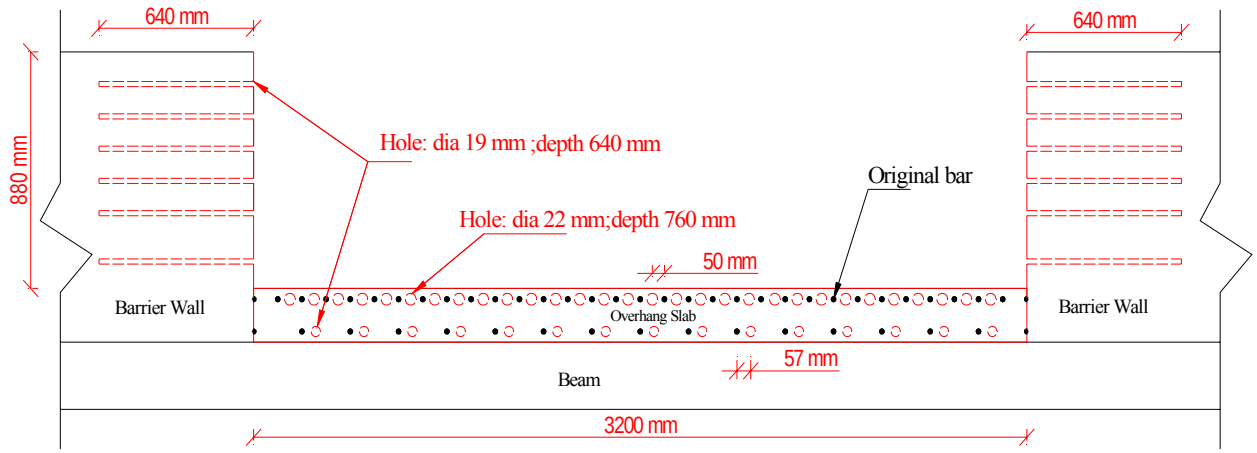

Figure (3.25): Longitudinal view of holes layout at middle

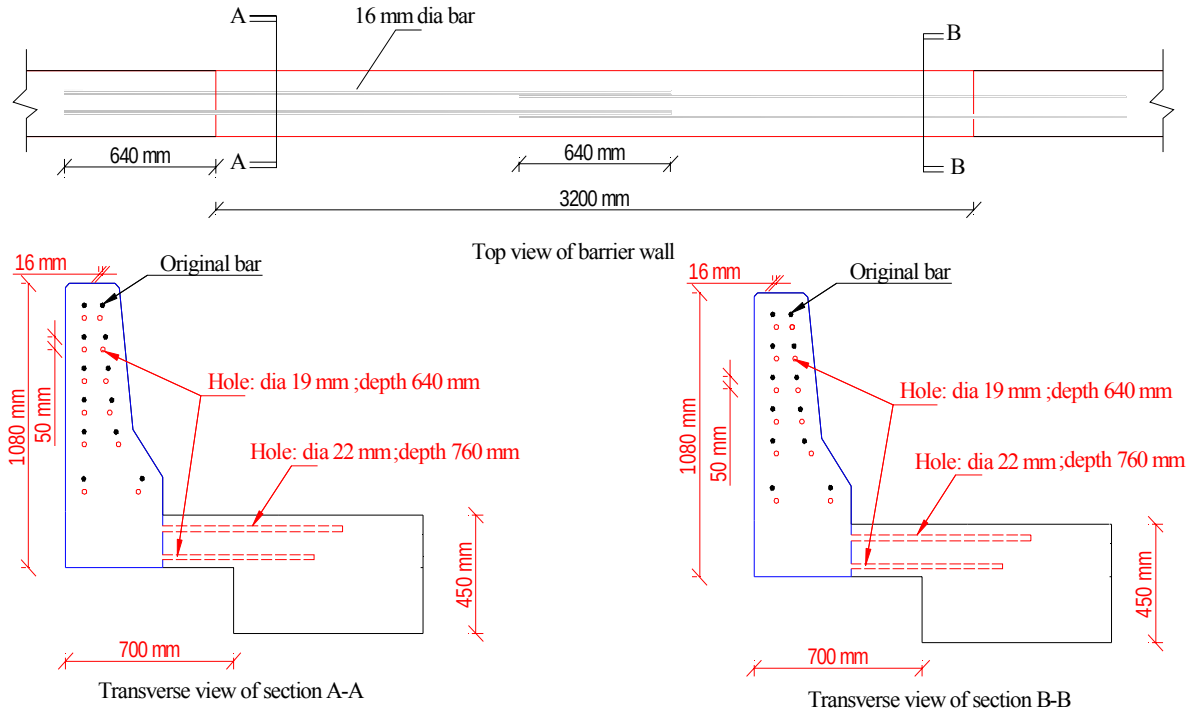

Figure (3.26): Transverse view of holes layout at middle

Figure (3.27): Drilling holes

- Strain gauges were placed on vertical, transverse and horizontal bars as shown in Figure 3.3 and 3.4.
- Epoxy was mixed and injected into the holes using injection gun, and then bars were inserted into holes. Figure 3.28 shows shapes of vertical bars used in repairing.

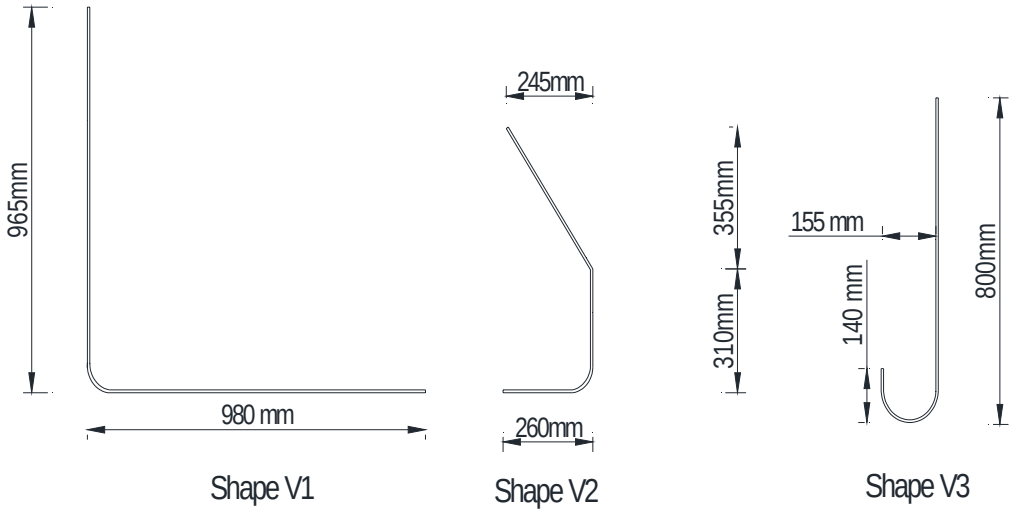

Figure (3.28): Shapes of vertical bars used in repairing

- Figure 3.29 to 3.32 shows bar plantation processes.

Figure (3.29): Mixing epoxy

Figure (3.30) Filling gun with epoxy

Figure (3.31): Injecting epoxy

Figure (3.32): Pushing bar inside the hole

- After finishing bar planting, new reinforcements were tied up. Figure 3.33 and 3.34 show new reinforcement cage.

a) Back view

b) Front view

Figure (3.33): New spliced (planted) reinforcement at middle

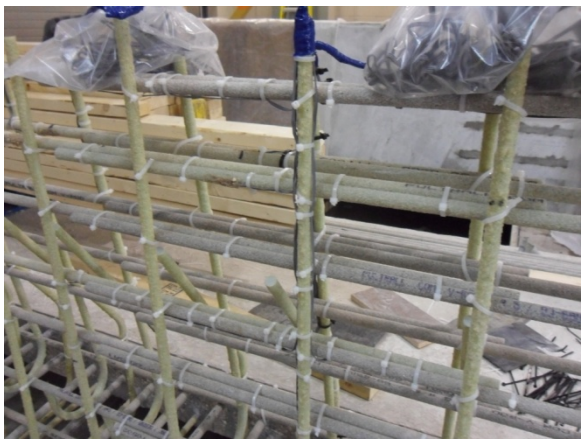

Figure (3.34): Lap splice of horizontal bar

- Then concrete was cast in the repaired part. Figure 3.35 shows splice repaired middle portion.

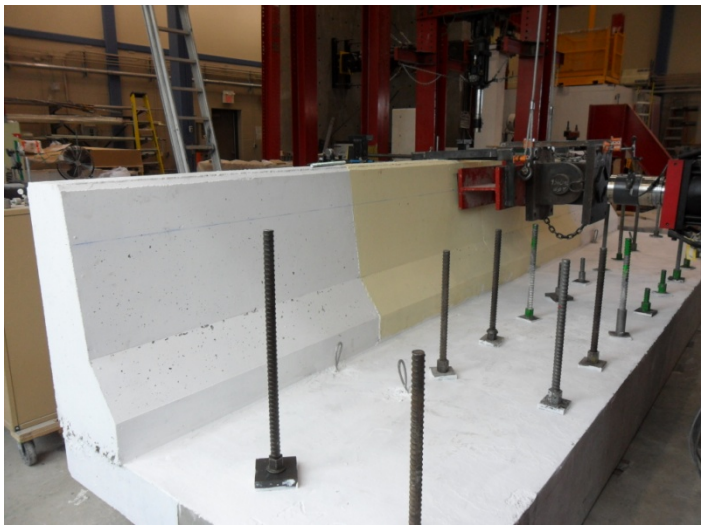

Figure (3.35): Splice repaired middle portion (in yellow color)

3.3.2.2. Repairing Edge Portion Using Splicing (Planting) Technique

In repairing damaged edge portion using splicing technique, the following procedure was used:

- A 2-m long damaged edge portion of the barrier wall including the underneath slab was cut using concrete saw.
- After removing the damaged portion, using concrete drilling machine, holes were drilled both on the barrier wall and the overhang deck slab. Figure 3.36 and 3.37 show the holes layout at the edge portion.

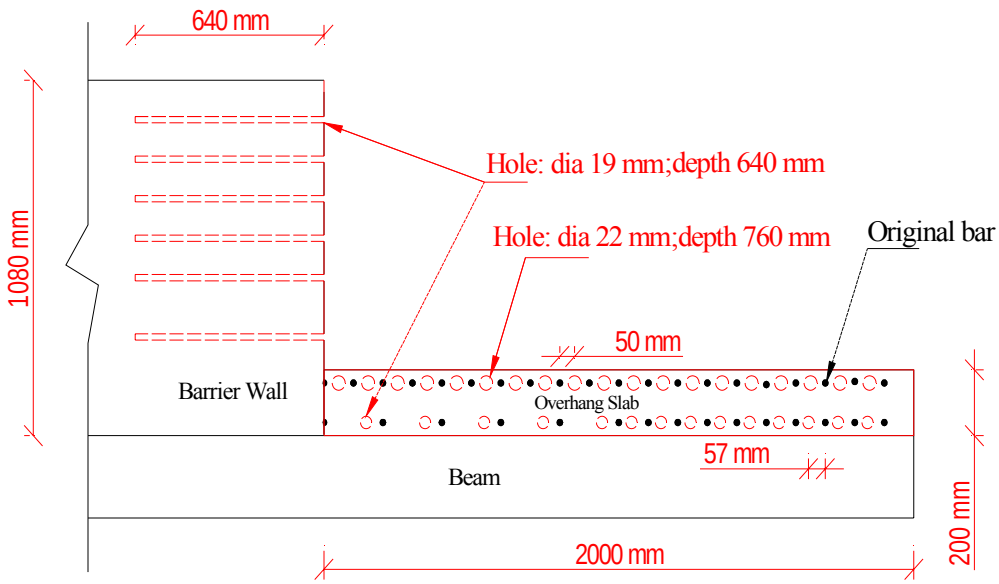

Figure (3.36): Longitudinal view of holes layout at the edge

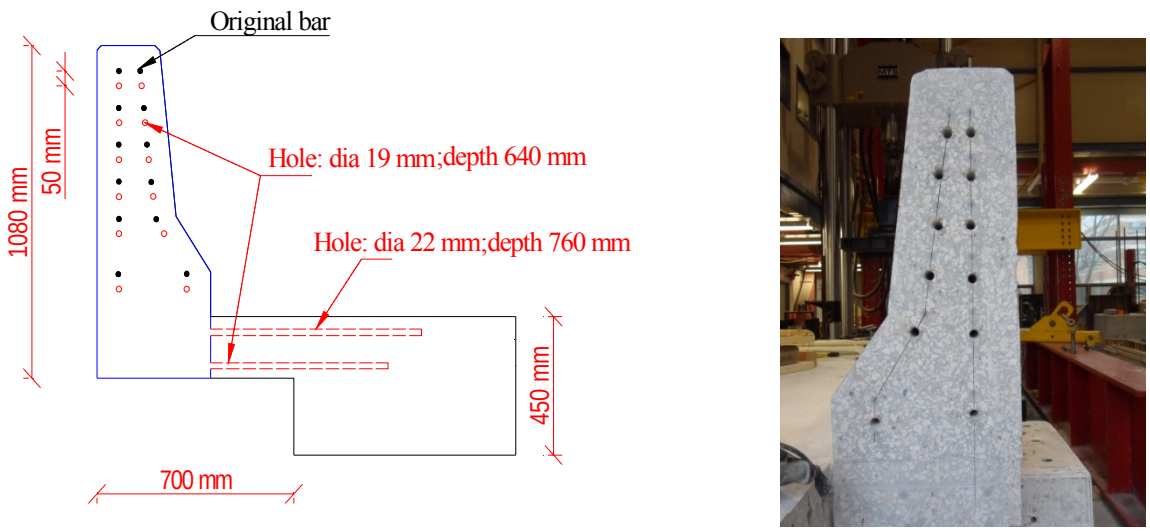

Figure (3.37): Transverse view of holes layout at the edge

- At the edge, all lose concrete of the overhang deck slab was removed. Figure 3.38 and 3.39 show the damaged edge portion and concrete removal.

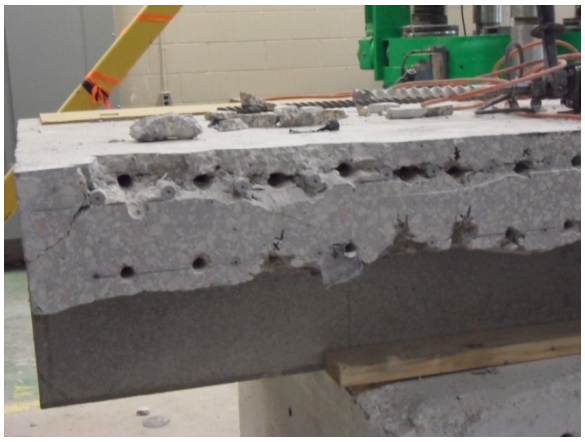

Figure (3.38): Edge condition

Figure (3.39): Edge Concrete removed

- After drilling, all holes were cleaned off using air blower to make them ready for bar planting. Interface surface was chipped off using jack hammer to make it rough for better bonding between new and old concrete.
- Strain gauges were placed on vertical, transverse and horizontal bars as shown in Figure 3.3 and Figure 3.5.
- Epoxy was mixed and injected into the holes using injection gun, and then bars were pushed into holes. Overhang edge was filled with epoxy.
- After finishing bar plantations, new reinforcements were tied up. Figure 3.40 and 3.41 show edge treatment and new reinforcement, respectively.

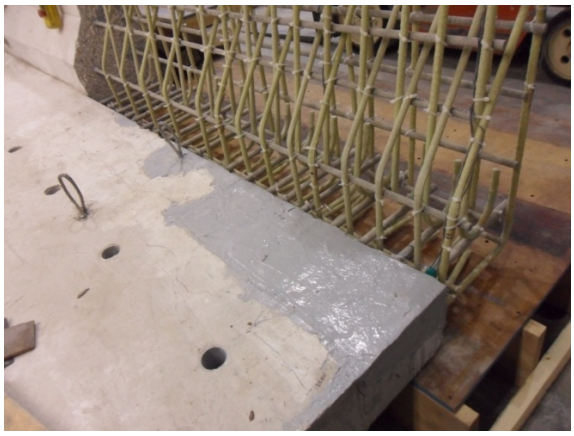

Figure (3.40): Edge treatment with epoxy

Figure (3.41): New spliced reinforcement at edge

- Then concrete was cast in the repaired edge. Figure 3.42 shows the repaired edge after concrete casting.

Figure (3.42): Splice repaired edge (in gray color)

3.3.3. Repairing Using NSM Technique

Near Surface Mounted (NSM) technique was used to repair both middle portion and edge of barrier wall prototypes. Repairing processes of both middle portion and edge portion are discussed below.

3.3.3.1. Repairing Middle Portion Using NSM Technique

In repairing damaged middle portion using NSM technique, the following procedure was used:

- Similar to planting technique, a 3.2-m long damaged middle portion of the barrier wall including the underneath slab was cut using concrete saw.
- After removing the damaged portion, using diamond blade concrete cutter machine and jack hammer, 30-mm wide × 25-mm deep and 30-mm wide × 50-mm deep grooves were cut both on the top of the overhang deck slab and both sides of the barrier wall, respectively. The grooves were cut right on top of the original reinforcement. Normally, 25 mm deep groove similar to deck slab groove would be good enough for NSM-GFRP bars of the barrier wall. However, in case of barrier wall, it would result in narrow gap (approximately 9 mm) between the formwork of repaired portion and NSM-GFRP bar; as a result new concrete (nominal aggregate size of concrete was 20 mm) would not be able to fill that gap. Therefore, 50 mm groove was cut on both sides of barrier wall to provide wider gap (approximately 35 mm) so that new concrete could fill that gap. Also, holes were drilled into the overhang deck slab to splice the bottom layer of GFRP reinforcement. Figures 3.43 and 3.44 show the grooves and holes layout. Figures 3.45 and 3.46 show grooves cutting and grooves on barrier wall. Figure 3.47 shows NSM grooves at middle portion.

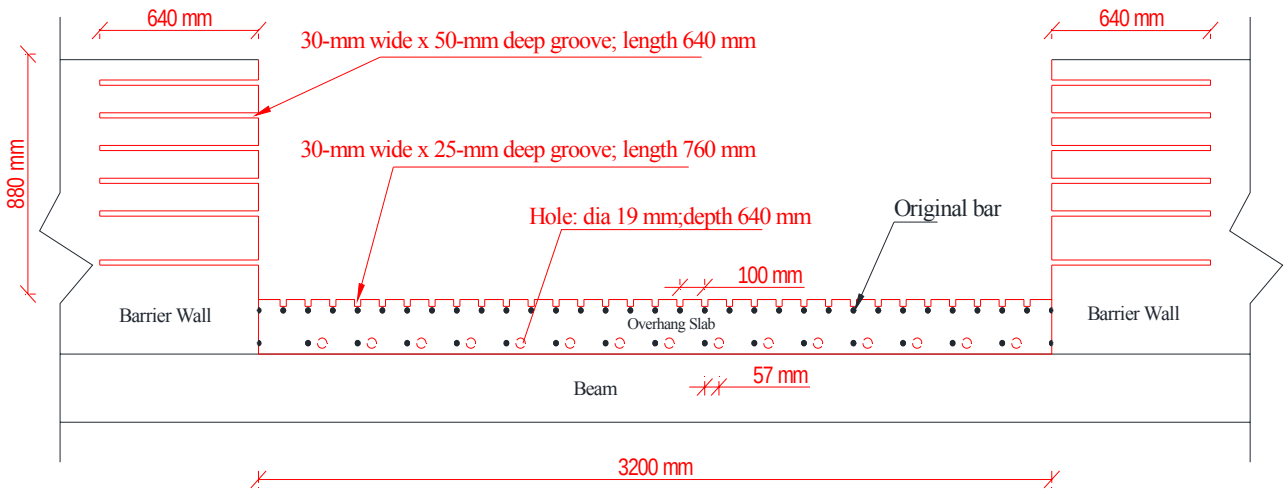

Figure (3.43): NSM Grooves and holes layout at middle portion in longitudinal direction

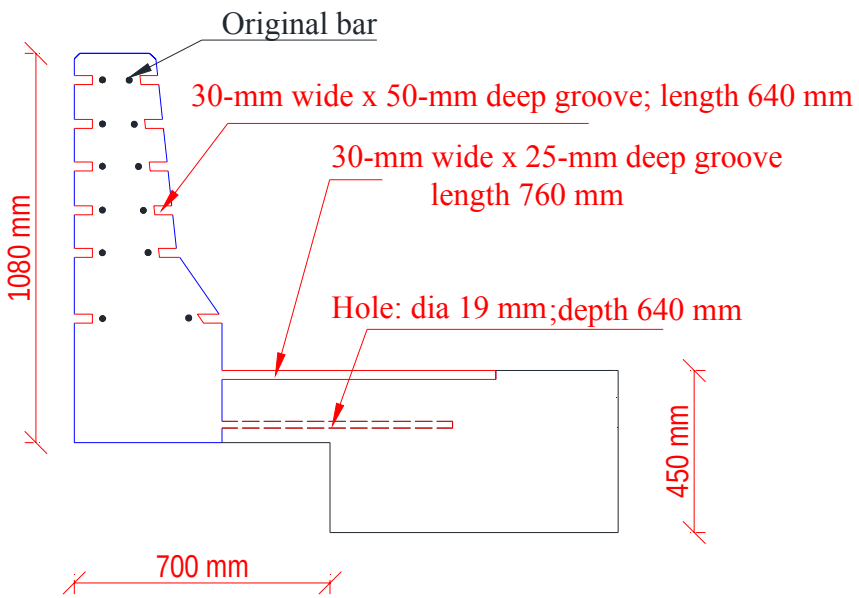

Figure (3.44): NSM grooves and holes layout in transverse direction

Figure (3.45): Cutting NSM grooves

Figure (3.46): NSM grooves on barrier wall

Figure (3.47): NSM grooves at middle portion of barrier wall

- After cutting and drilling, all grooves and holes were cleaned off using air blower to make them ready for bar installation. Interface surface was chipped off using jack hammer to make it rough for better bonding between new and old concrete.

- Strain gauges were placed on vertical, transverse and horizontal bars as shown in Figure 3.3 and 3.4.
- Barrier wall grooves were filled with epoxy up to 25 mm depth and then horizontal bars were placed in them and rest of the depth of grooves were filled by grout. Deck slab grooves were filled with epoxy fully and then transverse bars were placed.
- Epoxy was injected into the holes using injection gun, and then bars were pushed into holes. Figure 3.48 to 3.53 shows bar planting processes.

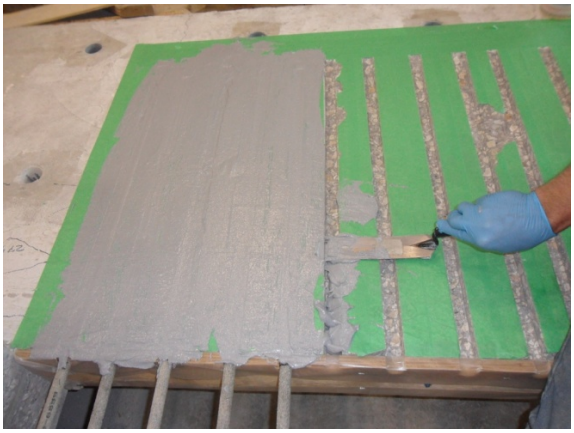

Figure (3.48): Filling deck slab grooves with epoxy

Figure (3.49): Placement of transverse bar

Figure (3.50): vertical bar at the middle portion

Figure (3.51): Filling epoxy in grooves

Figure (3.52): Placing bar in barrier wall grooves

Figure (3.53): Putting grout in grooves

- After finishing bar plantations, new reinforcements were tied up. Figure 3.54 shows new reinforcement at NSM repaired middle portion.

Figure (3.54): New reinforcement at NSM repaired middle portion

- Then concrete was casted in the repaired middle portion. Figure 3.55 shows NSM repaired middle portion during curing.

Figure (3.55): NSM repaired middle portion during curing

3.3.3.2. Repairing Edge Portion Using NSM Technique

In repairing damaged edge portion using NSM technique, following procedure was used:

- Similar to planting technique, a 2-m long damaged edge portion of the barrier wall including the underneath slab was cut using concrete saw.
- After removing the damaged portion, using diamond blade concrete cutter machine and jack hammer, 30-mm wide × 25-mm deep and 30-mm wide × 50-mm deep grooves were cut both on the top of the overhang deck slab and both sides of the barrier wall, respectively. The grooves were cut right on top of the original reinforcement. Here also, 50 mm deep groove were cut on the barrier wall for the same reason explained earlier. In addition, holes were drilled into the overhang deck slab to splice the bottom layer of GFRP reinforcement. Figure 3.56 and 3.57 show the holes layout.

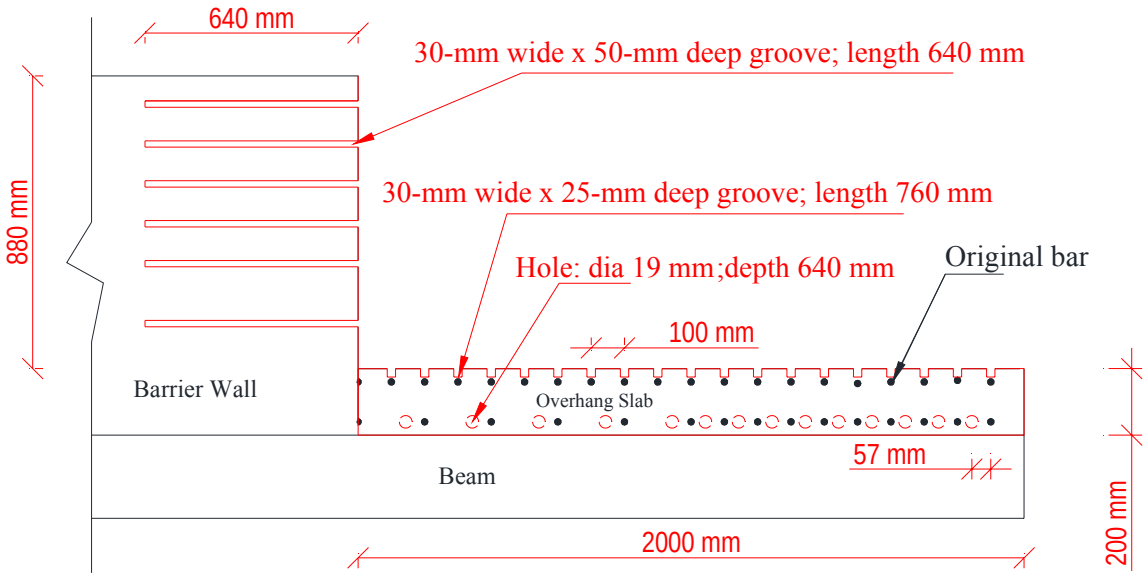

Figure (3.56): Longitudinal view of grooves and holes layout at the edge

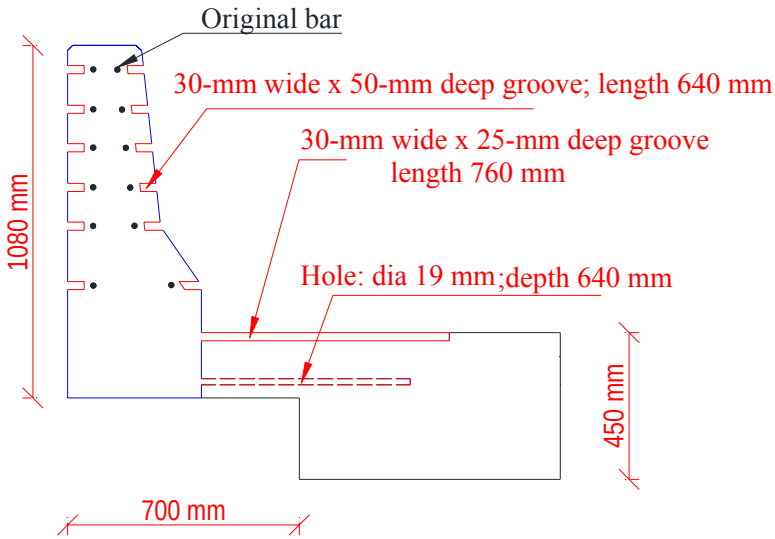

Figure (3.57): Transverse view of grooves and holes layout at the edge

- After cutting and drilling, all grooves and holes were cleaned off using air blower to make them ready for bar installation. Interface surface was chipped off using jack hammer to make it rough for better bonding between new and old concrete

- At the edge, all lose concrete of the overhang deck slab was removed. Figure 3.58 shows the damaged edge portion.

Figure (3.58): Edge condition

- Strain gauges were placed on vertical, transverse and horizontal bars as shown in Figure 3.3 and 3.5.
- Barrier wall grooves were filled with epoxy up to 25 mm depth and then horizontal bars were placed in them and rest of the depth of grooves were filled by grout. Deck slab grooves were filled with epoxy fully and then transverse bars were placed. Damaged overhang edge was filled with epoxy.
- Epoxy was injected into the holes using injection gun, and then bars were pushed into holes.
- After finishing bar plantations, new reinforcements were tied up. Figure 3.59 shows new reinforcement at edge

Figure (3.59) New NSM reinforcement at edge

- Then concrete was cast in the repaired edge. Figure 3.60 shows the repaired edge after concrete casting.

Figure (3.60): NSM repaired edge (in gray color)

Chapter 4

Test Results and Discussion

4.1. General

Both intact and repaired barrier wall prototypes were tested under monotonic load up to failure simulating vehicle crash test. All test data were recorded using DAQ (data acquisition system). In this chapter, test results are presented and discussed in terms of mode of failure, cracking pattern, deflection, and strains in reinforcements. As mentioned before, the experimental work included two phases; Phase I and Phase II. Tests results of Phase I are presented and discussed in this chapter. Phase II test results are presented, discussed and compared with Phase I test results in Chapter 5.

4.2. Test Results and Discussion of Phase I

Test results of intact barrier walls of Phase I are presented and discussed in terms of ultimate capacity and mode of failure, cracking pattern, deflection and strains in reinforcements. The overall behaviour of the replicate tests at the middle (M1, M2) and at the edge (LE, RE) was very similar and may be considered identical. Therefore, in the following discussion, typical results at both locations (middle and edge) will be presented. However, differences between replicates, if any, are highlighted.

4.2.1. Ultimate Capacity and Mode of Failure

Ultimate capacity and mode of failure of all the tested intact barrier walls are summarized in Table (4.1).

Table (4.1): Ultimate capacity and mode of failure

Test Designation	Ultimate Capacity (kN)	Compressive Strength of Concrete (MPa)	Mode of Failure
M1	391	50	Punching shear failure of the barrier wall
M2	373	45	
LE	237	45	Punching shear failure of the barrier wall along with failure of wall/deck slab joint
RE	245	45	

During testing of both M1 and M2, cracks first appeared on the overhanging deck slab. The first crack appeared at a load of approximately 90 kN (23% of the ultimate load). With the increasing load, more cracks started to appear on both the barrier wall and the overhang deck slab. At a load of approximately 150 kN (39% of the ultimate load), both specimens exhibited cracks at the joint between the barrier wall and the slab. Then at a load of approximately 250 kN (65% of the ultimate load), first vertical crack appeared on the back side of both specimens. Finally, both specimens failed due to punching shear through the barrier wall. Ultimate capacity of the M1 and M2 prototypes was close to each other (approximately 5% difference).

Similarly, during testing of both LE and RE, cracks first appeared at the free edge of the overhang deck slab. First crack appeared at a load of 75 kN (31% of the ultimate load) and 100 kN (41% of the ultimate load) in LE and RE, respectively. With the increasing load, more cracks started to appear both on the barrier wall and the overhanging slab. At a load of 125 kN (51% of the ultimate load), both specimen exhibited diagonal crack on the front face of the barrier wall. Then at a load of 150 kN (62% of the ultimate load), vertical crack appeared on the back side of both specimens. Finally, both specimens

failed due to punching shear through barrier wall along with failure of the joint between barrier wall and overhanging slab. Ultimate capacity of both edges was very similar (approximately 3% difference).

Ultimate capacity of all tested prototypes satisfied CAN/CSA-S6-06 strength requirement criterion of withstanding 100 kN longitudinal load spreading over 1050 mm length for PL-2 bridge barrier. Even though both edges of barrier have double the vertical reinforcement, they exhibited less capacity than the middle portion which was expected due to the discontinuity of edges. Figure 4.1 to 4.3 show mode of failure of intact barrier walls tested in Phase 1.

a) Front face

b) Back face

Figure (4.1): Punching shear failure of M1

Figure (4.2): Punching shear failure of RE

Figure (4.3): Joint failure of RE

The observed punching mode of failure confirms that the applied load on the barrier wall was carried by two-way action in both vertical and horizontal directions. In contrary, the work carried out by Ahmed et al. (2011) on 2.6-m long barrier segments failed by concrete splitting of overhang deck slab exhibiting much lower capacity (306 kN). This difference in mode of failure and capacity can be attributed to the difference in length of the tested prototypes. Long prototypes exhibited two-way action which is realistically simulating the long and continuous barriers in the field. Therefore, in real life bridge barriers will exhibit two-way action in resisting load in case of vehicle accidents.

4.2.2. Cracking Pattern

During testing, all test prototypes experienced lots of cracking on the top of the overhang deck slab, front face and back face of the barrier wall. Typically, longitudinal cracks initiated on the overhang slab first and then on the front face of barrier wall and finally at higher loading vertical appeared on the back face of barrier wall. In both M1 and M2 prototypes, critical length over which all cracks were distributed was approximately 3.2

m. In both LE and RE prototypes, this critical length was approximately 2.0 m. Cracks formed in trapezoidal shape on the front face of barrier wall. While on the back face, cracks were formed in the vertical direction. Typical cracking patterns are shown in Figure 4.4 to 4.7.

a) Front face

b) Back face

Figure (4.4): Cracking pattern of M1 prototype

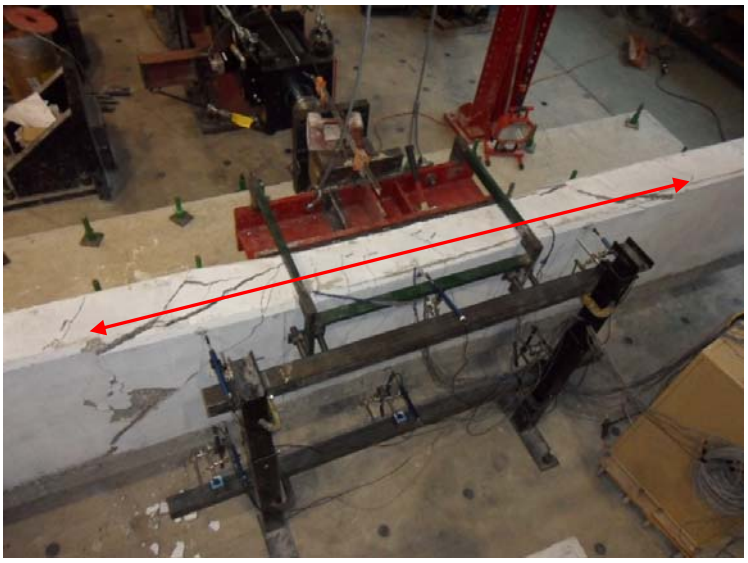

Figure (4.5): Critical length (3.2 m) of M2 (shown in arrow)

a) Front face b) Back face

Figure (4.6): Cracking pattern of LE prototype

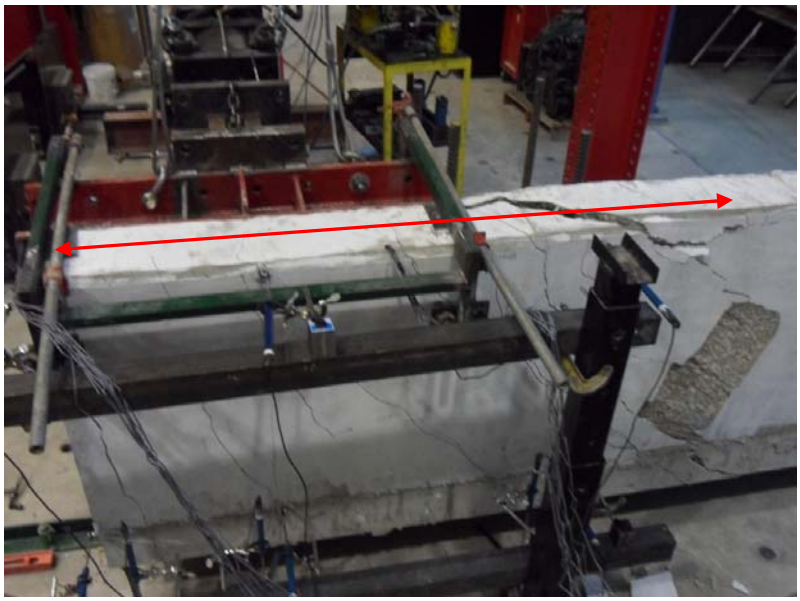

Figure (4.7): Critical length (2 m) of RE (shown in arrow)

4.2.3. Deflections

Linear variable displacement transducers (LVDTs) were used to measure horizontal deflection of the barrier wall as well as vertical deflection of the overhang slab of all the test prototypes. The following sections present and discuss typical load-deflection graphs based on average values of the replicated tests at middle (M1 and M2) and at edge (LE and RE). Individual load-deflection graphs for M1, M2, LE and RE tests can be found in Appendix G.

It should be noted that, in all tests, horizontal deflection was measured both at the top of the barrier wall and at the barrier wall-slab joint. The measurement at the bottom of the wall was intended to measure the rigid-body movement or slippage of the test prototype with the increasing load, if any. Since the reading at the bottom of the wall was zero, only horizontal deflection results at the top of the wall are presented.

4.2.3.1. Deflection for Middle Test

Figure 4.8 shows typical vertical deflection curves of the overhang deck slab while testing at the middle portion of the barrier wall.

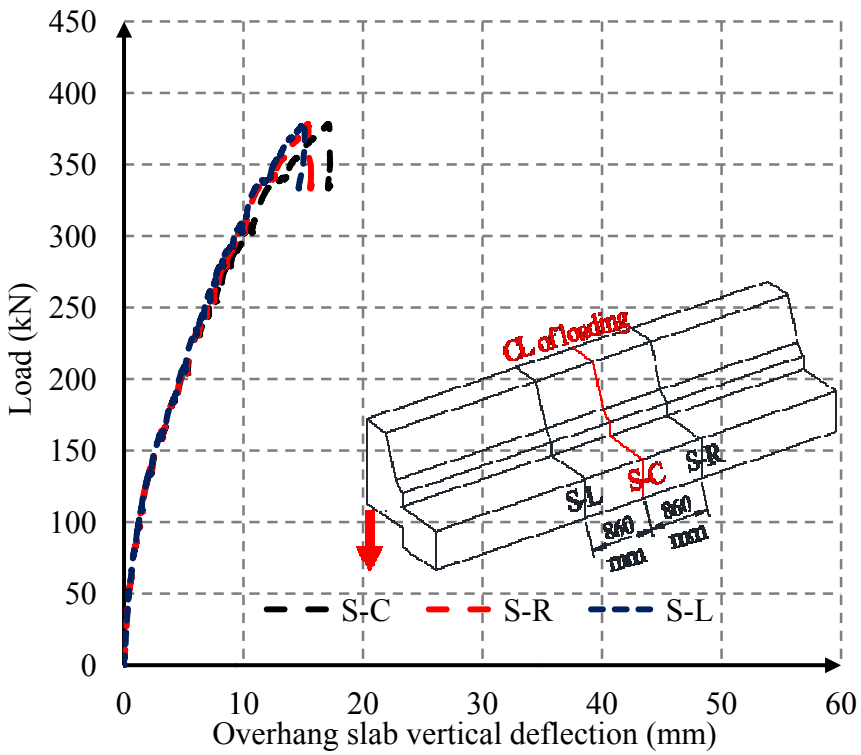

Figure (4.8): Vertical deflection of overhang deck slab for middle test (typical)

It can be noticed in the graph that the overhang deck slab exhibited almost equal vertical deflections at all three different locations up to a load of 300 kN (78% of the ultimate load). After that, higher vertical deflection appeared at the centerline of loading (S-C). Finally, as expected and due to the punching shear mode of failure, the overhang slab under the centerline of loading gave maximum vertical deflection. Furthermore, vertical deflection of overhang deck slab at equally spaced right and left side of the centerline of loading was almost equal. This means that overhang slab deflected symmetrically on both side of the centerline of loading, which indicates that load was transferred equally on both sides of the centerline of loading. At failure, in M1, maximum vertical deflection of overhang deck slab was 17.2 mm while, this value was 18 mm for M2 test. These two values were close to each other (approximately 4 % difference).

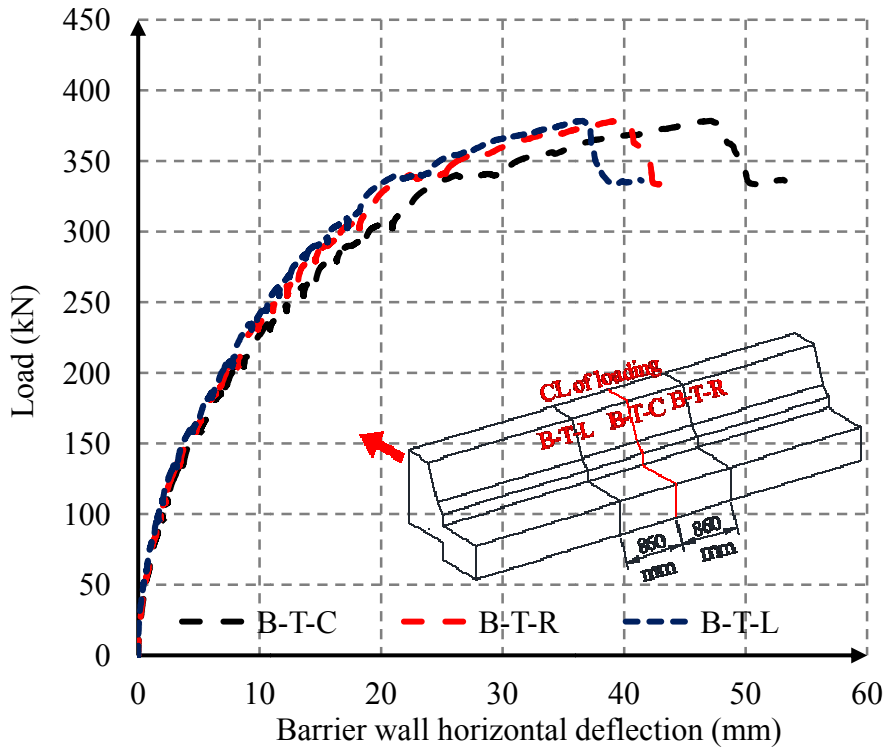

Figure (4.9): Barrier wall horizontal deflection for middle test (typical)

Figure 4.9 shows the typical horizontal deflection at the top of the barrier wall. Up to a load of 200 kN (52% of the ultimate load), horizontal deflection at all three different locations of the barrier wall was close to each other. Then, at the centerline of loading (B-T-C), higher horizontal deflection appeared. Similar to vertical deflection of overhang slab, barrier wall at the centerline of the loading gave maximum horizontal deflection at failure. Here also, equally spaced right and left side of the centerline of loading exhibited identical load-deflection path, which means that barrier wall exhibited symmetrical horizontal deflection around the centerline of loading. This confirms that load, on both side of the centerline of loading, was equally transferred. Finally at failure, maximum horizontal deflection in M1 and M2 was 51.4 mm and 48.7 mm, respectively. It can be

noticed that horizontal deflection of M1 at failure was higher than that of M2 by 2.7 mm (approximately 5%) due to the higher failure load of M1 than that of M2 (approximately 5%).

4.2.3.2. Deflections at Edge

Typical load vs. vertical deflection of the overhang deck slab for edge test is shown in Figure (4.10).

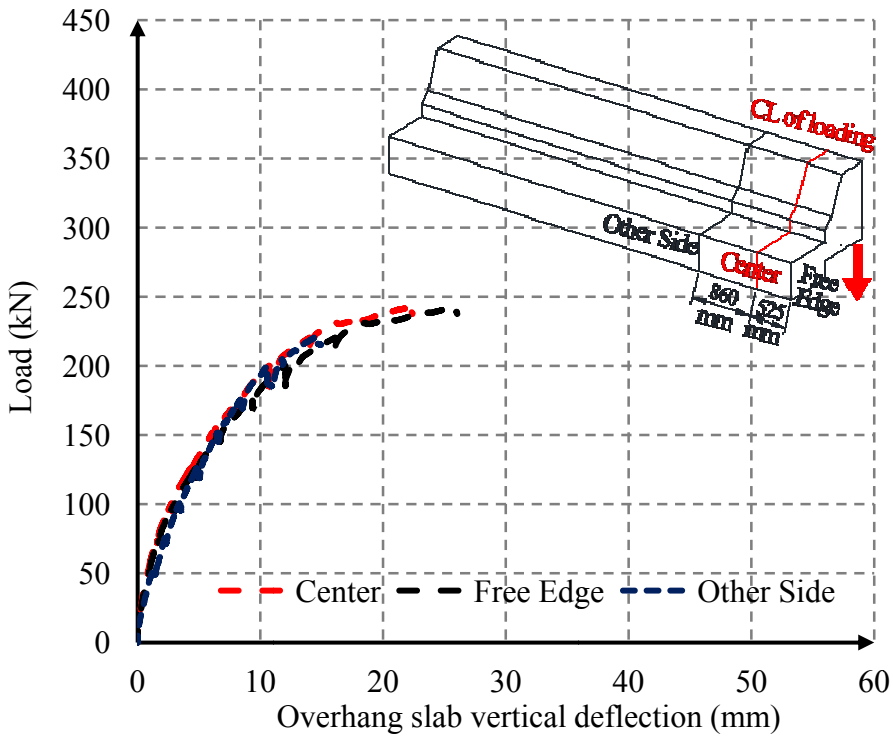

Figure (4.10): Vertical deflection of overhang deck slab for edge test (typical)

Typically, up to a load of 150 kN (62% of the ultimate load), overhang slab gave almost equal amount of vertical deflection at all three different locations. After that, as expected, overhang slab at its test side free edge gave higher vertical deflection; in LE at left side

free edge and in RE at right side free edge. Furthermore, vertical deflection decreased in locations away from the free edge. For example, in RE vertical deflection in S-L, which was 1385 mm away from the test side free edge, was the lowest among measured deflections. At failure, maximum vertical deflection of the overhang slab for LE test was 24.7 mm while, this value was 26.7 mm for RE test. These two values were close to each other (approximately 6% difference)

Figure 4.11 shows the typical horizontal deflection at the top of the barrier wall for edge test.

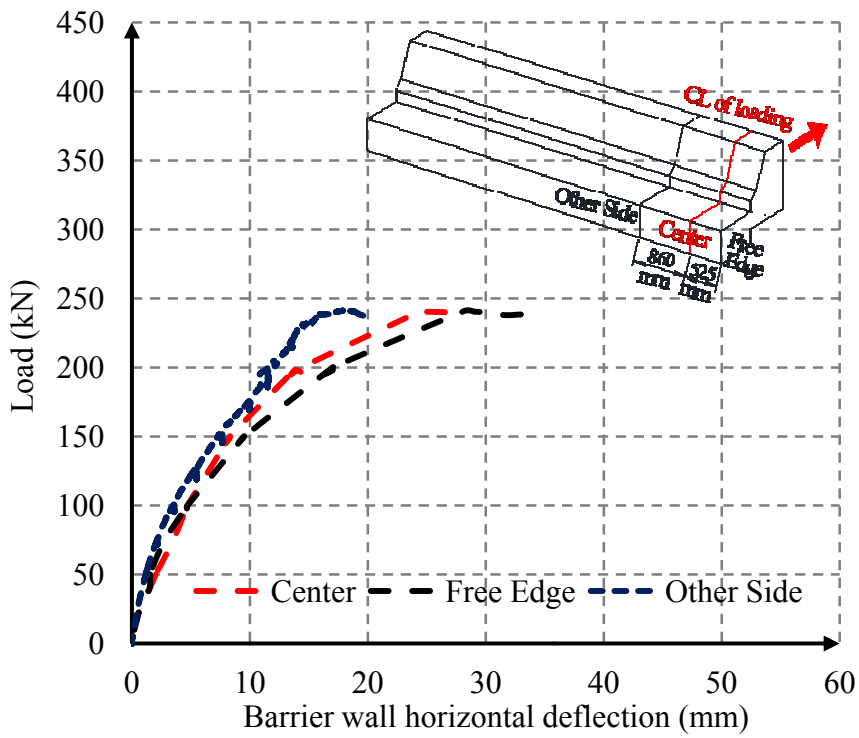

Figure (4.11): Barrier wall horizontal deflection for edge test (typical)

At edge, up to a load of 50 kN (21% of the ultimate load), barrier wall exhibited almost equal horizontal deflection at its different locations. With increasing load, as expected,

barrier wall gave higher horizontal deflection at its free edge. It can be noticed that almost equal horizontal deflection values were observed both at test side free edge and at centerline of loading up to a load of 100 kN (41% of the ultimate load). This is due to the fact that both the locations were inside of the 1050 mm load-application zone. Furthermore, minimum horizontal deflection was observed in location away from the free edge. Finally at failure, maximum horizontal deflection in LE and RE was 29.7 mm and 27.4 mm, respectively.

4.2.3.3. Summary of Deflection

Table 4.2 summarizes the maximum measured deflection values observed during the testing of the intact prototypes (at failure).

Table (4.2): Maximum deflections of intact prototypes

Test Designation	Location of Deflection	Maximum Overhang Slab Vertical Deflection (mm)	Maximum Barrier Wall Horizontal Deflection (mm)
M1	Centreline of loading	17.2	51.4
M2		18.0	48.7
LE	Free edge of testing side	24.7	29.7
RE		26.7	27.4

Based on the deflection values, it can be noticed that at middle portion horizontal deflection of barrier wall was much higher (approximately 3 times) than vertical deflection of overhang deck slab. However, at edges, barrier wall horizontal deflection and overhang deck slab vertical deflection became close to each other (approximately 10% difference). Furthermore, it can be noticed that at edges barrier wall horizontal

deflection was decreased and overhang deck slab deflection was increased by almost equal amount (approximately 43%) than those of middle portion of barrier wall. This means, at edges, barrier wall contribution in carrying load was decreased and overhang deck slab contribution in carrying load was increased than those of middle portion of the barrier wall. This indicates that two-way action of carrying load at middle portion of the barrier wall got decreased at the edges.

4.2.4. Strains in Reinforcements

During testing, readings from strain gauges were recorded using data acquisition system (DAQ). The following sections of this chapter present typical load-strain graph of the tested prototypes. Individual load-strain graphs for M1, M2, RE and LE can be found in Appendix G.

4.2.4.1. Strains in Reinforcements for Middle Test

For middle test, at the slab-barrier wall connection, two strain gauges were installed on two top transverse bars of overhang deck slab. One bar was located at the centerline of loading and another one was located 400 mm right to the centerline of loading. Figure 4.12 shows typical load-strain graph of overhang transverse bars for the middle test.

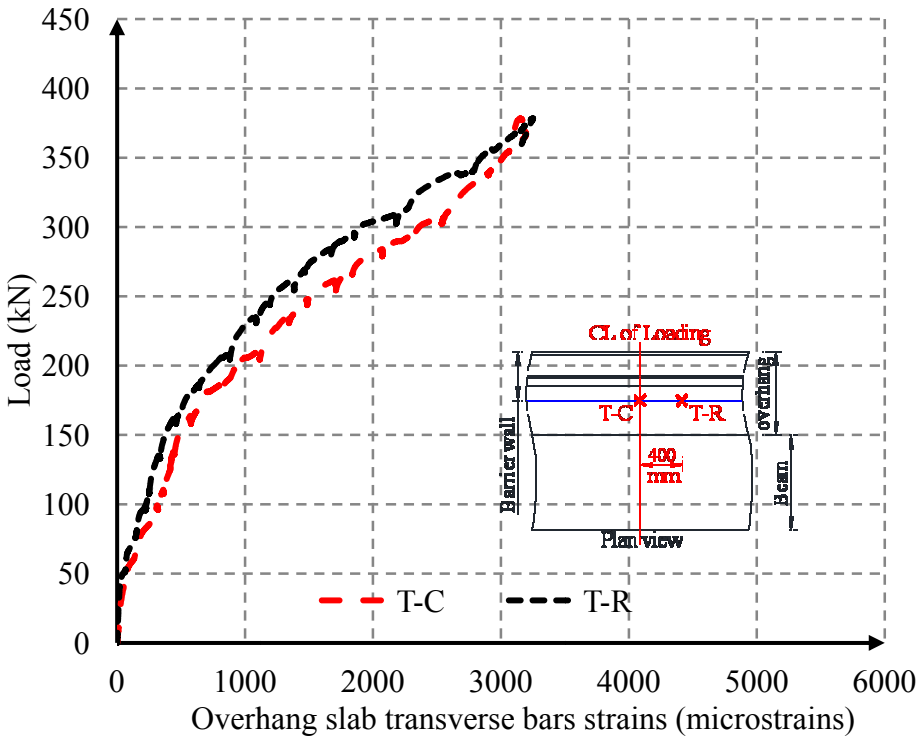

Figure (4.12): Overhang slab transverse bar strains for middle test (typical)

As expected, both the transverse bars of the overhang deck slab showed linear load-strain relationship up to failure. Initially, up to a load of 50 kN (13% of the ultimate load), amount of tensile strains in both the bars were negligible. Then overhang deck slab exhibited first longitudinal crack at a load of 100 kN (26% of the ultimate load) and significant strain appeared in both the bars; consequently, load-strain curve changed its slope. It can be noticed that T-C bar and T-R bar followed similar load-strain path and gave close strain values because both the bars were within the 1050 mm long load-application zone. In M1, maximum strain value at failure in T-R bar was 3624 micro-strains while, this value in T-C bar was 3328 micro-strains for M2 test; these values ranging between 22 and 23% of the ultimate strain of 19 mm GFRP bar (15300 micro-strains).

Strain gauges were installed on both front face and back face horizontal bars of the barrier wall. Figure 4.13 shows typical strain graphs of horizontal bars for middle test.

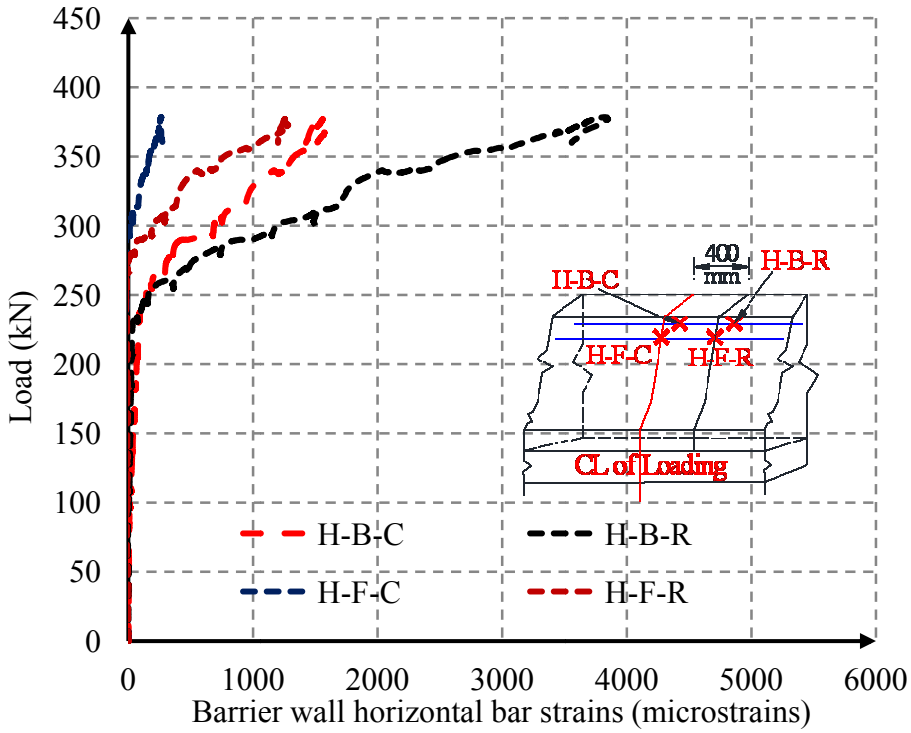

Figure (4.13): Barrier wall horizontal bar strains for middle test (typical)

Typically, all the horizontal bars started to have the considerable amount of strain after the load of 250 kN (65% of the ultimate load) because at that load first crack appeared on the barrier wall. With increasing load, back face horizontal bars exhibited higher tensile strains than those of front face bars. It was because barrier wall carried horizontal moments, which resulted tension at the back face of the wall. Finally, at failure, maximum tensile strain occurred at H-B-R location, which was 400 mm right to the centerline of loading on back face. It was because H-B-R was located close to the end of the 1050-mm long load-application zone, where stress concentration was expected to

occur. At failure, maximum tensile strain in H-B-R for M1 test was 4206 micro-strain while, this value was 3540 micro-strain for M2 which is much less than the ultimate strain of the 16 mm GFRP bar of 15600 micro-strain (73% less for M1 and 77% less for M2).

Strain gauges were installed on vertical bars of the barrier wall of both M1 and M2. Three different shapes of vertical bars, V1, V2 and V3, were used. Strain gauges were installed at different critical locations of all these bars as shown in Figure (3.18). In both M1 and M2, maximum tensile strain was occurred in V2 bars. It was due to the fact that V2 bars were located near the slab-barrier wall joint, where maximum vertical moment of the barrier wall was expected to occur. Furthermore, V2 bar provide anchorage against this vertical moment. Therefore, only V2 bar strains at different locations of the barrier are presented. Figure 4.14 shows typical strain graph of V2 bars. The remaining strain readings of the other bars are shown in Appendix G.

Typically, considerable amount of tensile strain appeared on V2 bars after the load of 300 kN (78% of the ultimate load) because at that load barrier wall front face diagonal cracks reached close of the slab-barrier wall junction. Finally, V2-R bar gave maximum tensile strains as it was near the end of load-application zone. Maximum tensile strain in V2-R bar for M1 test was 5081 micro-strains while, this value was 4724 micro-strains for M2 test which ranging between 43 and 46% of the ultimate strain of 16 mm GFRP bent bars (10920 micro-strain).

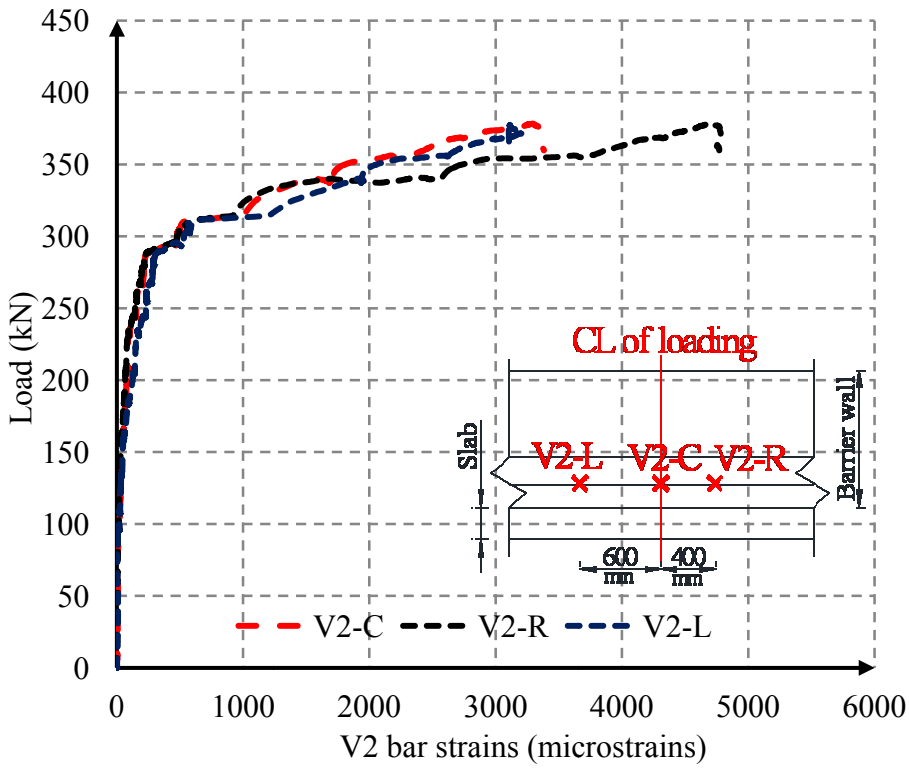

Figure (4.14): V2 bar strains along the length of the barrier wall for middle test (typical)

4.2.4.2. Strains in Reinforcements for Edge Test

Similar to middle test, strain gauges were installed on two top transverse bars of the overhang deck slab at barrier wall-slab junction. One bar was located at the centerline of loading and another one was located close to free edge of test side. Figure 4.15 shows typical load-strain graph of overhang transverse bars for edge test.

Typically, transverse bars of overhang deck slab exhibited linear load-strain relationship up to failure which was expected due to the linear stress-strain relationship of GFRP bars. Load-strain curve changed its slope at a load of 100 kN (41% of the ultimate load) because at that load longitudinal crack appeared on overhang deck slab. It can be noticed that T-Center and T-Free Edge bar followed similar load-strain path and gave close strain values because both the bars

were located within the 1050 mm long load-application zone. However, at failure, bar close to the free edge gave maximum tensile strain. In RE, maximum transverse tensile strain was observed in T-R bar, and the maximum value was 5462 micro-strains (35% of ultimate strain of the 19 mm GFRP bar). Similarly, in LE, maximum tensile strain was 4667 micro-strains (30% of ultimate strain of GFRP bar).

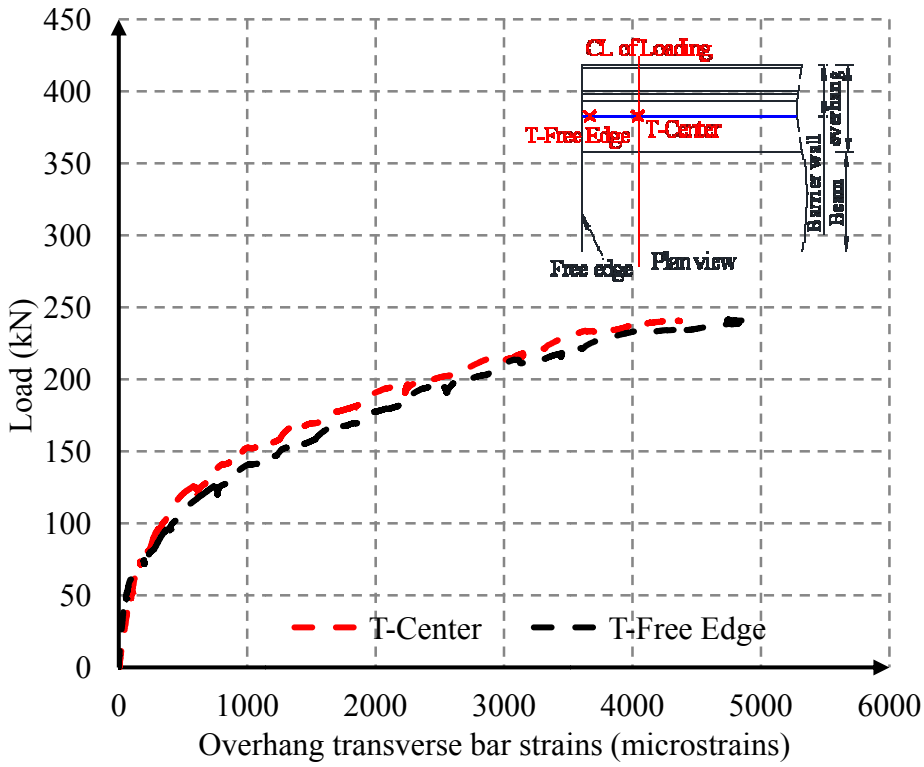

Figure (4.15): Overhang transverse bar strains for edge test (typical)

Figure 4.16 shows strains in horizontal bars of the barrier wall. Here also, strain gauges were installed on second horizontal bars (both front face and back face bar) from the top of the barrier wall. It can be noticed that all the horizontal bars started to exhibit considerable amount of strains after the load of 150 kN (62% of the ultimate load), at which first crack appeared on the barrier wall. After that back face horizontal bar, at a location close to the end of load-application

zone opposite to the free edge of barrier wall, showed the maximum tensile strain because maximum moment would occur at that location.

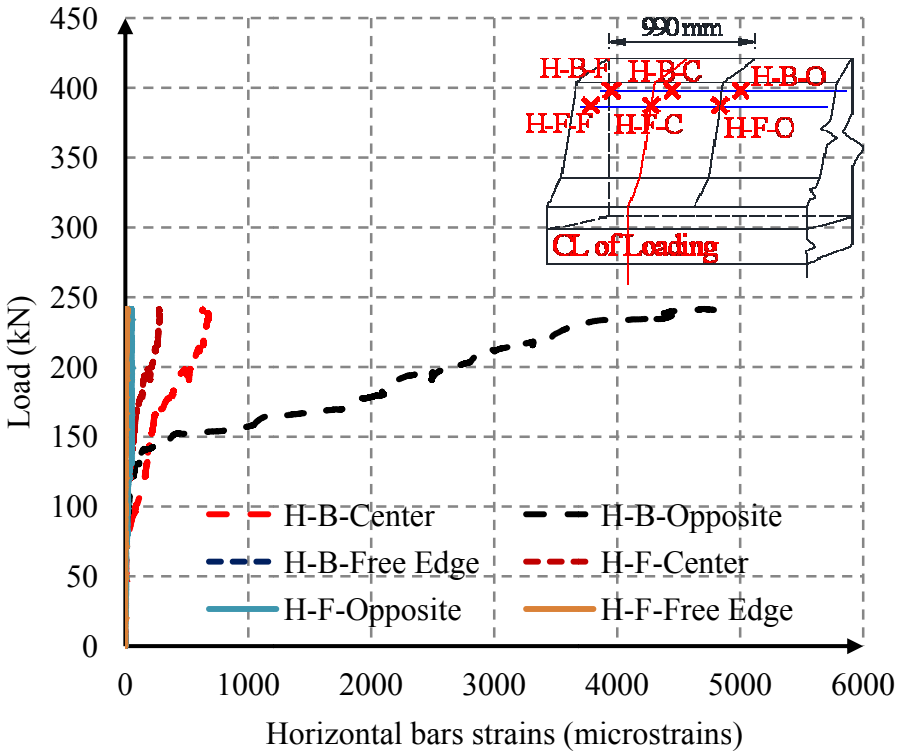

Figure (4.16): Barrier wall horizontal bar strains for edge test (typical)

In RE, maximum tensile strain observed in H-B-L was 5299 micro-strains (34% of ultimate strain of 16 mm GFRP bar). On the other hand, In LE, maximum tensile strain observed in H-B-R was 3845 micro-strains (25% of the ultimate strain of GFRP bar).

Strain gauges were installed on three different shapes (V1, V2 and V3) of vertical bars of barrier wall. However, maximum tensile strain was occurred on V2 shape bars similar to middle test. It was due to the fact that V2 bars were located near the slab-barrier wall junction, where maximum vertical moment of the barrier wall was expected to occur. Furthermore, V2 bar

provide anchorage against this vertical moment. Therefore, only V2 bar strains at different locations of the barrier are shown here. Figure 4.17 shows load vs. strains of V2 bar. The remaining strain readings of the other bars are shown in Appendix G.

Typically, considerable amount of tensile strain appeared on V2 bars after the load of 150 kN (62% of the ultimate load) because at that load first diagonal crack appeared on the barrier wall. Finally, V2 bar opposite to the centerline of loading exhibited maximum strains as it was close to the end of 1050 mm long load-application zone.

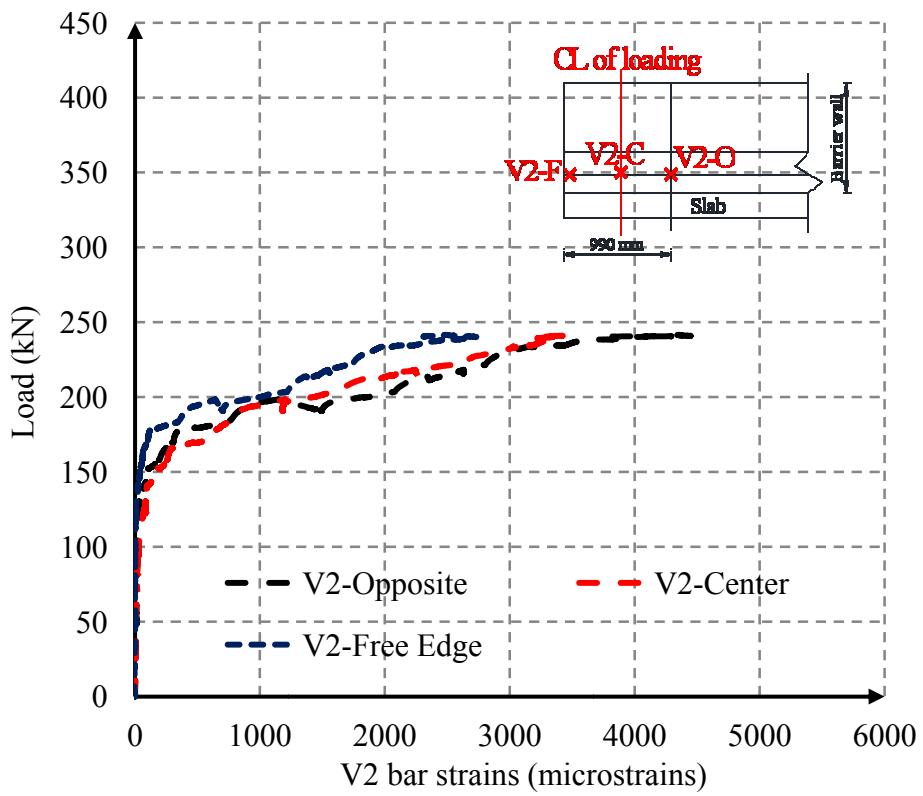

Figure (4.17): V2 bar strains along the length of the barrier wall for edge test (typical)

In RE, as expected, maximum observed tensile strain was 3846 micro-strains in V2-O. Similarly, in LE, maximum observed tensile strain in V2-O was 4293 micro-strains. These values ranging between 35 and 39% of the ultimate strain of 16 mm GFRP bent bars (10920 micro-strains).

4.2.4.3 Summary of Strains

Maximum strains measured at failure in horizontal and vertical bars of barrier wall and transverse bars of overhanging slab are summarized in Table 4.3.

Table (4.3): Maximum strains in GFRP reinforcements of intact prototypes

Test ID	Overhang transverse bar		Horizontal bar		Vertical bar (V2)	
	Strain gauge location	Strain (με)	Strain gauge location	Strain (με)	Strain gauge location	Strain (με)
M1	Centreline of loading	3624	Back face bar 400 mm right side to the CL of loading	4206	400 mm right the centreline of loading.	5081
M2	400 mm right side to the centreline of the loading	3328		3540		4724
LE	Free edge of barrier wall	4967	Back face bar 440 mm right side to the centreline of loading	3845	Centreline of loading	4293
RE		5462	Back face bar 440 left side to the centreline of loading	4299	left to the centreline of loading	3846

In both M1 and M2, at failure, contributions of vertical and horizontal bars of barrier wall in resisting the load were more than transverse bars of the overhanging slab. However, in both LE

and RE, contribution of transverse bars of the overhanging slab in resisting the load was more than the horizontal and vertical bars of the barrier wall which explains deck slab-barrier wall joint failure in addition to punching shear failure in those tests. These observations confirm that long or continuous barrier walls carry the concentrate/line loads in the two directions; vertical and horizontal.

4.2.5. Load Sharing

Test results of all the prototypes indicate that load within barrier wall was shared in two directions. However, many aspects of this load sharing such as mechanism of load sharing, percentage of load sharing in two directions, condition of load sharing at different load levels are yet to be fully explored. In order to clarify some of these aspects of load sharing using the obtained test results, a simple analysis at the middle portion of barrier wall was carried out. In this analysis, barrier wall was considered to act in one-way action up to the failure in order to calculate vertical bar strain because it was assumed that vertical bar of barrier wall when subjected to one-way action would result in higher strains than what it would give under two-way action. Therefore, theoretical and experimental values of strain would be different when barrier wall would start to carry load in two-way action; this difference in strains would travel in horizontal direction and thus load sharing percentage can be calculated. Furthermore, it was assumed that under one-way action, initially load would disperse at an angle of $45°$ on both sides of its application zone; this dispersion angle would decrease with increasing load due to the advent of cracks on the barrier wall. This means that with increasing load, un-cracked length along the horizontal cross section of barrier wall would decrease and finally it would reach to the

centerline of the loading. Then the whole section would be considered cracked and using cracked section properties vertical bar strain would be calculated.

Following these assumptions, initially, un-cracked section moment of inertia was used to find stress and strain in vertical bar at a particular load level. By using this approach and adjusting un-cracked length, calculated theoretical strain values matched with the experimental values. However, at higher load, theoretical strain and experimental strain no longer matched. Sudden increase in experimental strain value was observed than theoretical strain, which did not follow the initial assumptions. This was due to the fact that load within barrier wall after cracking redistributes itself and can travel to any bar. Thus on a particular bar, sudden increase of strain may be due to this redistributed strain. There is no theory available to measure this redistribution and test results also could not measure that. Due to these reasons, hand calculations of strains based on the stated assumptions could not yield any conclusive results on load sharing.

In order to get clear understanding on load sharing, a finite element modeling (FEM) of barrier wall can be carried out in future. Test results obtained in this phase can provide basis to do FEM of such full scale prototype and to investigate load sharing. Therefore, in this present research, test results of this phase are used for comparisons with the repaired prototypes to evaluate the efficiency of the repair techniques.

Chapter 5

Test Results, Comparisons and Discussion

5.1. Test Results of Phase II and Comparisons

In this chapter, test results of repaired barrier walls of phase II are presented and compared with corresponding intact barrier walls in terms of ultimate capacity and mode of failure, cracking pattern, deflection and strains in reinforcements.

5.2. Ultimate Capacity and Mode of Failure

In general, both spliced and NSM repaired middle portion of the barrier wall, similar to their intact counterparts, failed due to punching shear failure of the barrier wall. This punching shear failure was occurred within 3.2 m long repaired portion of the barrier wall. On the other hand, both spliced and NSM repaired edge portion of the barrier wall, similar to their corresponding intact prototypes, failed under combined punching shear failure and barrier wall-deck slab joint failure. Here also, failure happened within the 2.0 m long repaired edge portion. Furthermore, no visible failure occurred at the junction of new and old concrete in any of the repaired prototypes. In addition, in NSM repaired middle portion and edge portion, NSM grooves of both the overhang deck slab and barrier wall remained intact; no de-bonding failure occurred during test. The following sections present and discuss the ultimate capacity and mode of failure of individual tests (M1-P, M2-N, RE-P and LE-N) in detail.

Ultimate capacity and mode of failure of barrier walls repaired at the middle are summarized in Table 5.1.

Table (5.1): Ultimate capacity and mode of failure at middle

Test Designation		Ultimate Capacity (kN)		Compressive Strength of Concrete (MPa)		Mode of Failure	
Intact	Repaired	Intact	Repaired	Intact	Repaired	Intact	Repaired
M1	M1-P	391	348	50	37	Punching shear failure of the barrier wall	
M2	M2-N	373	451	45	51		

During testing of M1-P, repaired using splicing (planting) technique, first longitudinal crack appeared at a load of 50 kN (14% of the ultimate load) at the barrier wall-slab joint of the repaired portion. Then cracks appeared on both free edges of the overhanging slab at a load of 100 kN (29% of the ultimate load). With increasing load, more cracks appeared on the overhanging slab. After that at a load of 275 kN (79% of the ultimate load), first crack appeared on front face as well as on back face of barrier wall. Finally, M1-P failed due to punching shear failure of the barrier wall at a load of 348 kN. Thus, M1-P achieved 89% of the ultimate capacity of that of M1. This difference in obtained capacity (approximately 11 %) can be attributed to the lower concrete compressive strength of M1-P (approximately 25%) than that of M1. Figure 5.1 shows mode of failure of M1-P.

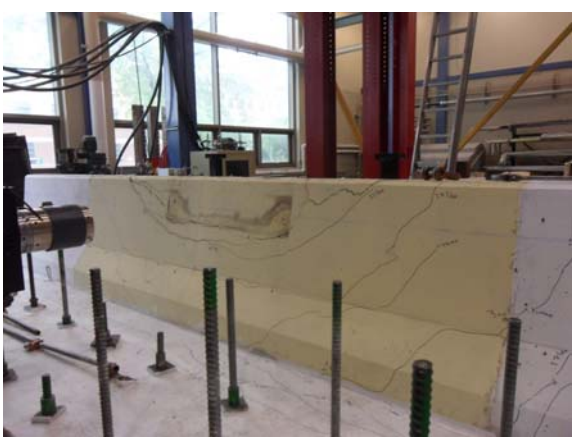

a) Front face

b) Back face

Figure (5.1): Punching shear failure of M1-P (repaired portion is painted yellow)

On contrary, in M2-N, repaired using NSM technique, first crack appeared at a load of 225 kN (50% of the ultimate load) on NSM grooves of overhang slab at barrier wall-slab junction. Then, at a load of 310 kN (69% of the ultimate load), crack appeared on the front face as well as back face of barrier wall. More cracks appeared on the front face and back face of barrier wall with increasing load. Finally, M2-N failed suddenly due to punching shear failure of the barrier wall at a load of 451 kN. Ultimate capacity of M2-N exceeded that of M2 by 20% because of NSM technique and higher concrete compressive strength of M2-N (approximately 13 %) than that of M2. This was expected since in NSM technique bars were placed near the surface that increased the effective depth of barrier wall and overhang slab, which in turn increased the moment capacity as well as stiffness of the repaired portion. Mode of failure of M2-N is shown in Figure (5.2).

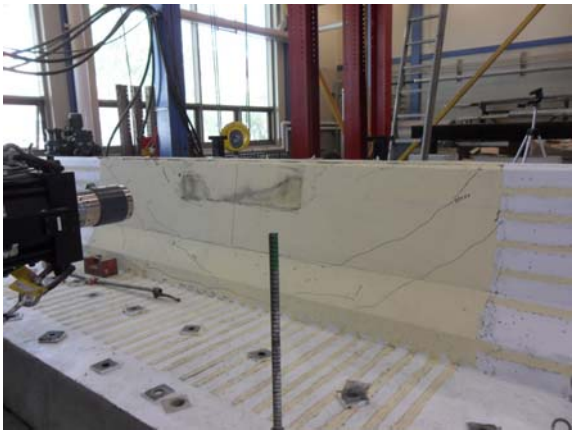

a) Front face

b) Back face

Figure (5.2): Punching shear failure of M2-N (repaired portion is painted yellow)

Ultimate capacity and mode of failure of barrier walls repaired at edges are summarized in Table (5.2).

Table (5.2): Ultimate capacity and mode of failure at edge

Test Designation		Ultimate Capacity (kN)		Compressive Strength of Concrete (MPa)		Mode of Failure	
Intact	Repaired	Intact	Repaired	Intact	Repaired	Intact	Repaired
RE	RE-P	245	208	45	38	Punching shear failure of the barrier wall along with failure of wall/deck slab joint	
LE	LE-N	237	230	45	51		

In RE-P, longitudinal crack first appeared on the test side free edge of the overhanging slab at a load of 75 kN (36% of the ultimate load). Then, at a load of 125 kN (60% of the ultimate load), diagonal crack appeared rack on the front face of the barrier wall while, on the back side of the barrier wall vertical crack appeared at a load of 150 kN (72% of the ultimate load). With increasing load, more cracks started to appear both on the barrier wall and the overhanging slab. Finally, RE-P failed due to punching shear failure of the barrier wall along with failure of the joint between barrier wall and overhanging slab at a load of 208 kN. As such, RE-P achieved approximately 85% of the ultimate capacity of its corresponding intact RE prototype. This difference in obtained capacity can be attributed to the lower concrete compressive strength of RE-P (approximately 15%) than that of RE. Figure 5.3 shows mode of failure of RE-P.

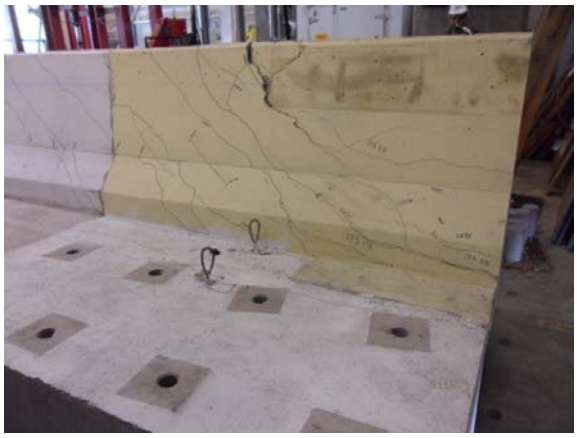

a) Front face

b) Back face

c) Joint failure

Figure (5.3): Mode of failure of RE-P (repaired portion is painted yellow)

On the other hand, while testing LE-N, first longitudinal crack appeared on the test side free edge of the overhanging slab at a load of 100 kN (43% of the ultimate load). Then, test side free edge of the barrier wall exhibited diagonal crack at a load of 125 kN (54% of the ultimate load). With increasing load, crack appeared on both the front face and back face of the barrier wall at a load of 150 kN (65% of the ultimate load). Finally, LE-N failed due to punching shear failure of the

barrier wall along with failure of the joint between barrier wall and overhanging slab at a load of 230 kN similar to corresponding intact LE. Ultimate capacity of LE-N was 97% of that of intact LE. Figure 5.4 shows mode of failure of LE-N.

a) Front face b) Back face

Figure (5.4): Punching shear failure of LE-N (repaired portion is painted yellow)

The ultimate capacity of all the tested repaired prototypes satisfied CAN/CSA-S6-06 strength requirement criterion of withstanding a longitudinal load of 100 kN spreading over 1050 mm length for PL-2 bridge barrier. It can be noticed that obtained concrete compressive strength of NSM and spliced repaired prototypes (both middle and edge) varied approximately 30% from each other even though normal strength concrete was used in all prototypes. In terms of ultimate capacity, NSM repaired prototypes (M1-N and LE-N) achieved higher ultimate strength than those of Spliced (planting) repaired prototypes (M1-P and RE-P). However, in terms of mode of failure, all the repaired prototypes exhibited identical failure mode to their corresponding intact prototypes. Furthermore, the observed mode of failure confirms that the applied load on the repaired barrier wall was carried by two-way action similar to the intact prototypes.

5.3. Cracking Pattern

During testing M1-P, longitudinal cracks initiated on the overhang slab first, then, cracks appeared on front face of barrier wall, and finally, at higher loading vertical cracks appeared on back face of barrier wall. This crack propagation was similar to the corresponding intact M1 prototype. In addition, almost all the cracks were confined within new concrete region. Only few crack appeared on old concrete region. Thus, critical length over which all cracks were distributed was 3.2 m, identical with M1. Similar to M1, in M1-P, cracks formed in trapezoidal shape on the front face of barrier wall while, on the back face, cracks were formed in the vertical direction. Figure 5.5 shows the cracking pattern of M1-P.

a) Front face b) Back face

Figure (5.5): Cracking pattern of M1-P

On contrary, in M2-N, first, cracks initiated on NSM grooves of overhang slab at barrier wall-slab junction, second, cracks appeared on the front face of barrier wall, and finally at higher loading vertical cracks appeared on back face of barrier wall. Unlike the corresponding intact M2, no longitudinal crack occurred on the overhang slab; cracks only appeared on the barrier

wall. Furthermore, fewer numbers of cracks was observed on the repaired barrier wall than that of the intact one. This may be due to the increase in stiffness of NSM repaired barrier wall resulted from NSM technique. In M2-N, all the cracks were occurred in new concrete zone, no cracks occurred in old concrete region. Here, critical length over which all cracks were distributed was 3 m. Similar to M2, in M2-N, cracks formed in trapezoidal shape on the front face of barrier wall while, on the back face, cracks were formed in the vertical direction. Figure 5.6 shows the cracking pattern of M2-N.

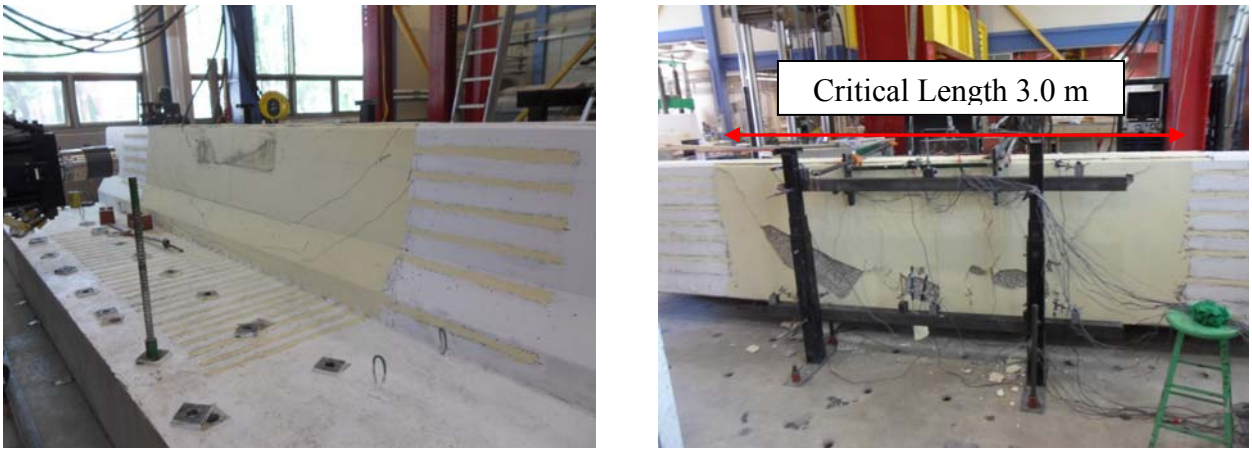

a) Front face b) Back face

Figure (5.6): Cracking pattern of M2-N

In both RE-P and LE-N, overhang deck exhibited longitudinal cracks in the initial stage of loading. Then diagonal crack appeared on the front face of barrier wall. Finally, back face of the barrier wall exhibited crack at the higher amount of loading. This crack propagation pattern of edge repaired prototypes was in good agreement with corresponding intact prototypes. In both case, critical length over which all cracks were distributes was approximately 1.8 m and almost all the cracks occurred in new concrete of the repaired portion. Only few cracks appeared on old

concrete portion. Furthermore, in both RE-P and LE-N, cracks formed in diagonal direction on both front face and vertical direction on back face of the barrier wall, identical to corresponding intact RE and LE. Cracking patterns of RE-P and LE-N are shown in Figure 5.7 to 5.8.

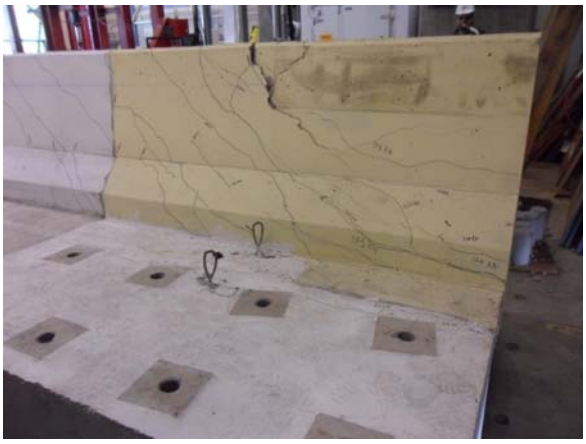

a) Front face

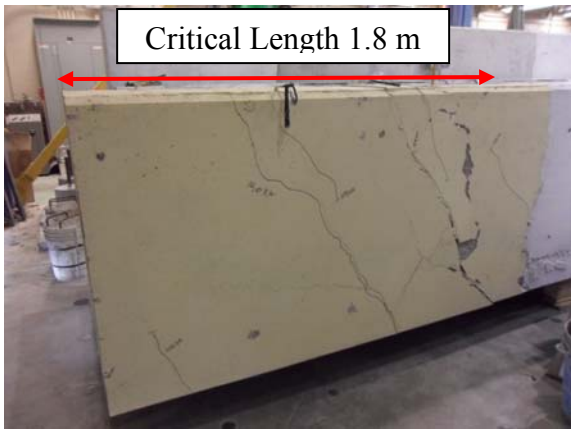

b) Back face

Figure (5.7): Cracking pattern of RE-P

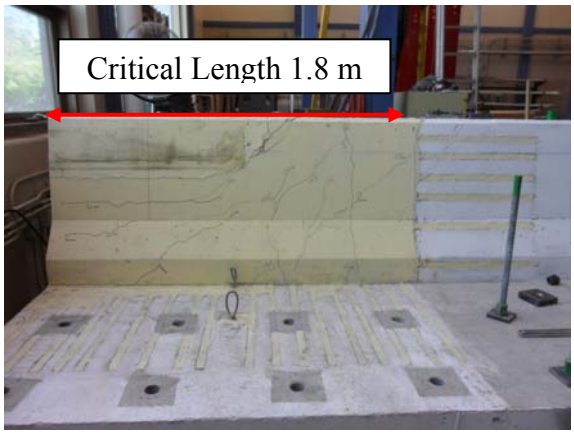

a) Front face

b) Back face

Figure (5.8): Cracking pattern of LE-N

NSM repaired M2-N exhibited fewer number of cracks and lower critical length (3 m) than that of Spliced repaired M1-P (3.2 m). Furthermore, in M2-N, cracks did not appear on overhang deck slab unlike the M1-P. However, spliced repaired edge prototype RE-P and NSM repaired edge prototype LE-N showed identical cracking behavior and critical length.

5.4. Deflections

Barrier wall horizontal and overhang deck slab vertical deflection was measured using LVDTs. Similar to intact prototypes repaired barrier wall horizontal deflection at the slab-barrier wall joint was zero, therefore, only barrier wall top horizontal deflections are considered. These deflection values are presented and compared with the corresponding intact barrier walls in the following sections.

Both spliced and NSM repaired middle portion (M1-P and M2-N) gave maximum overhang deck slab vertical deflection as well as maximum barrier wall horizontal deflection at the centerline of the loading similar to their corresponding intact prototypes. Furthermore, both overhang deck slab and barrier wall exhibited equal amount of deflections at equally spaced right and left side of the centerline of the loading. This indicates that both overhang deck slab and barrier wall deflected symmetrically around the centerline of loading similar to their intact counterparts. On the other hand, both spliced and NSM repaired edge portion (RE-P and LE-N) showed maximum overhang deck slab vertical deflection as well as maximum barrier wall horizontal deflection at the test side free edge. In addition, these deflections decreased in locations away from the test side free edge. These observations were in good agreement with intact prototypes.

5.4.1. Deflection of M1-P

Vertical deflection of the overhang deck slab is shown in Figure (5.9). It can be noticed that, overhang deck slab exhibited almost identical deflection at its three different locations up to failure. However, at failure, maximum vertical deflection was (9.9 mm) occurred at the centerline of loading, similar to corresponding intact M1.

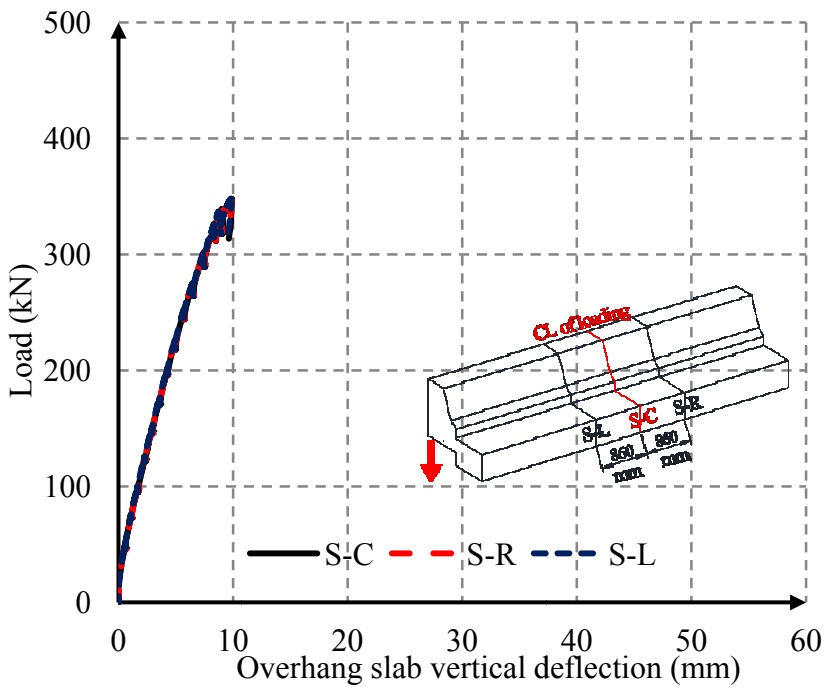

Figure (5.9): Vertical deflection of overhang slab for M1-P test

Figure 5.10 shows barrier wall top horizontal deflection of M1-P.

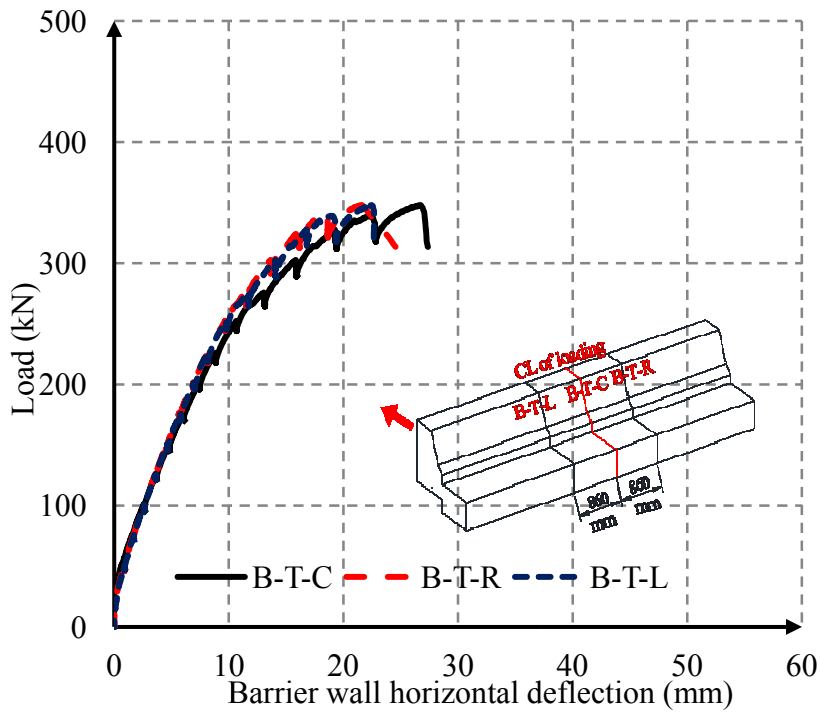

Figure (5.10): Horizontal deflection of barrier wall for M1-P test

It can be noticed that up to a load of 200 kN (57% of the ultimate load), horizontal deflection at different locations of the barrier wall was almost equal. After that, higher deflection value appeared at the centerline of loading up to the failure. At failure, maximum horizontal deflection occurred at the centerline of loading, and the deflection was 26.7 mm. Left and right side deflection was 22.4 mm and 21.6 mm respectively.

For deflection comparison purposes, only maximum overhang slab vertical deflections and barrier wall horizontal deflections before and after repair (M1 & M1-P) are considered. Figure 5.11 shows maximum deflections of both M1-P and M1.

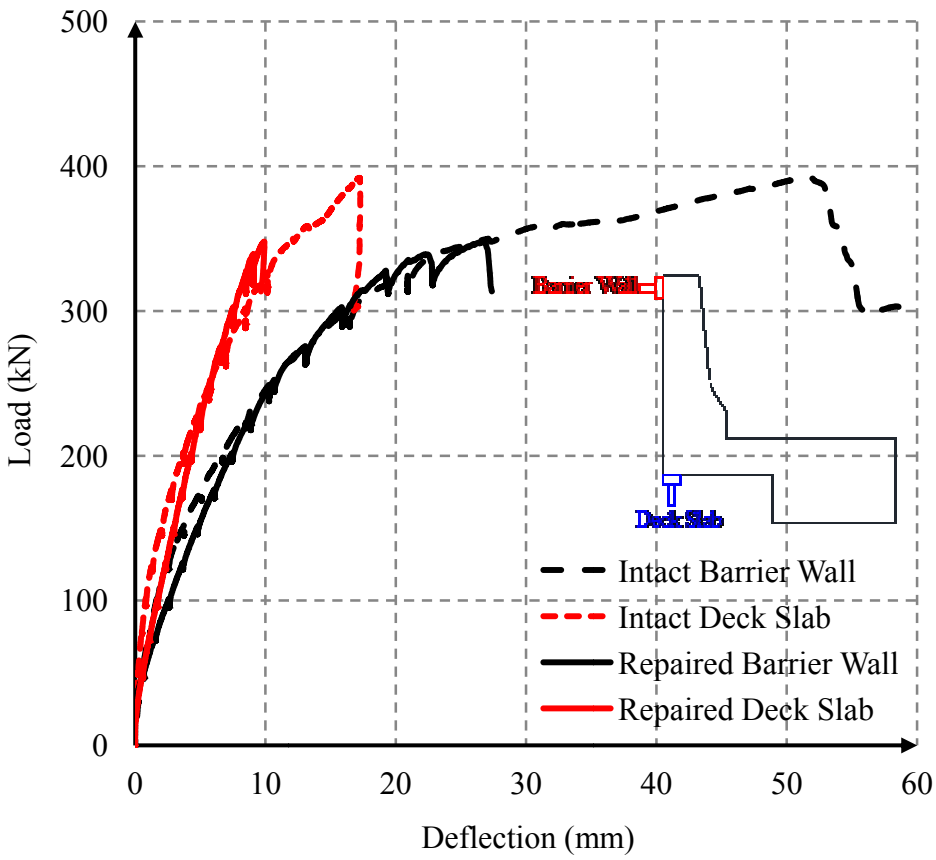

Figure (5.11): Comparisons of deflections of M1-P with M1

It can be noticed that both vertical deflection of overhang deck slab and horizontal deflection of barrier wall of repaired M1-P followed the identical load-deflection path of that of corresponding intact M1 until failure. However, at failure, M1-P exhibited lower vertical and horizontal deflection than that of M1. This is due to the fact that M1-P failed at lower load than M1, which in turn caused lower vertical and horizontal deflection in the repaired prototype.

5.4.2. Deflection of M2-N

Figure 5.12 shows load vs. overhang slab vertical deflection of M2-N. Almost equal amount of vertical deflection of overhang deck slab was found at different locations up to the load of 350

kN (77% of the ultimate load). After that, as expected, centerline of loading gave higher vertical deflection of overhang deck slab.

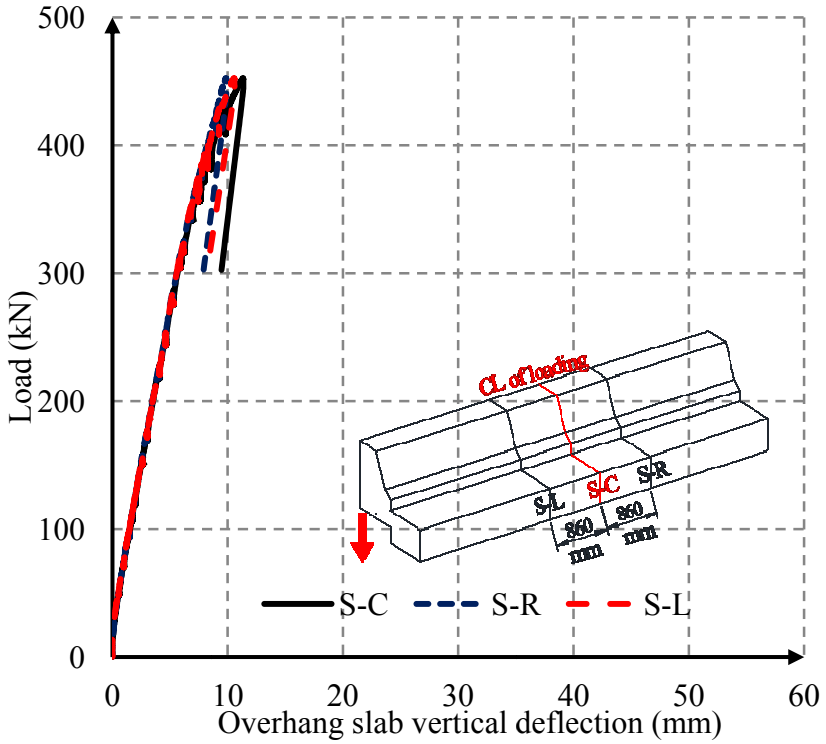

Figure (5.12): Vertical deflection of overhang slab of for M2-N test

At failure, maximum vertical deflection occurred at the centerline of loading was 11.3 mm while, left and right side deflection was 10.5 mm and 9.8 mm, respectively.

Barrier wall top horizontal deflection for M2-N is shown in Figure (5.13). As expected, centerline of loading gave higher horizontal deflection than other two locations. Ay failure, maximum horizontal deflection occurred at the centerline of loading was 31 mm while, left and right side deflection was 22 and 26 mm, respectively.

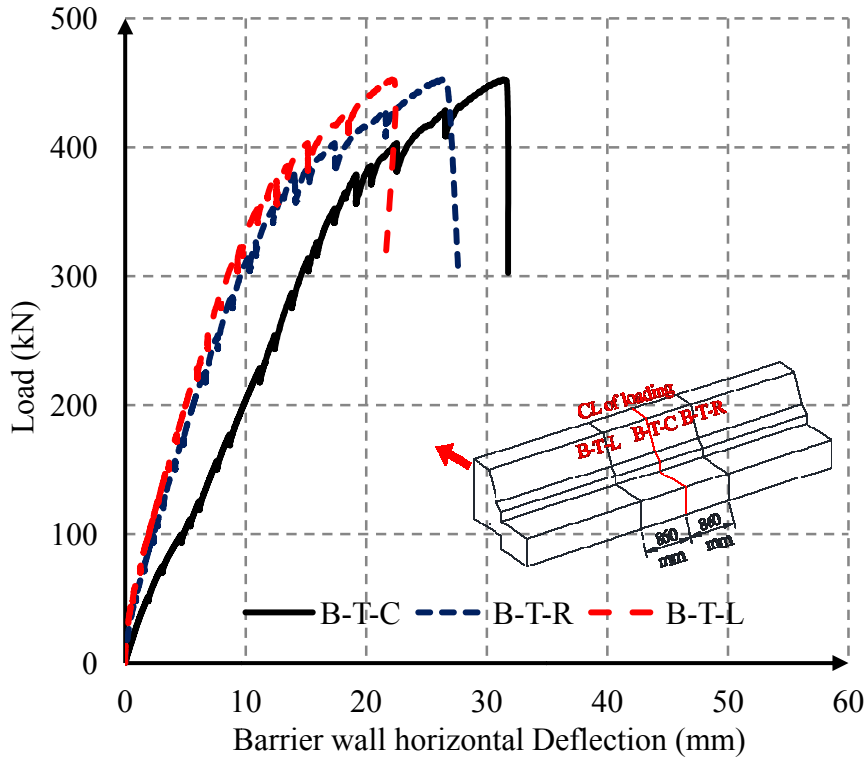

Figure (5.13): Horizontal deflection of barrier wall for M2-N test

Figure 5.14 shows maximum horizontal and vertical deflection of both M2-N and M2 in order to make comparison between them.

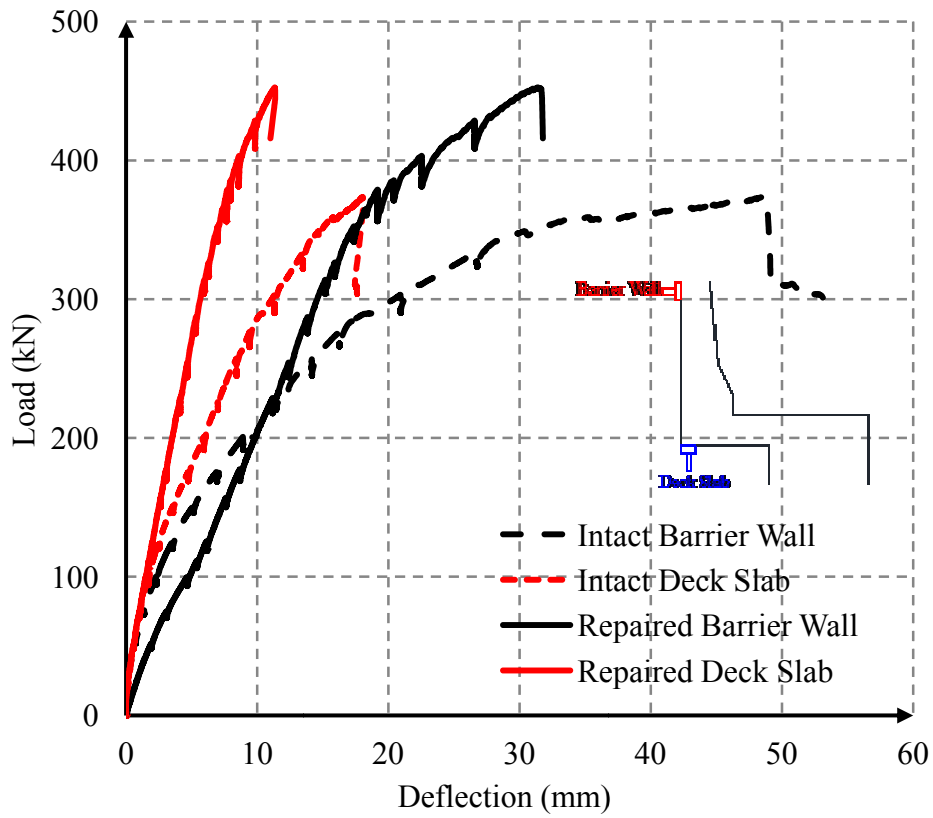

Figure (5.14): Comparisons of deflections of M2-N with M2

It can be noticed that load-deflection path of both overhang deck slab and barrier wall for M2-N was steeper (approximately 2 times) than that of corresponding intact M2. This indicates that stiffness of M2-N was higher than that of M2 due to the NSM technique. Though M2-N failed at higher load than that of M2, horizontal and vertical deflection of M2-N was lower than that of M2. This can be attributed to the increase of stiffness as well as moment capacity resulted from NSM technique.

5.4.3. Deflection of RE-P

During testing of RE-P, repaired using splicing (planting) technique, both overhang slab vertical deflection and barrier wall horizontal deflection was measured using LVDTs.

Vertical deflection of the overhang deck slab of RE-P is shown in Figure (5.15).

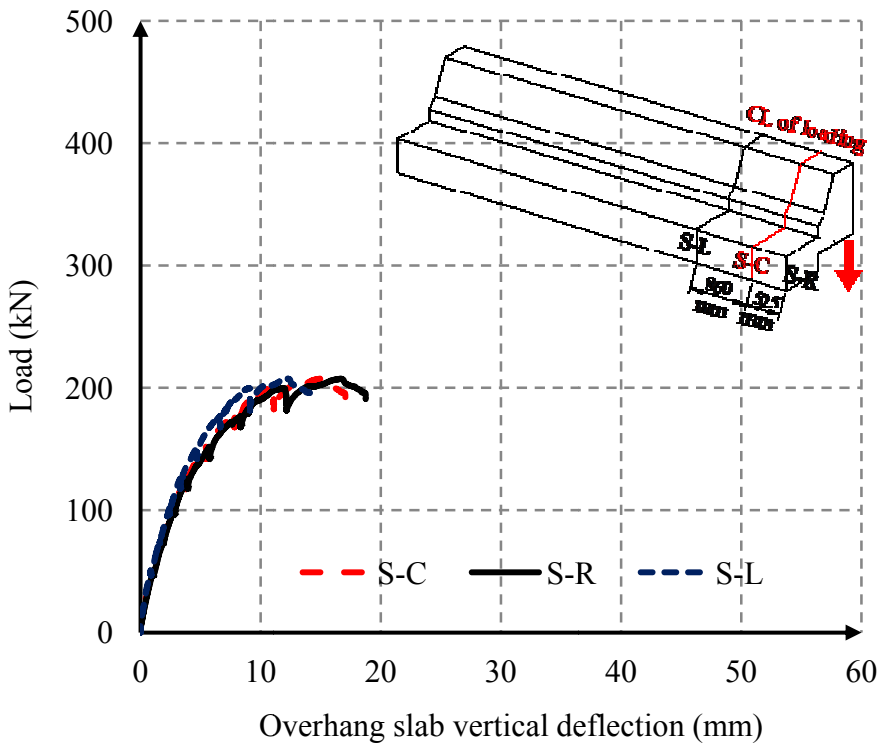

Figure (5.15): Overhang slab vertical deflection for RE-P test

It can be noticed that up to a load of 100 kN (48% of the ultimate load), vertical deflection of overhang deck slab at different locations was close to each other. After that, as expected, test side free edge (right side) gave maximum vertical deflection. At failure, maximum vertical deflection observed at the test side free edge of the overhang slab was 16.6 mm while, at the center line of loading this vertical deflection was 14.9 mm and at the left side to the center line of loading was 12.3 mm; decreased away from the test side free edge.

Horizontal deflection of barrier wall of RE-P is shown in Figure (5.16). It can be noticed that, barrier wall exhibited identical load-deflection curve at the test side free edge and at the centerline of loading up to failure. This is due to the fact that both these locations were within

1050 mm long load-application zone. At failure, as expected, maximum horizontal deflection of 33.2 mm occurred at the test side free edge. On the other hand, horizontal deflection at the centerline of loading and left side of it was 32.4 mm and 29.2 mm, respectively.

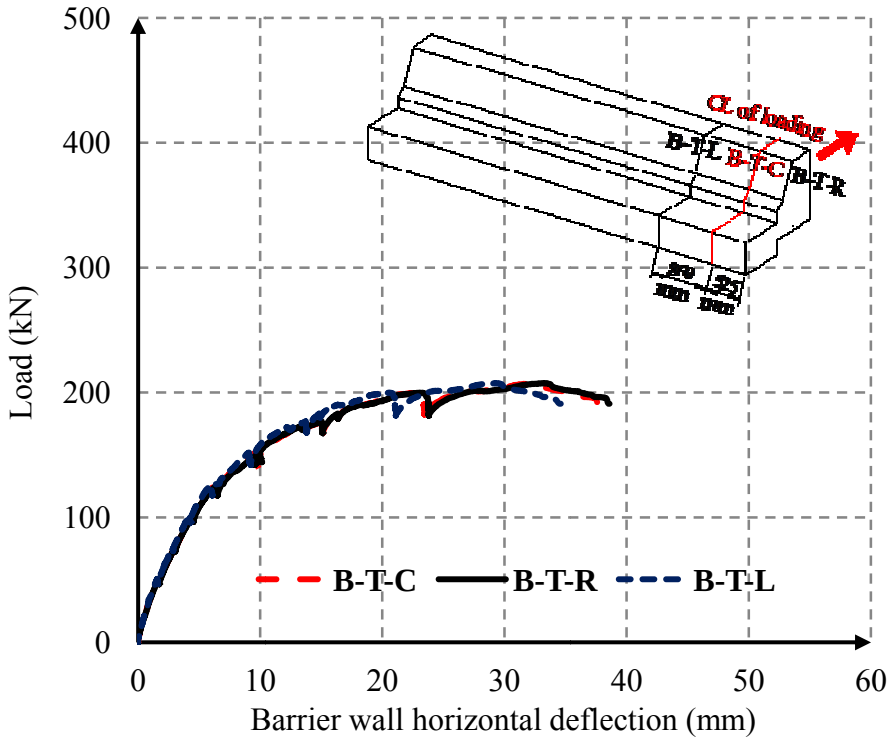

Figure (5.16): Horizontal deflection of barrier wall for RE-P

In order to compare maximum vertical and horizontal deflection of RE-P with corresponding intact RE, deflection values of both repaired RE-P and intact RE is plotted in Figure (5.17). Both overhang slab vertical deflection and barrier wall horizontal deflection of RE-P exhibited identical load-deflection path to that of intact RE up to the load of 200 kN. However, at failure RE-P showed lower vertical and higher horizontal deflection than that of RE.

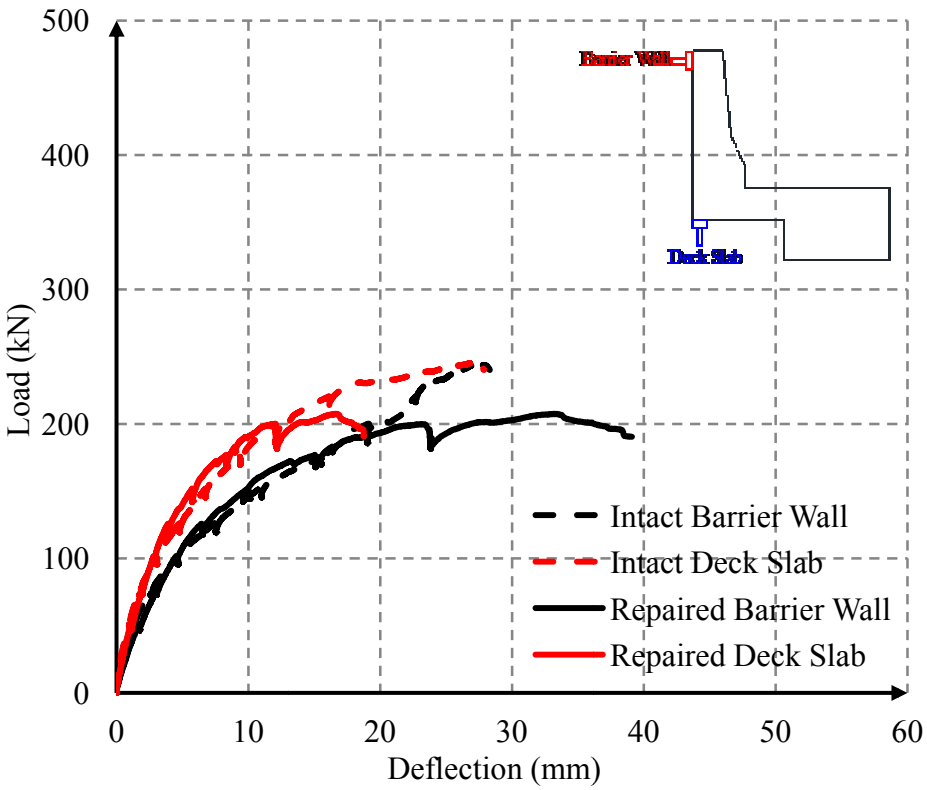

Figure (5.17): Comparisons of deflections of RE-P with RE

5.4.4. Deflection of LE-N

Figure 5.18 shows vertical deflection of the overhang slab for LE-N test. During testing, overhang deck slab exhibited identical load-deflection path up to a load of 100 kN (43% of the ultimate load). At failure, maximum vertical deflection at the free edge of the overhang slab was 9.1 mm. On the other hand, this deflection at the center line of loading was 8.1 mm and at left side to the center line of loading was 7.2 mm.

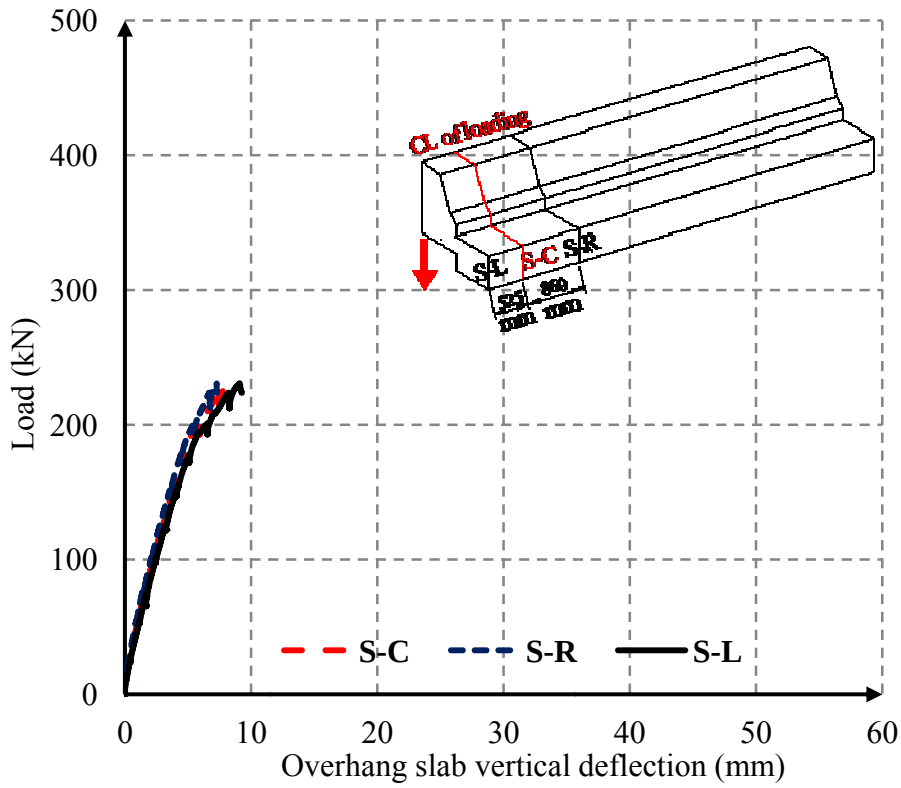

Figure (5.18): Overhang slab deflection for LE-N test

Figure 5.19 shows barrier wall top horizontal deflection for LE-N test. It can be noticed that up to a load of 100 kN (43% of the ultimate load), barrier wall exhibited almost equal horizontal deflection at all three different locations. At failure, maximum horizontal deflection at the free edge was 18.1 mm. This deflection at the centerline of loading and left side of it was 17.8 mm and 14.7 mm, respectively.

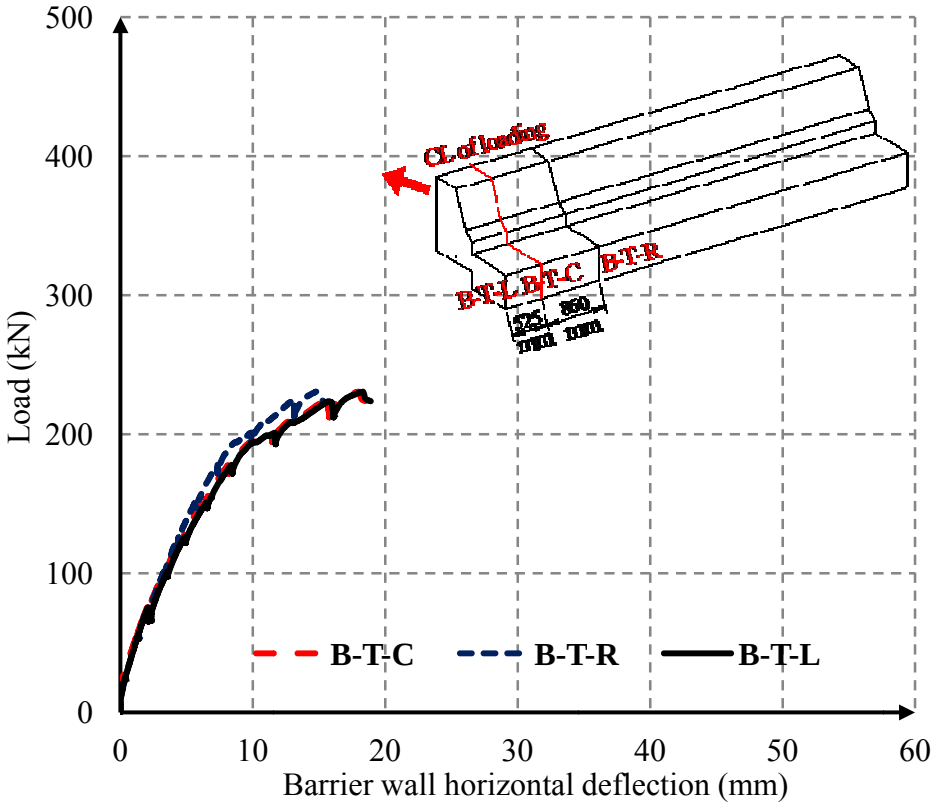

Figure (5.19): Horizontal deflection of barrier wall for LE-N test

Maximum vertical and horizontal deflection of LE-N is plotted with the corresponding intact LE, to make comparisons between them. Figure 5.20 shows deflection curves of both LE-N and LE. It can be noticed that repaired LE-N exhibited lower barrier wall horizontal deflection and overhang slab vertical deflection than that of corresponding intact LE because NSM technique increased the stiffness as well as moment capacity of both overhang deck slab and barrier wall of repaired LE-N.

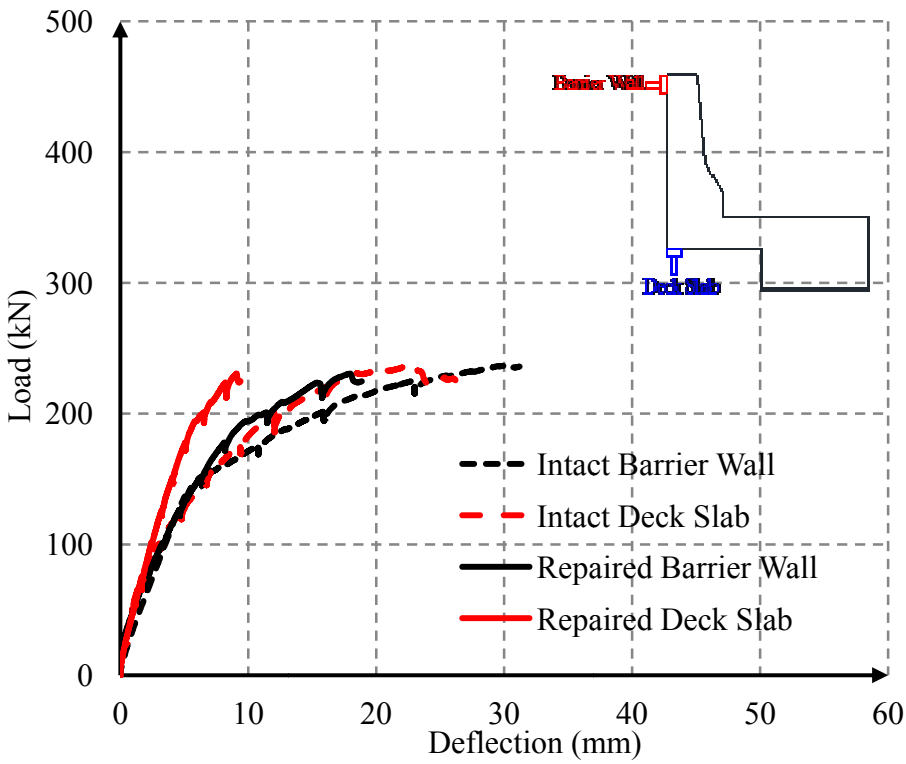

Figure (5.20): Comparisons of deflections of LE-N with LE

5.4.5. Summary of Deflections

Table (5.3) summarizes the maximum deflection values observed during the testing of the prototypes.

Table (5.3): Maximum deflections of repaired and intact prototypes

Test Designation		Repairing Technique	Test Location	Overhang Slab Vertical Deflection (mm)		Barrier Wall Horizontal Deflection (mm)	
Intact	Repaired			Intact	Repaired	Intact	Repaired
M1	M1-P	Planting	Middle	17.2	9.9	51.4	26.7
M2	M2-N	NSM	Middle	18	11.3	48.7	31
RE	RE-P	Planting	Right edge	26.7	16.6	27.4	33.2
LE	LE-N	NSM	Left edge	24.7	9.1	29.7	18.1

- In M1-P, 42% decrease in vertical deflection and 48% decrease in horizontal deflection was observed when compared to M1 because failure load of M1-P was 13% lower than that of M1.
- In M2-N, 37% decrease in vertical deflection and 36% decrease in horizontal deflection was observed when compared to M2 even though failure load of M2-N was 20% higher than that of M2. This can be attributed to the increase in stiffness as well as moment capacity in M2-N resulted from NSM technique.
- In RE-P, 38% decrease in vertical deflection and 21% increase in horizontal deflection was observed when compared to RE. However, failure load of RE-P was 15% lower than that of RE.
- In LE-N, 63% decrease in vertical deflection and 39% decrease in horizontal deflection was observed when compared to LE even though failure load of both of them was almost same. This can be attributed to the increase in stiffness as well as moment capacity of LE-N resulted from NSM technique.

Therefore, NSM repaired middle and edge portions exhibited lower overhang slab vertical deflection as well as barrier wall horizontal deflection than their corresponding intact portions, even though the ultimate capacity of repaired portion was similar (edge) or higher (middle) than that of intact ones. On the other hand, spliced (Planting) repaired middle and edge portion, due to the lower achieved ultimate capacity, gave lower vertical deflection as well horizontal deflection (except horizontal deflection of RE-P) than that of intact portions.

5.5. Strains in Reinforcements

Strains in horizontal and vertical bars of repaired barrier wall and in transverse bar of overhang deck slab were measured using 6 mm electrical strain gauges. These strain values are presented and compared with the corresponding intact barrier walls.

In general, reinforcements of all the repaired prototypes exhibited linear load-strain relationship up to failure similar to their intact counterparts, which was expected due to the linear stress-strain relationship of GFRP bars. In both spliced and NSM repaired prototype overhang deck slab bar at the centerline of loading gave maximum strain similar to their corresponding intact prototypes. Since repaired barrier wall carried moment horizontally, back face horizontal bar of the barrier wall exhibited maximum tension. This maximum tension occurred at the location close to the end of load-application zone as stress concentration was expected to occur at that location similar to their intact counterparts. Among vertical bars, due to the location near to the barrier wall-deck slab joint, V2 bars gave maximum strains and thus, only V2 bars strains are presented here. Remaining vertical bars strain graph can be found in appendix G. Furthermore, similar to the intact prototypes V2 bar close to the end of the load-application zone showed maximum strains.

On the other hand, both spliced and NSM repaired edge portion exhibited maximum strain in transverse bar of overhang deck slab at the test side free edge similar to the corresponding intact prototypes. Back face horizontal bar gave maximum strain at location opposite to the test side free edge. Here also, for the same reason explained earlier, only V2 bar strains are presented. Remaining vertical bar strain graphs can be found in Appendix G. In addition, V2 bar exhibited maximum strain in location opposite to the test side free edge similar to the corresponding intact prototypes.

5.5.1. Strains in Reinforcements of M1-P

Strain gauges were installed on two top transverse bars of M1-P, similar to M1, at its barrier wall-slab junction. One bar was located at the centerline of loading and another one was located 400 mm right to the centerline of loading. Figure 5.21 shows strains in transverse bars of M1-P.

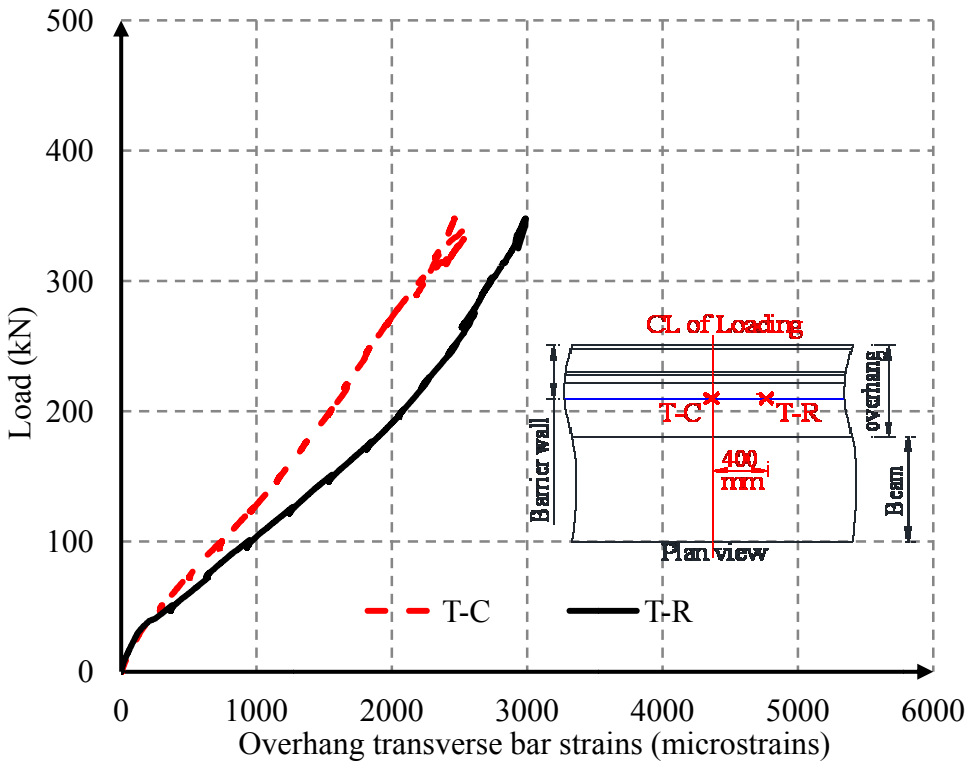

Figure (5.21): Overhang transverse bars strain for M1-P test

It can be noticed in the graph that both the transverse bars gave equal strains up to a load of 50 kN (14% of the ultimate load). After that longitudinal crack appeared on overhang deck slab; T-R bar close to end of 1050 mm long load-application zone gave higher strains value than that of T-C up to failure. Finally at failure, maximum strain observed in T-R bar was 2989 micro-strains (19% of the ultimate strain of 19 mm GFRP bar).

Strain gauges were installed on second horizontal bars (both front side and back side bar) from the top of the barrier wall as maximum horizontal moment would have occurred at that location. Figure 5.22 shows horizontal bars strains of M1-P.

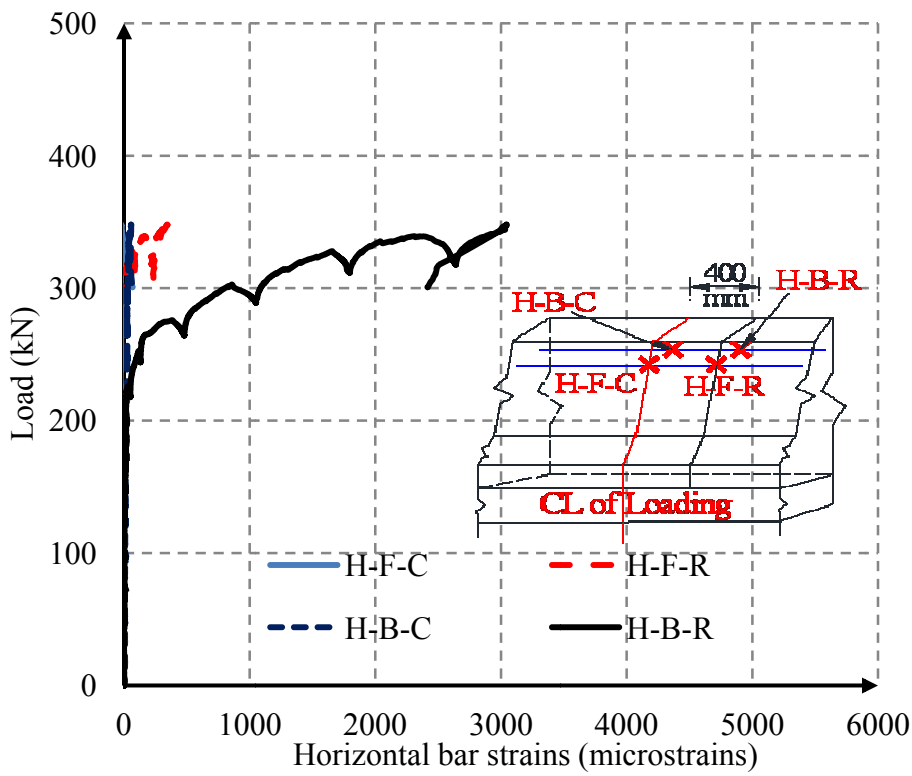

Figure (5.22): Barrier wall horizontal bar strains for M1-P test

It can be noticed from the graph that back face bar at H-B-R location exhibited considerable amount of strain after the load of 275 kN (79% of the ultimate load) because barrier wall exhibited crack on its both front and back face at that load. Furthermore, negligible amount of tensile strain appeared in front face bar at its two locations, and in back face bar at the centerline of loading. Finally at failure, maximum tensile strain was occurred at H-B-R location similar to

intact M1 and this strain was 3042 micro-strains (20% of the ultimate strain of 16 mm GFRP bar).

In M1-P, strain gauges were installed on three different shape (V1, V2 and V3) vertical bars of the barrier wall. Figure 5.23 shows V2 bar strains at different locations.

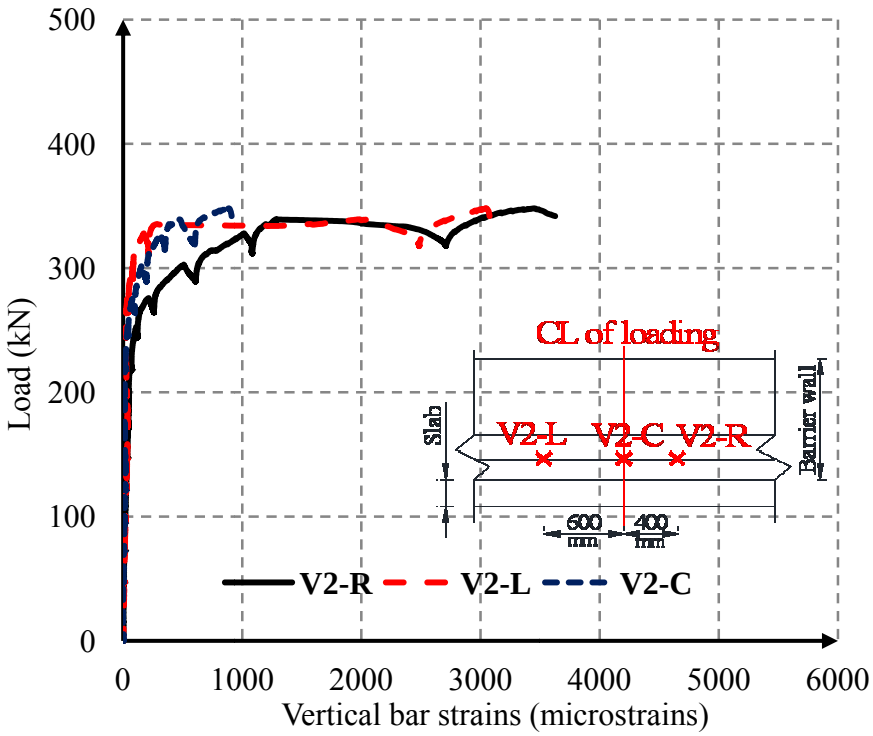

Figure (5.23): V2 bar strains along the length of the barrier wall for M1-P test

It can be noticed that considerable amount of strains appeared in V2 bar after the load of 275 kN (79% of the ultimate load) at which first crack appeared on the barrier wall. Among V2 bars, V2-R bar gave higher tensile strains similar to M1. Finally at failure, maximum ensile strains in V2-R was 3452 micro-strains (32% of ultimate strain) while, in V2-L and in V2-C this value was 3046 and 888 micro-strains (ranging between 9 and 29% of ultimate strain), respectively.

In order to compare strains of M1-P with corresponding intact M1, only maximum transverse, horizontal and vertical bar strains of M1-P and M1 are shown in Figure (5.24).

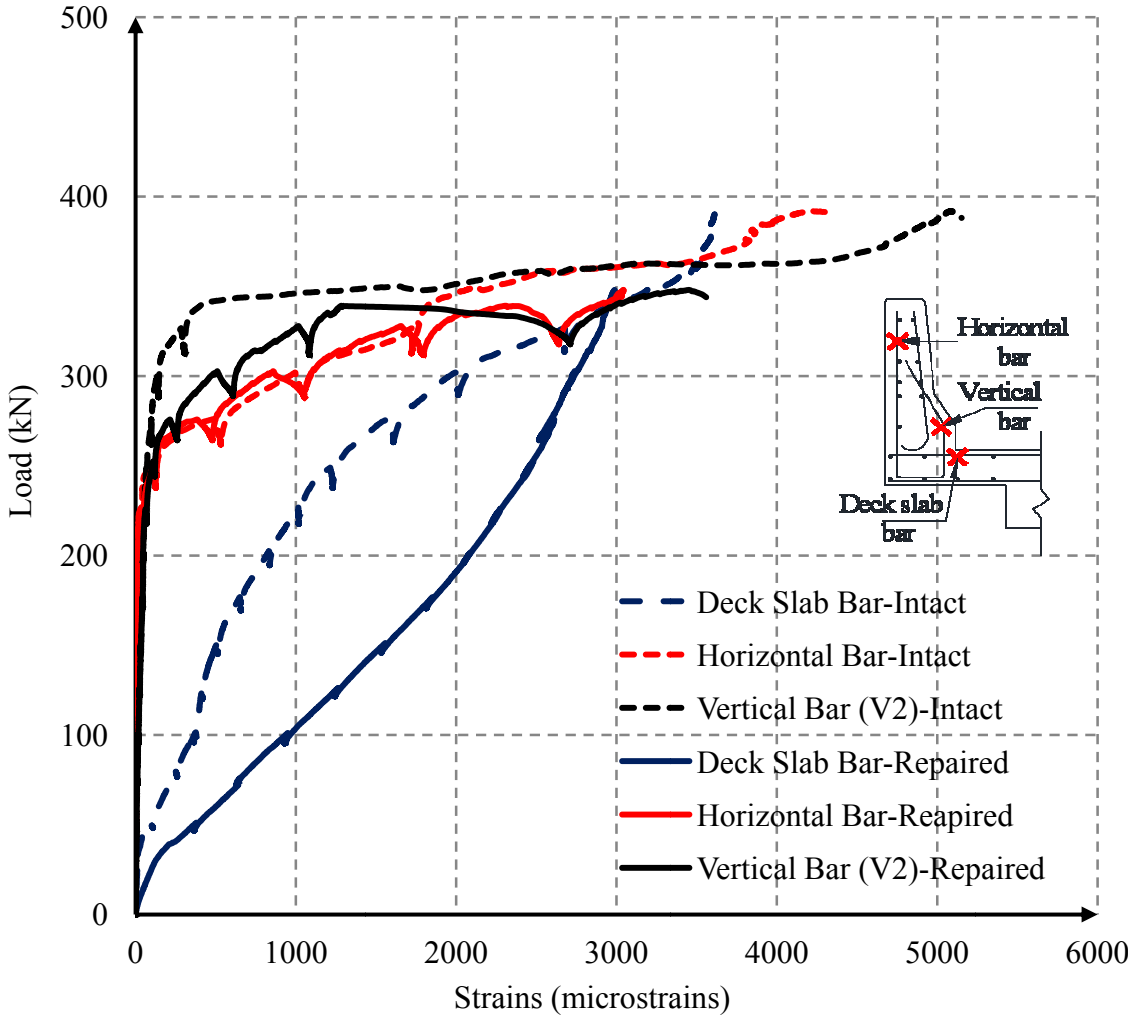

Figure (5.24): Comparison of strains of M1-P with M1

In M1-P, deck slab bar exhibited much higher strain than that of intact M1 after the load of 50 kN (14% of the ultimate load) up to failure. On the other hand, horizontal and vertical bar of barrier wall of M1-P gave considerable amount of strain after the load of 275 kN (79% of the ultimate load), similar to the intact M1. Similar to deck slab bar, barrier wall vertical bar of M1-P

gave higher strains than that of intact M1 up to failure. However, horizontal bar of M1-P exhibited less strain than that of M1 up to failure. Finally, because M1-P failed at lower load (approximately 13%) than that of M1, at failure, strains in three types of bars of M1-P were less than those of M1.

In general, load-strain curve of the bars of M1-P and M1 were similar in shape and followed similar trend of propagation. Furthermore, strains in bars of M1-P, similar to M1, confirms that load within barrier wall was carried in two-way action.

5.5.2. Strains in Reinforcements of M2-N

Similar to M2, in M2-N, two strain gauges were installed on two top transverse of overhang deck slab. Figure 5.25 shows strains in transverse bars of M2-N.

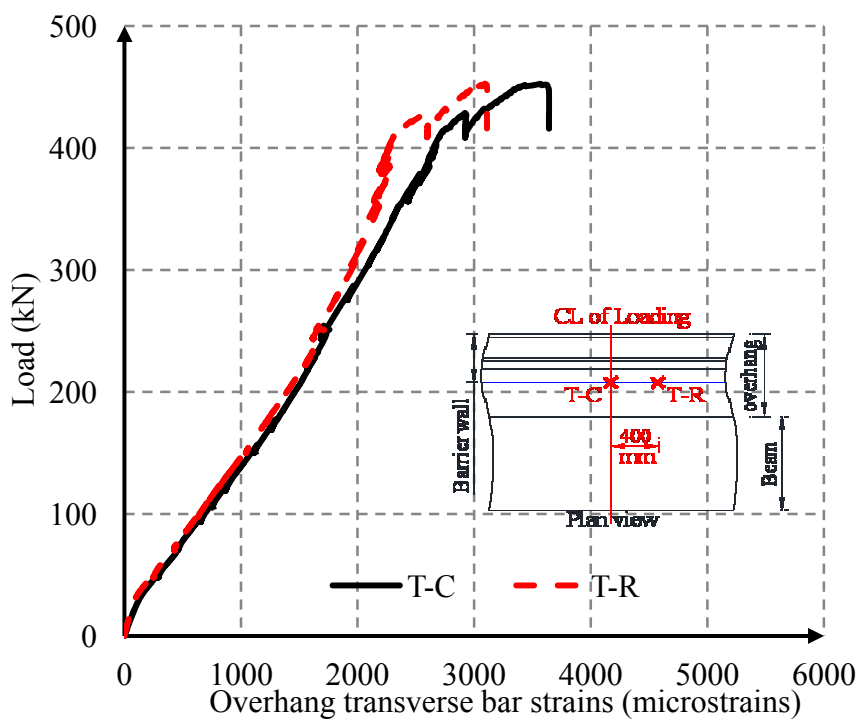

Figure (5.25): Overhang transverse bar strains for M2-N

In M2-N, both the transverse bars followed identical linear load-strain path up to a load of 250 kN (55% of the ultimate load). After that, crack appeared at NSM groove-barrier wall junction and T-C bar at the centerline of loading, exhibited higher strain similar to M2 up to failure. Maximum strain, at failure, in T-C bar was 3565 micro-strains (23% of ultimate strain).

Figure (5.26) shows strains in horizontal bars of M2-N.

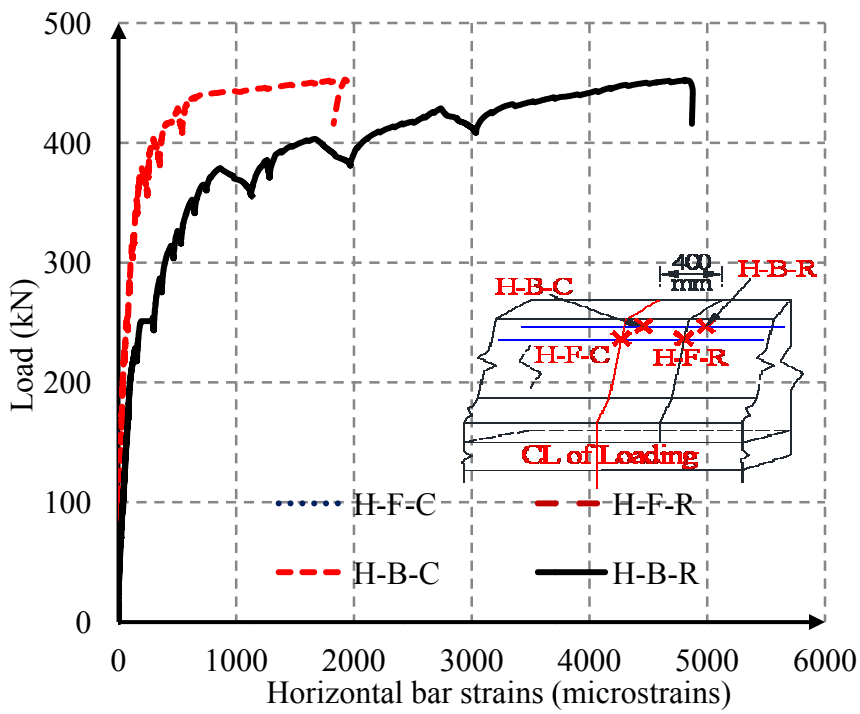

Figure (5.26): Barrier wall horizontal bar strains of M2-N

It can be noticed from the graph that only back face horizontal bars exhibited tensile strain as barrier wall carried horizontal moment, which caused tension at the back face of the barrier wall. Furthermore, horizontal bar gave considerable amount of strains after barrier wall exhibited its first crack at a load of 300 kN (66% of the ultimate load). Finally, similar to M2, at a location

close to the end of 1050 mm load-application zone (H-B-R) maximum strain was measured. At failure, maximum tensile strain in H-B-R bar was 4812 micro-strain (30% of ultimate strain).

Figure (5.27) shows V2 bar strains at different locations. Here also, V2 bar gave significant amount of strain after the barrier wall first crack load of 300 kN (66% of the ultimate load). Both V2-C and V2-R bar showed close load-strain relationship because both of them were within 1050 mm load-application zone. Finally, at failure, V2-C bars exhibited maximum strain of 6202 micro-strains (57% of ultimate strain) while, V2-R and V2-L gave 6084 and 4499 micro-strains (ranging between 41 and 66% of ultimate strain), respectively.

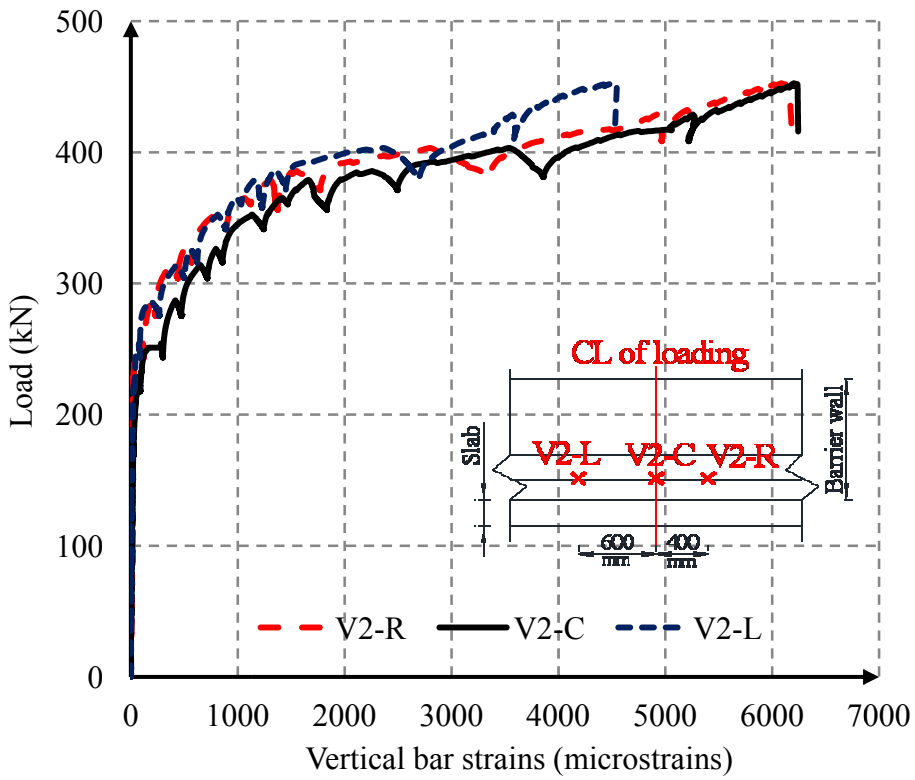

Figure (5.27): V2 bar strains along the length of barrier wall for M2-N test

Maximum strains of transverse, horizontal and vertical bars of M2-N and corresponding intact M2 is shown in Figure (5.28). From this graph, it can be noticed that at failure load (373 kN) of intact M2, repaired M2-N exhibited lower transverse, vertical and horizontal bar strains than those of intact M2. This is due to the increase in stiffness and moment capacity of M2-N resulted from NSM technique. Finally, M2-N failed at higher load (approximately 20%) than that of M2, which resulted higher strains in all three types of bars bar than that of M2.

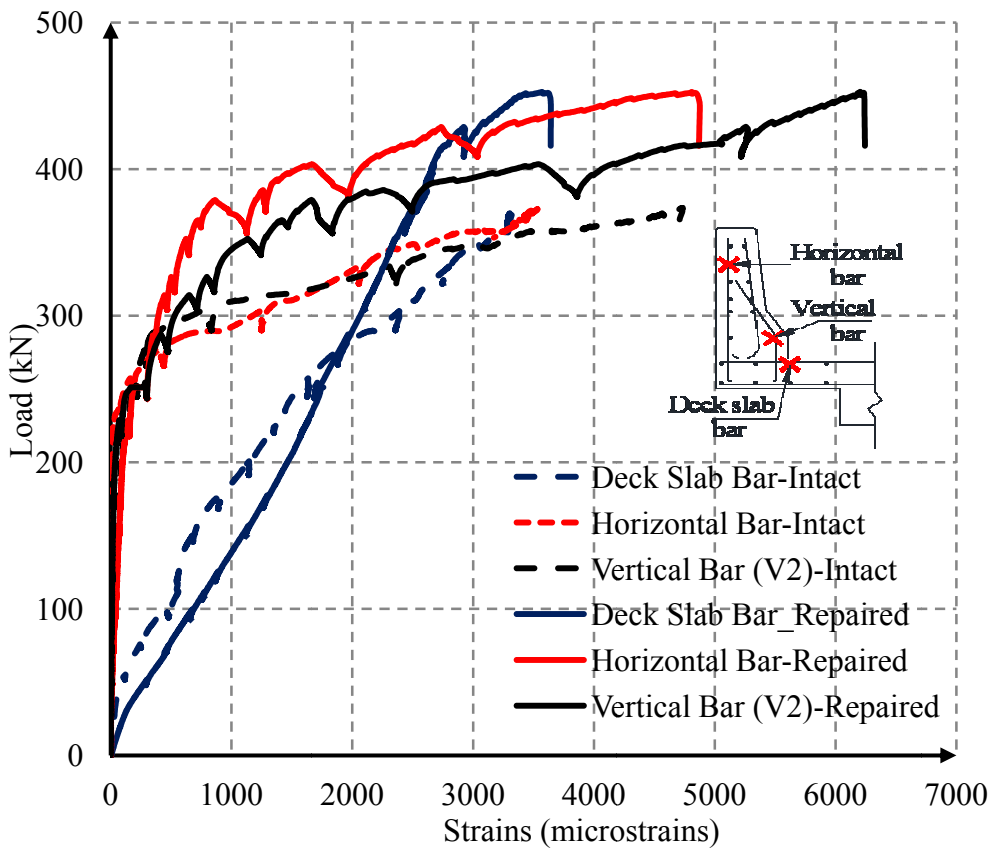

Figure (5.28): Comparison of strains of M2-N with M2

In general, both M2-N and M2 exhibited similar load-strain curve in terms of shape. In addition, strain values of M2-N confirm that load on repaired barrier wall is carried by two-way actions similar to the intact M2.

5.5.3. Strains in Reinforcements of RE-P

Figure 5.29 shows strains in transverse bars of overhang deck slab for RE-P test. Both T-C and T-R bar gave almost equal amount of strain up to the load of 75 kN (36% of the ultimate load). After that first longitudinal crack appeared on overhang deck slab and T-R bar close to the test side free edge gave higher amount of strain than T-C up to the failure.

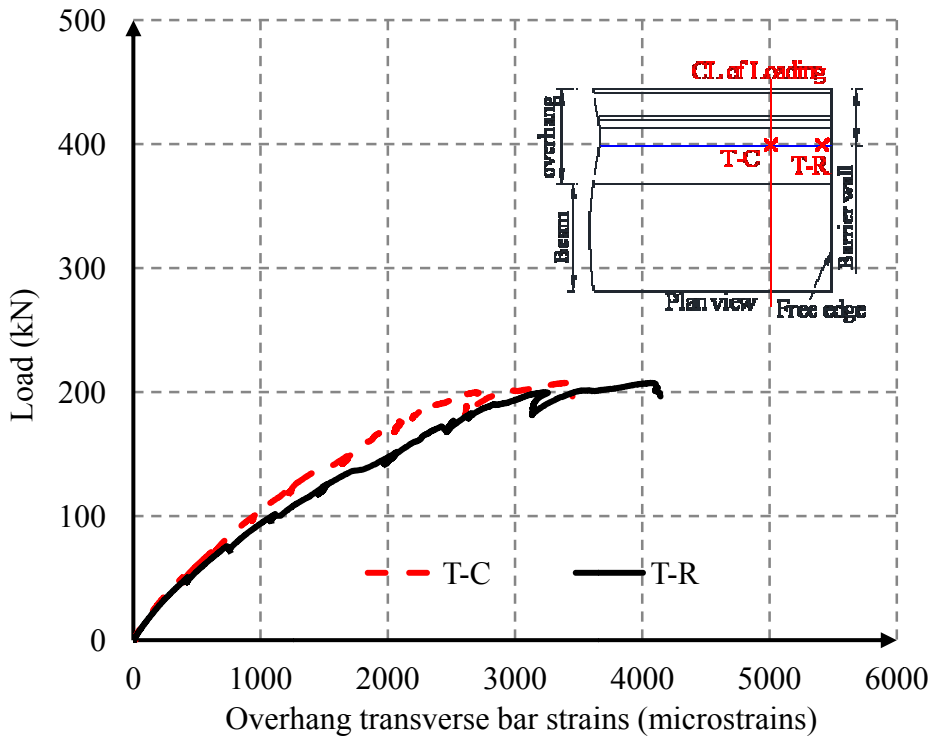

Figure (5.29): Overhang transverse bar strain for RE-P test

Finally, at failure, maximum strain observed in T-R bar was 4065 micro-strains (26% of ultimate strain).

Figure 5.30 shows load vs. barrier wall horizontal bar strains for RE-P test. As expected, back face horizontal bars of the barrier wall experienced higher tensile strain than those of front face horizontal bars. It can be noticed from the graph that back face bar started to have the considerable amount of strain after the load of 150 kN (72% of the ultimate load) because at that load the barrier wall exhibited its first crack on both front and back face. At failure, maximum tensile strain of 3114 (20% of ultimate strain) micro-strain was observed in H-B-L bar, which was close to the end of 1050 mm long load-application zone.

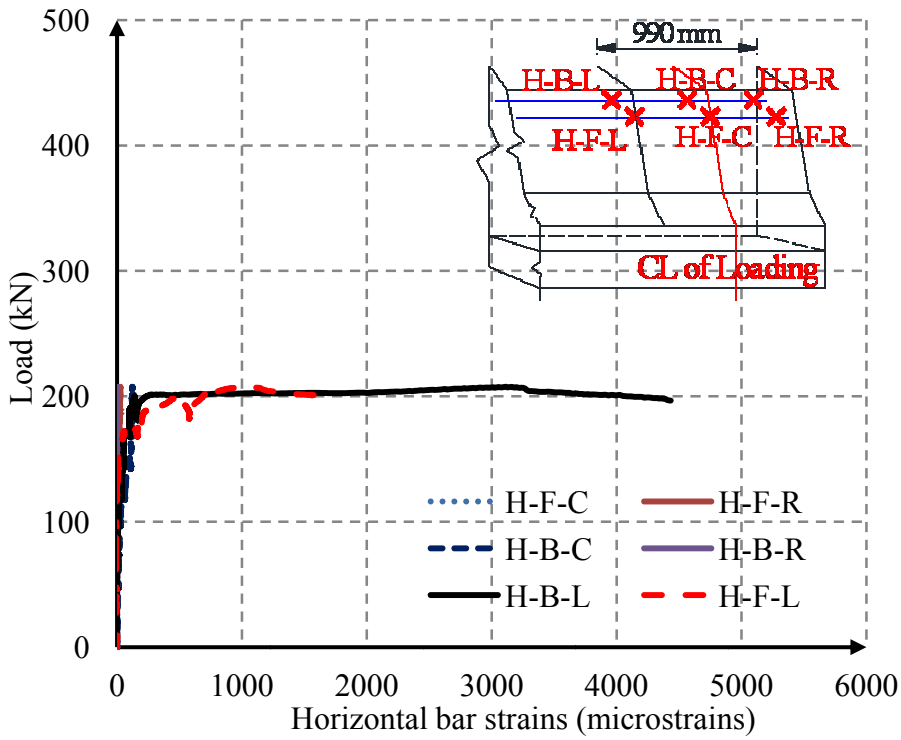

Figure (5.30): Barrier wall horizontal bar strains for RE-P test

Figure 5.31 shows strain values of V2 bars of RE-P. It can be noticed that all the V2 bars exhibited considerable amount of strain after the barrier wall had its first crack at a load of 150 kN (72% of the ultimate load). After that all the vertical bars showed close load-strain

relationship because all of them were within 1050 mm load-application zone. At failure, V2-L bars exhibited maximum strain of 4380 micro-strains (40% of the ultimate strain of 16 mm GFRP bent bars) similar to corresponding RE while, V2-C and V2-R gave 3948 and 3491 micro-strains (ranging between 32 and 36% of ultimate strain), respectively.

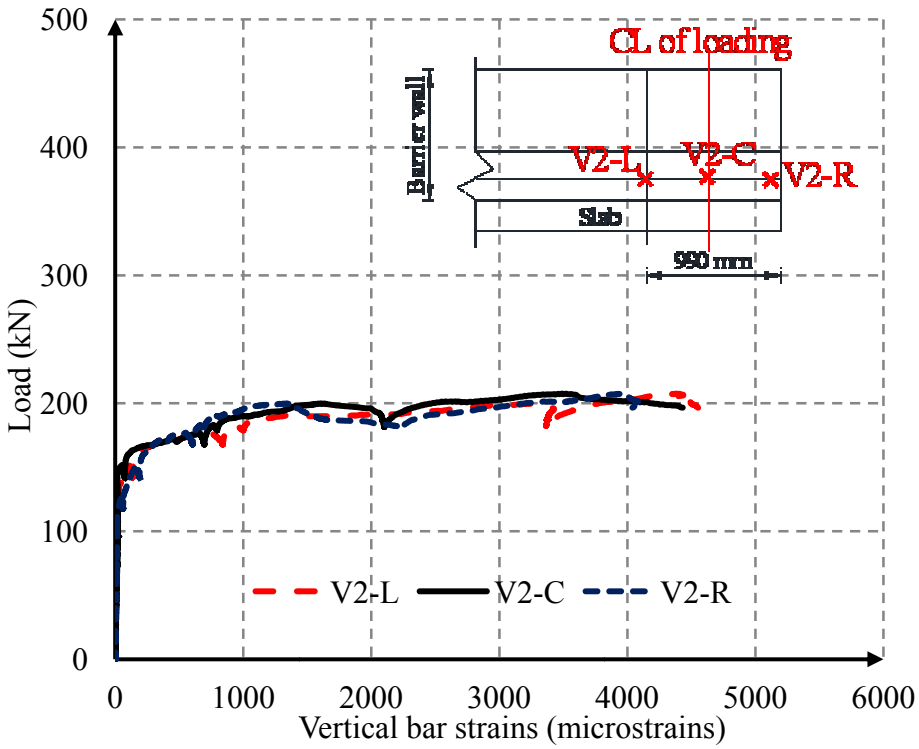

Figure (5.31): V2 bar strains of the barrier wall for RE-P test

Maximum strains of transverse, horizontal and vertical bars of both RE-P and corresponding intact RE is shown in Figure (5.32). It can be noticed that up to the failure load of RE-P (208 kN) both transverse and vertical bar of repaired barrier wall gave higher strain than that of intact RE. However, horizontal bar in the barrier wall of RE-P exhibited lower strain than that of the intact RE. Finally at failure, strains in all the bars of RE-P were lower than those of RE.

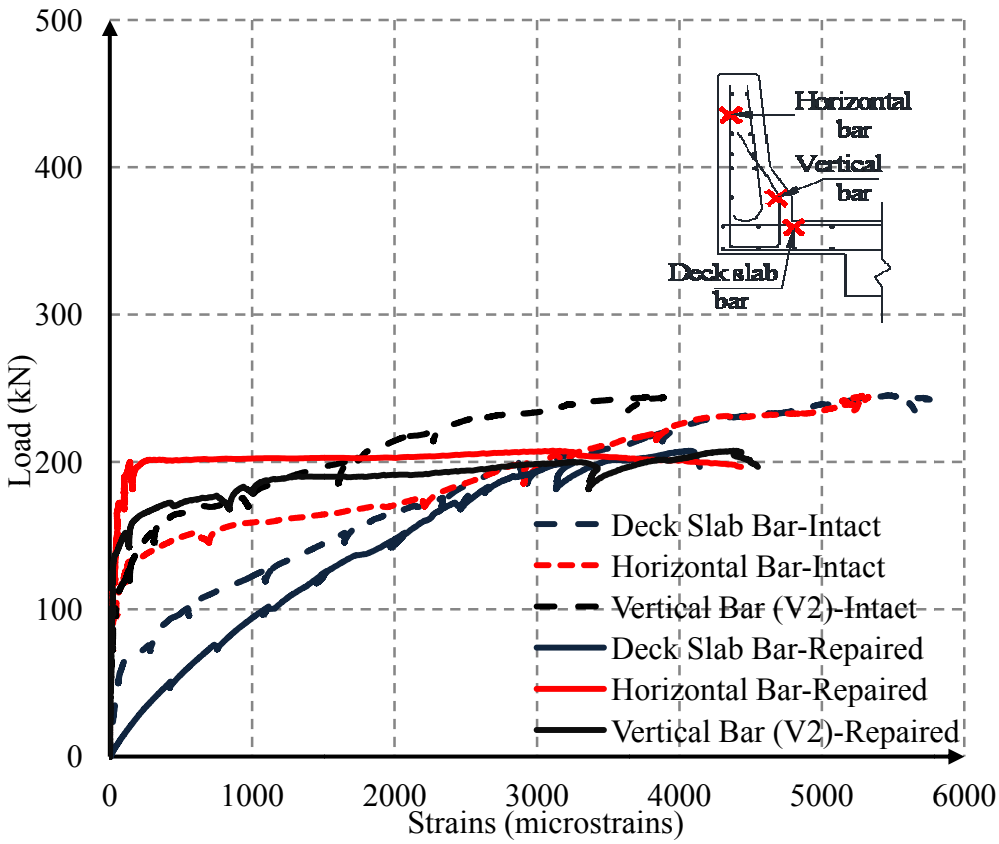

Figure (5.32): Comparison of strains of repaired RE-P with intact RE

In general, load-strain pattern in both intact (RE) and repaired barrier wall (RE-P) was similar, and load was carried by two-way action both in intact and repaired barrier wall.

5.5.4. Strains in Reinforcements of LE-N

Figure 5.33 shows strains in transverse bars of overhang deck slab for LE-N. It can be noticed that up to a load of 70 kN (30% of the ultimate load), both the bars gave almost equal strains. After that at a load of 100 kN (43% of the ultimate load), overhang deck slab exhibited first crack, and as expected, T-R bar close to the test side free edge gave maximum strain up to the failure. Similar to LE, in LE-N both the bars followed linear load-strain relationship. Finally at failure, maximum strain observed in T-L bar was 2754 micro-strains (18% of ultimate strain).

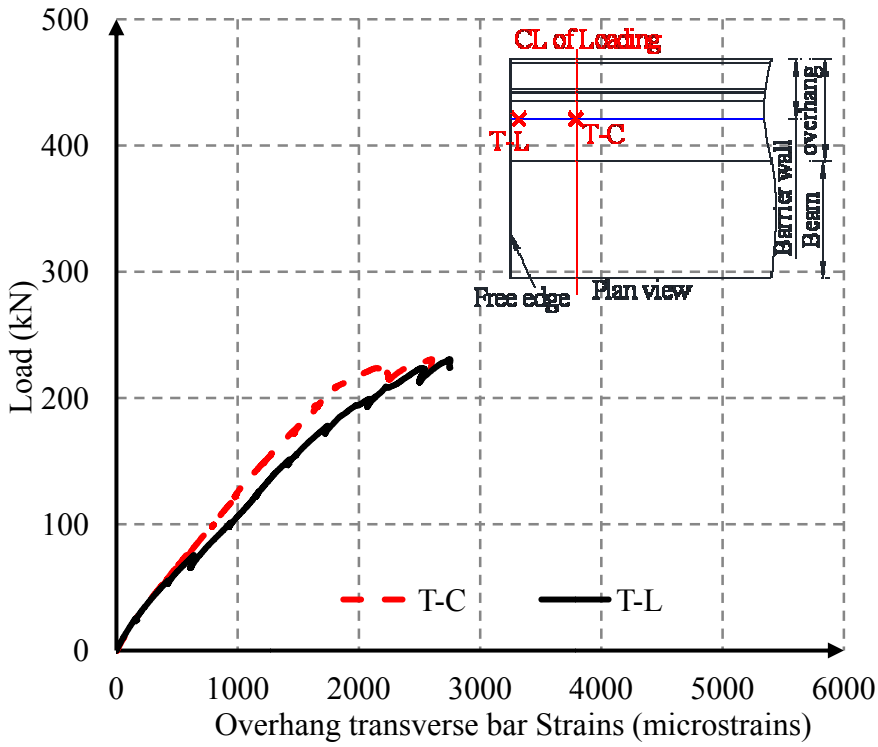

Figure (5.33): Overhang transverse bar strains for LE-N test

Barrier wall horizontal bars strain for LE-N test is shown in Figure (5.34). In LE-N, back face bars, similar to LE, experienced tensile strain and front face bars experienced negligible amount of tensile strain. Considerable amount of strain appeared in back face bar after the load of 100 kN 943% of the ultimate load) at which barrier wall showed crack on both front and back face. Furthermore, maximum tensile strain at failure was observed in H-B-R location, which was close to the end of load-application zone opposite to the test side free edge. At failure, maximum tensile strain in H-B-R was 2524 micro-strain (16% of ultimate strain).

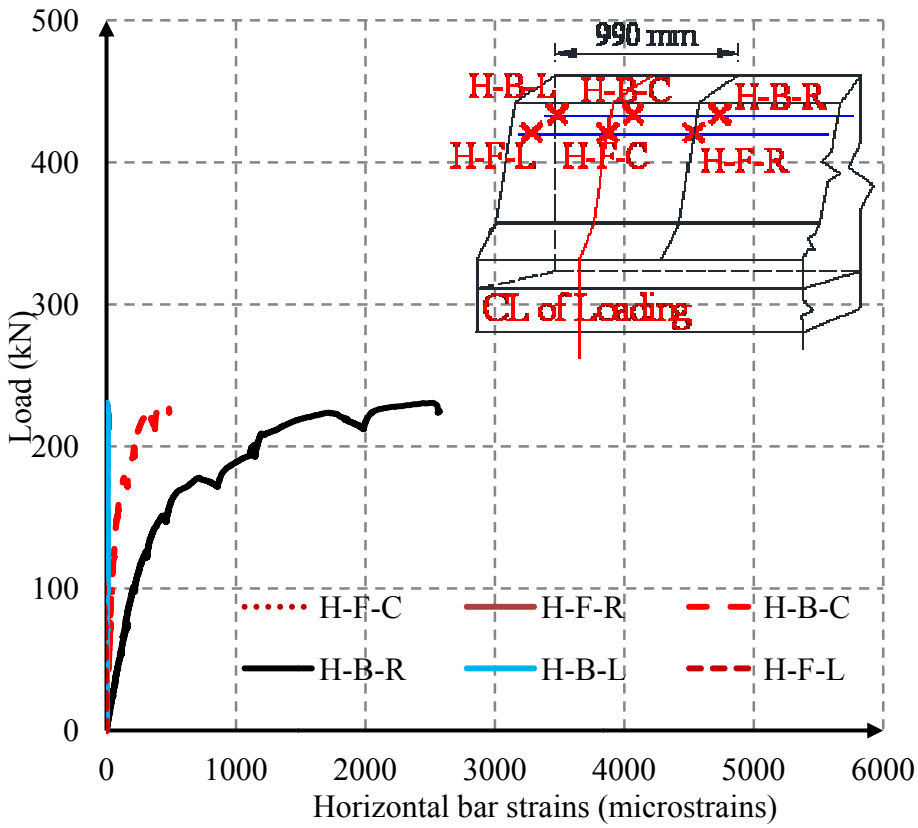

Figure (5.34): Horizontal bar Strains for LE-N test

Figure 5.35 shows V2 bar strains at different locations along the length of the barrier wall. Considerable amount of strain appeared in all the V2 bars after the load of 150 kN (65% of the ultimate load), at which barrier wall exhibited first crack. Furthermore, all the vertical bars showed close load-strain relationship because all of them were within 1050 mm load-application zone. At failure, V2-R bars exhibited maximum strain of 2448 micro-strains (22% of ultimate strain) similar to corresponding LE while, V2-C and V2-L gave 1887 and 1627 micro-strains (ranging between 15 and 17%), respectively.

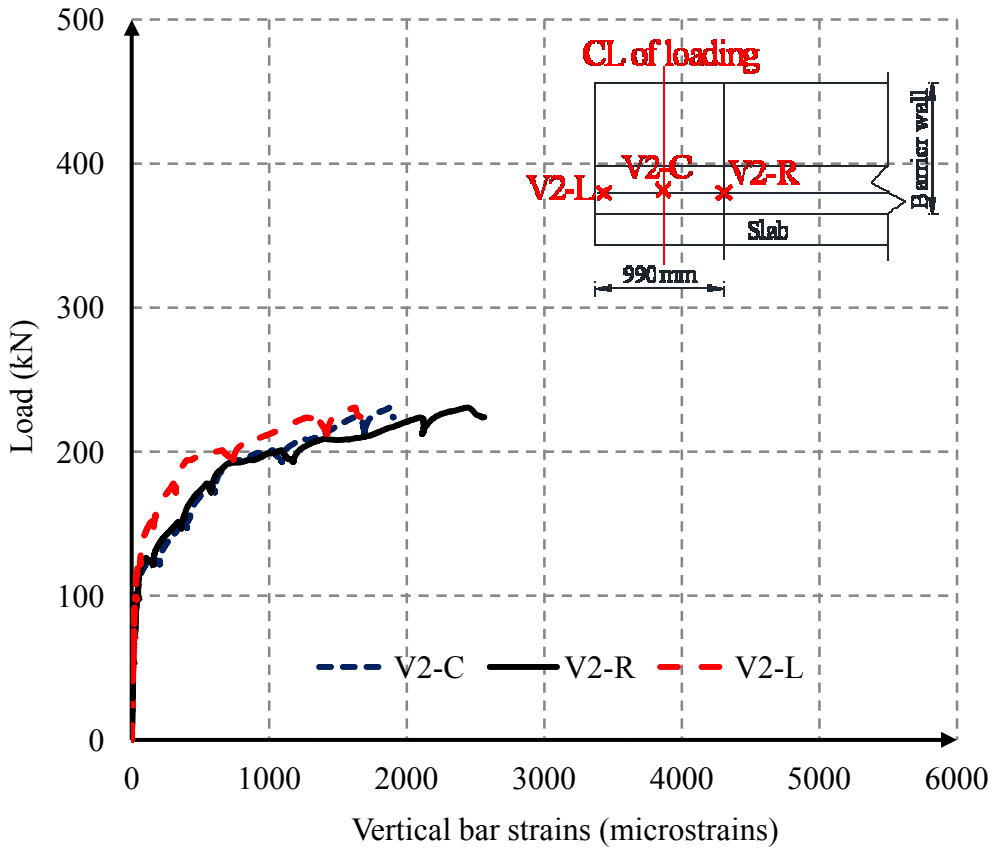

Figure (5.35): V2 bar strains along the length of the barrier wall for LE-N test

Maximum strains of transverse, horizontal and vertical bars of LE-N and intact LE are plotted in Figure 5.36. It can be noticed from the graph that initially up to a load of 170 kN (74% of the ultimate load) deck slab bar of LE-N exhibited higher strain than that of LE. However, other two bars, horizontal and vertical bar of barrier wall, exhibited lower strain than those of LE from the very beginning up to the load of failure. Finally, at failure, strains in all the bars of LE-N were lower than those of LE even though ultimate capacity of both of them was close. This is due to the fact that NSM technique increased the stiffness and moment capacity of repaired LE-N than that of intact LE.

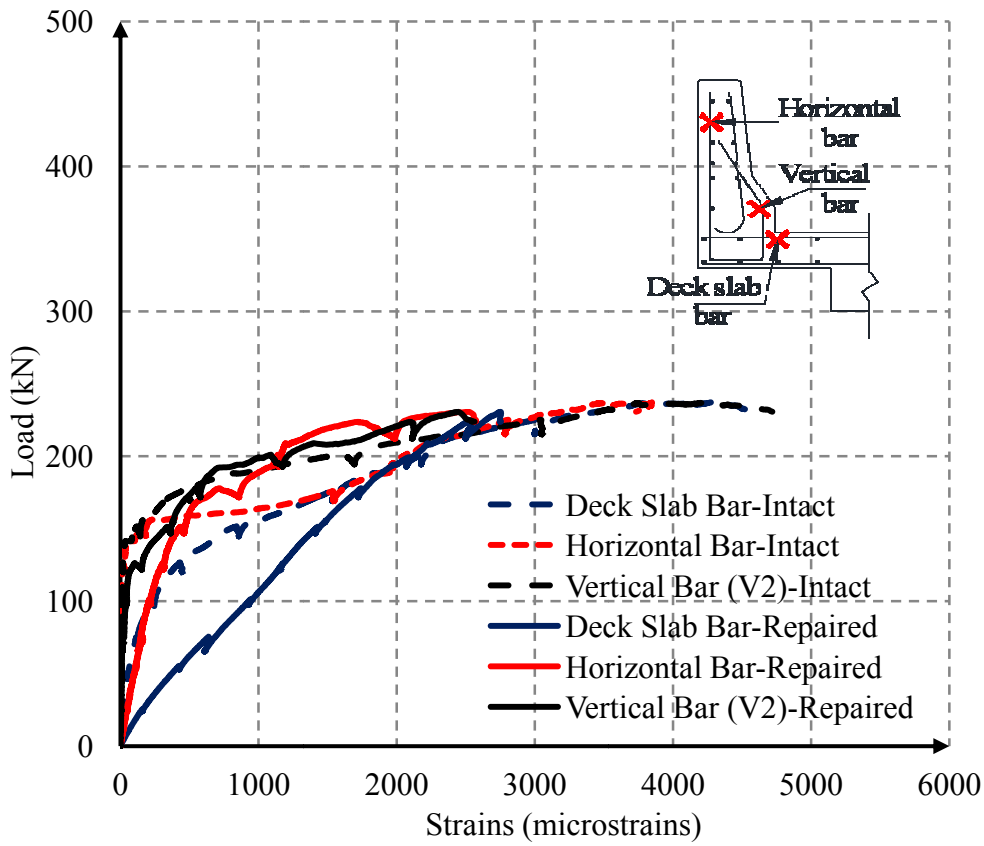

Figure (5.36): Comparison of strains of repaired LE-N with intact LE

5.5.5. Summary of Strains in Reinforcements

Table 5.4 summarizes the maximum strain values observed during the testing of the both repaired prototypes and their corresponding intact prototype.

- In M1-P, strain in transverse bar of overhang deck slab (approximately 18%), vertical bar (approximately 23%) and horizontal bar (approximately 28%) of barrier wall was lower than those of corresponding intact M1. This can be attributed to the ultimate capacity of M1-P which was lower (approximately 13%) than that of intact M1.

Table (5.4): Summary of strains in GFRP reinforcements for repaired and intact prototypes

Test ID		Overhang transverse bar		Horizontal bar		Vertical bar (V2)	
		Strain (με)		Strain (με)		Strain (με)	
Intact	Repaired	Intact	Repaired	Intact	Repaired	Intact	Repaired
M1	M1-P (Planting)	3624	2989	4206	3042	5081	3452
M2	M2-N (NSM)	3328	3565	3540	4812	4724	6202
LE	LE-N (NSM)	4667	2754	3845	2524	4293	2448
RE	RE-P (Planting)	5462	4065	5299	3114	3846	4380

- Due to higher ultimate capacity of M2-N (approximately 20%) than that of M2, overhang deck slab bar (approximately 7%). barrier wall vertical bar (approximately 31%) and barrier wall horizontal bar (approximately 35%) exhibited higher strain than those of intact M2.
- LE-N, NSM repaired edge portion, exhibited lower strains in deck slab bar (approximately 40%), barrier wall vertical bar (approximately 43%) and barrier wall horizontal bar (approximately 35%) than those of corresponding intact LE. Though ultimate capacity of LE-N and intact LE was almost same (approximately 3% difference), due to the NSM technique, LE-N gave lower strains in bars than that of LE.
- Because ultimate capacity of RE-P, spliced repaired edge portion, was lower (approximately 16%) than that of corresponding intact RE, strains in deck slab bar (approximately 26%) and in barrier wall horizontal bar (approximately 41%) was lower

than that of RE. However, vertical bar of the barrier wall of RE-P showed higher strain (approximately 14%) than that of RE.

In general, measured strains in both intact and repaired prototypes (using either repair technique) followed similar pattern and confirm that load within barrier wall was carried in two directions; horizontal and vertical.

Chapter 6

Summary, Conclusions and Future Work

6.1. Summary

In this research, repair techniques of GFRP-reinforced concrete bridge barriers were investigated. To do so, an extensive experimental program was conducted at the W.R. McQuade Heavy Structures Laboratory of the University of Manitoba. The entire experimental program was divided into two phases; Phase I and Phase II.

In Phase I, three full scale 6-m long GFRP reinforced PL-2 concrete bridge barrier wall prototypes were constructed. These barrier wall prototypes were tested at middle and at both edges under monotonic loading up to failure simulating vehicle crash test. Test results were analysed in terms of ultimate capacity, modes of failure, cracking pattern, load-deflection and load-strain. Furthermore, tested prototypes exhibited damage that can occurr in a bridge barrier in case of an accident.

In Phase II, damaged barriers of Phase I were repaired using two different repair techniques: Splicing (Planting) technique and Near Surface Mounted (NSM) technique. After the repair, all barrier walls were re-tested using identical loading conditions of Phase I. Test results were used to evaluate the structural performance of repaired GFRP-reinforced concrete bridge barrier as well as efficiency of repair techniques compared to those of the undamaged ones.

6.2. Conclusions

The findings of the present investigation support the following conclusions.

6.2.1. Conclusions from Phase I

1. The average ultimate capacity of a middle portion of PL-2 GFRP-reinforced concrete bridge barrier walls was 382 kN. This value decreased to 241 kN (approximately 37% decrease) near the edge of the barrier wall even though the vertical reinforcement is doubled for the first 1.0 m at the edge.
2. Barrier walls tested at the middle failed due to the punching shear failure. While barrier walls tested near the edges failed due to a combined punching shear and deck slab-barrier wall joint failure.
3. Critical length over which most of the cracks formed for middle portion of barrier wall was 3.2 m and for edges of barrier wall were 2.0 m, which is in good agreement with the yield line prediction adopted by AASHTO LRFD (2007) and CAN/CSA-S6-06. Cracks formed in trapezoidal shape on the front face of barrier wall. While on the back face, cracks were formed vertically.
4. Measured strains and deflections in the barrier wall and overhang deck slab confirms that bridge barrier walls are resisting line/concentrated loads in two directions; vertical and horizontal. Near the edge of the barrier walls, load resisted in the horizontal direction is less than that for a middle portion of the wall.
5. The obtained critical length for both middle and edge tests as well as the measured strains indicates that the 6.0-m long barrier prototypes used in this investigation better represent real field applications where barrier walls are typically long and continuous.

6.2.2. Conclusions from Phase II

1. Barrier wall repaired at middle, using splicing (planting) technique, achieved 89% (348 kN) of the ultimate capacity of corresponding intact barrier wall (391 kN). This decrease in obtained capacity (approximately 11 %) can be attributed to the lower concrete compressive strength of spliced repaired middle portion (approximately 25%) than that of intact barrier wall.
2. NSM-GFRP repaired middle portion of barrier wall (451 kN) showed 20% increase in ultimate capacity than that of corresponding intact barrier wall (373 kN). This was due to NSM technique and higher concrete compressive strength of NSM-GFRP repaired middle portion (approximately 13%) than that of intact barrier wall.
3. Edge portion of barrier wall, repaired using splicing (planting) technique, achieved 85% (208 kN) of the ultimate capacity of corresponding intact barrier wall (245 kN). This may be attributed to the concrete compressive strength of spliced repaired edge which was lower (approximately 16%) than that of intact barrier wall.
4. Barrier wall repaired at edge, using NSM technique, achieved 97% (230 kN) of the ultimate capacity of corresponding intact barrier wall (237 kN) even though concrete compressive strength of repaired portion was approximately 13% higher than that of intact barrier wall.
5. Mode of failure of the repaired barrier walls was very similar to their intact counterparts. At middle portion, using either splicing technique or NSM technique, the mode of failure was punching shear. While mode of failure of the repaired edge portion, using either splicing technique or NSM technique, was combined punching shear and slab-barrier wall joint failure.

6. Cracking pattern and critical length over which most of the cracks formed in spliced and NSM-GFRP repaired barrier walls were very similar to those of the corresponding intact barriers, both at middle and edge portions.
7. Spliced repaired middle and edge portion of barrier wall followed the same load-deflection path of that of corresponding intact barrier walls up to failure. While NSM-GFRP repaired middle and edge portion of barrier wall exhibited steeper load-deflection path than that of corresponding intact barrier walls. This was due to the increase in stiffness as well as moment capacity of NSM-GFRP repaired middle and edge portion resulted from NSM technique (bigger effective depth).
8. Measured strains in reinforcements of spliced repaired barrier wall (both middle and edge) and only NSM-GFRP repaired edge were lower than those of intact barrier walls due to lower ultimate capacity (ranging between 11 and 15% for splicing and 3% for NSM technique). At failure, transverse bar of overhang deck slab, horizontal and vertical bar of barrier wall exhibited lower strains (ranging between 18 and 43%) than those of their intact counterparts. However, vertical bar of the spliced repaired edge gave higher strains (approximately 14%) than that of corresponding intact barrier wall.
9. On contrary, in NSM-GFRP repaired middle portion, measured strains in transverse bar of overhang deck slab, and vertical and horizontal bar of barrier wall were higher (ranging between 7 and 35%) than that of intact barrier wall due to higher ultimate capacity (approximately 20%).
10. Measured strains and deflections as well as mode of failure in the repaired barrier wall and overhang deck slab confirms that repaired bridge barrier walls are similar to intact barrier walls in resisting load in two-way action.

11. In general, GFRP reinforced concrete bridge barrier wall can be efficiently repaired using either splicing technique or NSM technique used in this research.

6.3. Future Work

1. Further experimental and analytical studies are required to formulate general equations for ultimate capacity and critical length of GFRP reinforced concrete bridge barrier.
2. A finite element model (FEM) can be built to investigate the effects of different parameters such as concrete cover, reinforcement ratio in each direction, and compressive strength of concrete on ultimate capacity and cracking pattern of GFRP reinforced concrete bridge barrier. Furthermore, that model can be used to investigate load sharing within the barrier wall at different load stages.
3. A FEM model for repaired barrier wall can be built to investigate the effects of different parameters such as compressive strength of concrete, bonding agent, groove size, bar-hole diameter and anchorage length on behaviour of repaired barrier wall.

REFERENCES

ACI Committee 355. (2001). "Evaluating the Performance of Post-Installed Mechanical Anchors in Concrete (ACI 355.2-01) and Commentary (355.2R-01)," *American Concrete Institute*, Farmington Hills, Mich., 29 p.

ACI Committee 555. (2001). "Removal and Reuse of Hardened Concrete," (ACI 555R-01), *American Concrete Institute*, Farmington Hills, Mich., 26 p.

ACI Committee 408. (2003). "Bond and Development of Straight Reinforcing Bars in Tension," (ACI 408R-03), *American Concrete Institute*, Farmington Hills, Mich., 49 p.

AASHTO. (2007). "LRFD Bridge Design Specifications," AASHTO LRFD 2007, *American Association of State Highway and Transportation Officials*, Washington, DC.

Ahmed, E., Benmokrane, B. (2011). "Static Testing of Full-Scale Concrete Bridge Barriers Reinforced with GFRP Bars." *10th International Symposium on Fibre Reinforced Polymer Reinforcement for Concrete Structures*, *ACI*, SP-275, pp. 1-20.

Alberson, D.C., Williams, W.F., Menges, W.L. and Haug, R.R. (2004). "Testing and Evaluation of The Florida Jersey Safety Shaped Bridge Rail," *Report No. 9-8132-1*, February, Texas Transportation Institute (TTI), The Texas A&M University System, College Station, Texas.

Alves, J., El-Ragaby, A. and El-Salakawy, E. (2011). "Durability of GFRP Bars Bond to Concrete under Different Loading and Environmental Conditions," *Journal of Composites for Construction, ASCE*, V. 15, No. 3, pp. 249-262.

Bakht, B., Mufti, A.A. and Tadros, G. (2004). " Discussion of Fiber-reinforced polymar bars for the concrete deck slab of Wotton Bridge," *Canadian Journal of Civil Engineering*, V. 31, pp. 530-531.

Canadian Standards Associations. (2004). "Concrete Materials and Methods of Concrete Construction," CAN/CSA-A23.1-04, *Canadian Standards Association*, Rexdale, Ontario.

Canadian Standards Associations. (2006). "Canadian Highway Bridge Design Code," CAN/CSA-S6-06, *Canadian Standards Associations*, Rexdale, Ontario.

Canadian Standards Associations. (2006). "Commentary on CAN/CSA-S6-06, Canadian Highway Bridge Design Code," *Canadian Standards Associations*, Rexdale, Ontario.

Deitz, D., Harik, I.E. and Gesund, H. (2000), "GFRP Reinforced Concrete Bridge Decks," *Research Report KTC-00-9*, Kentucky Transportation Center, College of Engineering, University of Kentucky, Kentucky, USA, 185 p.

Deitz, D.H., Harik, I.E., Gesund, H. and Zatar, W.A. (2004). "Barrier Wall Impact Simulation of Reinforced Concrete Decks with Steel and Glass Fiber Reinforced Polymer Bars," *Journal of Composites for Construction*, *ASCE*, V. 8, No. 4, pp. 369-371.

El-Salakawy, E.F., Benmokrane, B. and Desgagné, G. (2003). "Fibre-reinforced polymer composite bars for the concrete deck slab of Wotton Bridge," *Canadian Journal of Civil Engineering,* V. 30, pp. 861-870.

El-Salakawy, E.F., Masmoudi, R., Benmokrane, B., Brière, F. and Desgagné, G. (2004). "Pendulum Impacts into Concrete Bridge Barriers Reinforced with Glass Fibre Reinforced Polymer Composite Bars," *Canadian Journal of Civil Engineering*, V. 31, pp. 539–552.

El-Salakawy, E.F., Mufti, A. and Elragaby, A. (2010). "Laboratory Investigations on the Repair of GFRP-Reinforced Concrete Bridge Deck Slabs," *Recent Advances in Maintenance and Repair of Concrete Bridges*, *ACI*, SP-235, 20 p.

Hasan, T., Rizakalla, S., Abdelrahman, A. and Tadros,G. (1999). "Design Recommendations for Bridge Slabs Reinforced by Fiber Reinforced Polymars," *ACI Special Publication*, V. 188, pp. 313-324.

Hassan T. and Rizkalla S. (2004) "Bond Mechanism of NSM FRP Bars for Flexural Strengthening of Concrete Structures," *ACI Structural Journal*, V. 101, No. 6, pp. 830–839.

Hirsch, T.J. (1978). "Analytical evaluation of Texas bridge rails to contain buses and trucks," *Tex. Research Report 230-2*, Texas Transportation Institute, Texas A&M University, College Station, Texas.

Jeon, S.J., Choi, M.S. and Kim, Y.J. (2011). "Failure Mode and Ultimate Strength of Precast Concrete Barrier," *ACI structural Journal*, V. 108, No. 1, pp. 99-107.

Lorenzis, D. and Nanni, A. (2002) "Bond Between Near Surface Mounted FRP Rods and Concrete in Structural Strengthening," *ACI Structures Journal*, V. 99, No. 2, pp. 123-133.

Matta, F. and Nanni, A. (2009). "Connection of Concrete Railing Post and Bridge Deck with Internal FRP Reinforcement," *Journal of Bridge Engineering*, *ASCE*, V. 14, No. 1, pp. 66-76.

Mitchell, G., Tolnai, M., Gokani, V., Picon, R., Yang, S., Klingner, R.E. and Williamson, E.B. (2006). "Design of Retrofit Vehicular Barriers Using Mechanical Anchors," *Report No. 0-4823-CT-1*, October, Centre for Transportation Research (CRT), The University of Texas at Austin, Red River, Austin.

Quayyum, S. (2010). "Bond Behavior of Fiber Reinforced Polymer (FRP) Rebars in Concrete'" M.A.Sc. Thesis, The University of British Columbia, Okanagan, British Columbia, Canada.

Sennah, K., Juette, B., Weber, A., Witt, C. (2011). "Vehicle Crash Testing on a GFRP-Reinforced PL-3 Concrete Bridge Barrier," *Annual Conference of the Transportation Association of Canada*, Edmonton, Alberta, Canada, 8 p.

Soliman, S.M., El-Salakawy, E.F., and Benmokrane, B. (2011). "Bond Performance of Near-Surface-Mounted FRP Bars," *Journal of Composites for Construction*, *ASCE*, V. 15, No. 1, pp. 103-111.

U.S. Army Corps of Engineers. (1995). "Evaluation and Repair of Concrete Structures," EM-1110-2-2002, *U.S. Army Corps of Engineers*, Washington, DC.

Vorster, M.C., Merrigan, J.P., Lewis, R.W., Weyers, R.E. (1992). "Techniques for Concrete Removal and Bar Cleaning for Bridge Rehabilitation Projects," SHRP-S-336, Strategic Highway Research Program, Washington, DC.

APPENDIX A:

DESIGN OF OVERHANG DECK SLAB

A.1. Transverse design moment in the overhang

Figure A-1 shows transverse cross section of overhang slab, barrier wall and supporting beam. It also shows locations of dead load, wheel load and overhang moment induced by these loads.

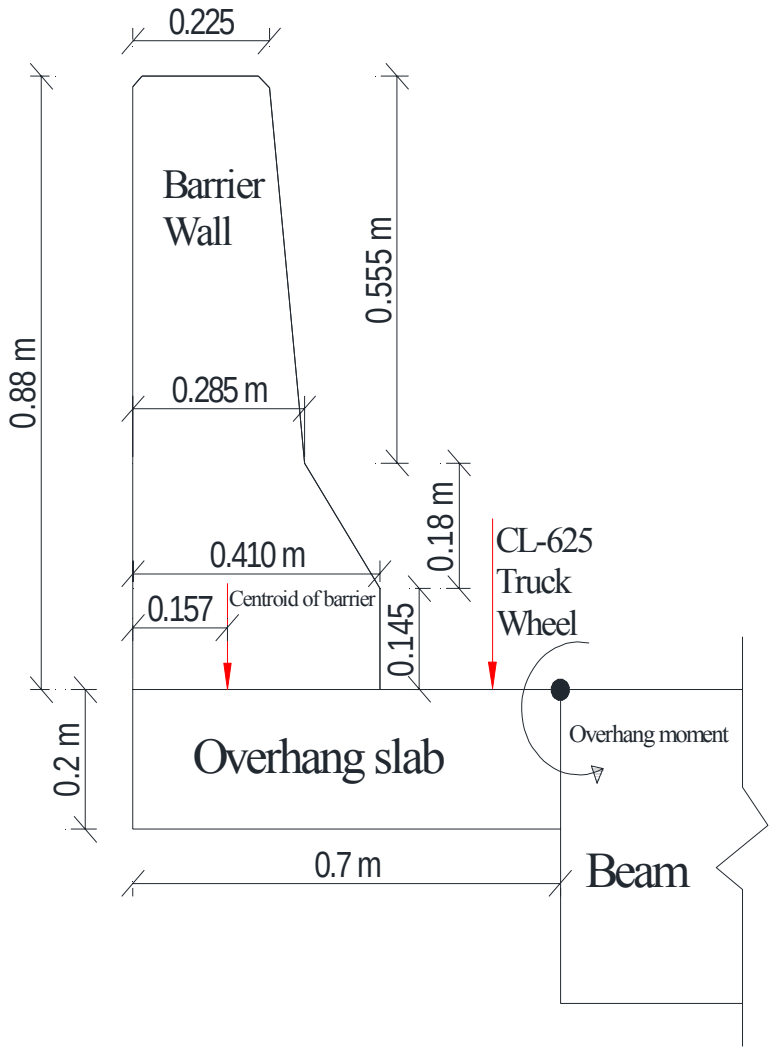

Figure (A-1): Transverse moment in overhang due to dead load and wheel load

Moment due to dead load

The perpendicular span of the overhang, S = 0.7 m

Average cross sectional area of PL-2 barrier

$$\frac{1}{2}(225+285)*555+\frac{1}{2}(285+410)*180+410*145=0.2635m^2$$

Unit weight of concrete = 24 kN/m^3

Dead Load of PL-2 concrete barrier = 0.2635 × 24 = 6.32 kN/m

Dead Load of Concrete slab = 0.20 × 24 = 4.8 kN/m^2

Un-factored moment due to dead load

$$6.32*(0.7-0.157)+4.8*(0.7)^2/2=4.61\,kN-m/m$$

Factored moment due to dead load = 1.2*4.61= 5.53 kN-m/m

Moment induced by the wheel load (service load) (Clause 5.7.1.6.1, CAN/CSA-S6-00)

Here, Span of overhang S_c = 0.7 m; r_t = 1 (as overhang slab thickness is constant)

Overhang slab has PL-2 barrier wall on its free edge.

From Table 5.7.1.6.1. (a) of CAN/CSA-S6-06

Maximum un-factored cantilever moment for CL-625 truck wheel = 32 kN-m/m

For Serviceability Limit State (SLS No.1), from Table 3.5.1 (a) of CAN/CSA-S6-06

the load combination factor = 0.9

The service design moment for the overhang is 32*0.9+4.61 = 33.41 kN-m/m

The ultimate design moment due to dead load for the overhang is M_u = 1.7 × 32 + 5.53

= 60 kN-m/m

Moment induced by the load on the barrier (ultimate load) (Clause 3.8.8.1and Clause 12.5.2.4, CAN/CSA-S6-00)

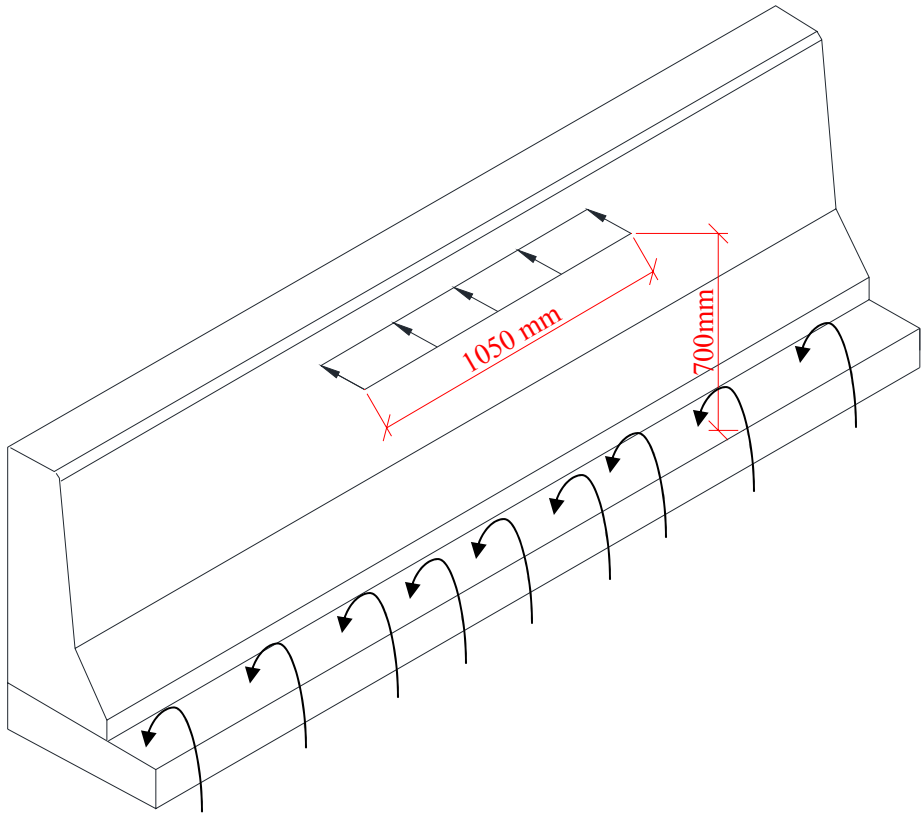

Figure (A-2): Moment induced by transverse impact load

Here,

Transverse load applied over 1050 mm long at 700 mm height, P_t = 100 kN

The service moment, $M_y = \frac{100 * 0.7}{1.05} = 66.7\ kN - m/m$

The ultimate design moment (due to impact) Mu = 1.7*66.7 = 113.4 kN-m/m (Governs)

Therefore, transverse design moment in the overhang = <u>113.4 kN-m/</u>

A.2. Amount of GFRP bars for the overhang slab

In overhang deck slab 19 mm sand coated GFRP bar was used. Properties of 19 mm sand coated GFRP bars are as follows:

$$Area\ A_f = 285\ mm^2$$

$$Modulus\ of\ Elasticity\ E_f = 42\ GPa$$

$$Design\ Strengt\ f_{fu} = 428.5\ MPa$$

Properties of concrete used in casting overhang deck slab are as follows:

$$Concrete\ Compressive\ Strength\ f_c' = 45\ MPa;$$

$$Modulus\ of\ Elasticity\ of\ Concrete\ E_c = 4500\sqrt{45} = 30\ GPa$$

$$Ultimate\ Strain\ of\ Concrete\ \varepsilon_{cu} = 0.0035$$

Here,

Slab thickness h =200 mm

Slab width b = 1000 mm

For a concrete clear cover (cc), dc = 38 mm

Effective depth d = 200 – 38 – 19.05/2 = 152.5 m

Try, A_f = 2850 mm²/m (No.19 @ 100) as top reinforcement assembly in the overhang.

Therefore,

Reinforcement ratio $\rho_f = \dfrac{285}{152.5*100} = 1.875\%$

Now,

$$Stress\ block\ parameter\ \beta_1 = 0.97 - 0.0025 * f_c' = 0.8575$$

$$Resistance\ factor\ of\ GFRP\ \varphi_f = 0.7$$

Stress in GFRP:

$$f_f = \left[\sqrt{\left(\frac{\left(E_f \varepsilon_{cu}\right)^2}{4} + \frac{0.85\beta_1 f_c^{'}}{\rho_f} E_f \varepsilon_{cu} \right)} - 0.5 E_f \varepsilon_{cu} \right] = 425 < f_{fu}(428.5Mpa) \text{ OK}$$

Moment resistance:

$$M_r = \phi_f \rho_f f_f \left(1 - 0.59 \frac{\rho_f f_f}{f_c^{'}} \right) bd^2 = 124.5\ kN - m > M_U (113.4\ kN - m) \text{ OK}$$

Clause 16.8.2 (CAN/CSA-S6-00) requires that the maximum stress in the FRP bars under factored loads shall not exceed $\phi_{frp} * F * f_{fu}^{*}$.

Where,

ϕ_{frp} = FRP strength reduction factor = 0.75

F = 0.8 for GFRP bars (Table 16.8.2 of CAN/CSA-S6-06)

f_{fu}^{*} = ultimate tensile strength of GFRP bar = 600 MPa

Depth of the neutral axis at cracking:

$$c = d.\left(\sqrt{\left(2\rho_f n_f + \left(\rho_f n_f\right)^2\right)} - \rho_f n_f \right)$$

$$Modular\ ratio\ n_f = E_f / E_c = 1.45$$

$$c = 0.1525.\left(\sqrt{\left(2 * 0.01875 * 1.45 + \left(0.01875 * 1.45\right)^2\right)} - 0.01875 * 1.45 \right) = 31.62mm$$

Moment at cracked section:

$$I_{cr} = \frac{b.c^3}{3} + n_f.A_f.(d-c)^2 = 7.092x10^{-5} m^4$$

$$Maximum\ stress\ in\ GFRP\ under\ \ factored\ load\ \ f_u = \frac{M_u n.(d-c)}{I_{cr}}$$

$$= \frac{113.4*1.45*(0.1525-0.03162)}{7.092x10^{-5}} = 280Mpa < 0.75*0.8*600 = 366Mpa \quad OK$$

Therefore, Use No. 19 @ 100 mm spacing in the overhang top assembly.

According to Hassan et al. (1999) and Bakht et al. (2004) minimum longitudinal reinforcement ratio should be 0.6 % and according to clause 16.8.7 and clause 8.18.4.2 of CHBDC (CAN/CSA S6-00) this ratio should be 0.35%. Here, 0.6% longitudinal reinforcement ratio is selected; top longitudinal reinforcement spacing is No. 16 @ 200 mm. Spacing of Overhang bottom transverse and longitudinal reinforcement is also taken as No. 16 @ 200 mm.

Figure A-4 shows the reinforcement layout in the overhang deck slab.

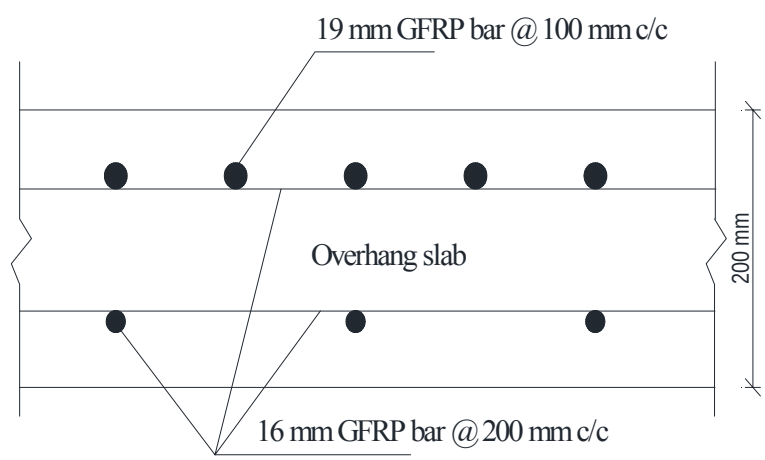

Figure (A-3): Transverse section and reinforcement layout of overhang deck slab

APPENDIX B:

DESIGN OF PROTOTYPE SUPPORTING BEAM

B.1. Supporting beam cross section selection

The supporting beam width must be wide enough so that it can fit NSM groove and splicing hole in repairing phase. The length of NSM groove and splicing hole was chosen to be 40 d_b. Where, d_b is the diameter of the overhang transverse bar that is 19 mm.

Length of NSM groove or splicing hole $40\,d_b$ = 40*19 = 760 mm

As such, width of the supporting beam = 800 mm

Allowing 250 mm depth underneath the overhang to allow for deflection and rotation, depth of supporting beam = 450 mm.

B.2. Torsion design of supporting beam

Figure B-1 shows locations of loads and resulting torque in the supporting beam.

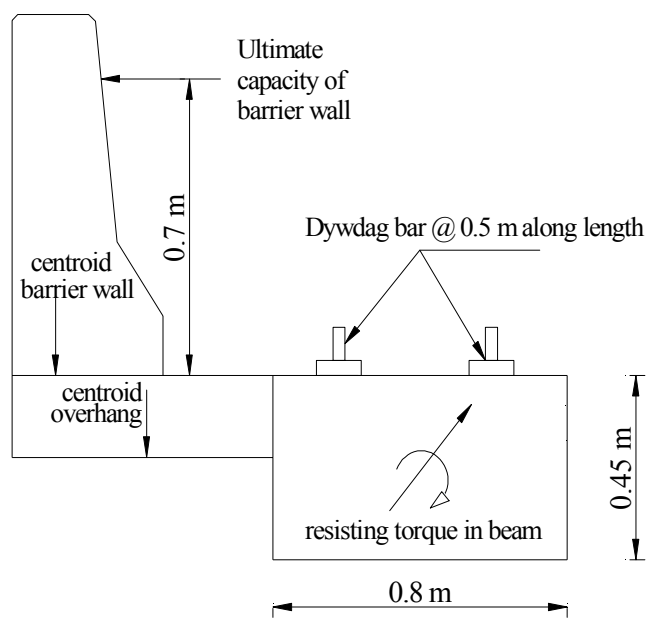

Figure (B-1): Load locations and resulting torque in supporting beam

Ultimate torsion:

Deal load of PL-2 concrete barrier: 0.2635 × 24 = 6.32 kN/m

Dead load of Concrete slab: 0.20 × 24 = 4.8 kN/m^2

Uniformly distributed torque due to these loads

= 6.32*(0.7-0.157) + 4.8*0.7*0.7*0.5 = 4.61 kN-m/m

Assume maximum load capacity of bridge barrier 400 kN

Load is applied at 700 mm high from the top of the slab.

Assuming failure load will spread over the critical length (3 m) of the barrier wall and as supporting beam is fixed at each 0.5 m distance along its length.

Therefore, Ultimate torsion $T_f = \frac{400*0.7}{3} + 4.61*0.5*0.25 = 93.9\ kN-m$

Cracking Torque:

Torque that causes cracks in the supporting beam = $T_{cr} = \frac{A_c^2}{P_c} 0.38\lambda\phi_c\sqrt{f_c^{'}}$

Where,

A_c = Cross sectional area of the supporting beam = 800*450

P_c = Perimeter of the supporting beam = 2(800+450)

λ = Concrete density factor = normal density concrete = 1

ϕ_c = Concrete strength reduction factor = 0.65

$f_c^{'}$ = Compressive strength of concrete = 45 MPa

Now,

$$T_{cr} = \frac{A_c^2}{P_c} 0.38\lambda\phi_c\sqrt{f_c^{'}} = \frac{(800*450)^2}{2(800+450)} *0.38*1*0.65*\sqrt{45}*10^{-6} = 85.89\ kN-m$$

Ultimate torsion $T_f > 0.25T_{cr}(21.47\ kN-m)$

Therefore, Torsion must be considered in designing supporting beam

To design supporting beam against ultimate torsion, both longitudinal bars and transverse stirrups need to be provided. Subsequent portion shows the design process.

Transverse stirrups:

$$\frac{A_t}{S} = \frac{T_f}{2A_0\phi_s f_y \cot\theta}$$

Here, S = spacing of transverse stirrups; T_f = ultimate torsion;

Using 10M stirrups (Area A_t = 100 mm^2) and assuming cover = 40 mm

Using simplified method cracking angle θ = 35°

Figure B-2 shows the different parameters in resisting torque of supporting beam

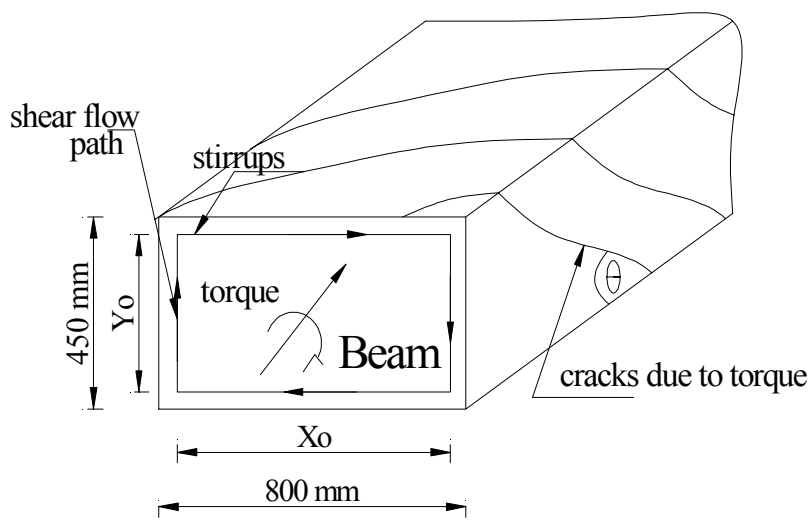

Figure (B-2): Different parameters in resisting torque

Now,

$$x_0 = 800 - 2*38 - 11 = 713\ mm$$
$$y_0 = 450 - 2*38 - 11 = 363\ mm$$
$$A_{oh} = 713*363 = 258819\ mm^2$$
$$A_0 = 0.85*A_{oh}$$
$$p_h = 2*(713+363) = 2152\ mm$$

$$\frac{100}{S} = \frac{93.9x10^6}{2*0.85*258819*0.85*450*\cot 35}$$
$$\Rightarrow S = 256\ mm$$

Check Maximum spacing:

Assuming 15M steel as longitudinal reinforcement

$$\text{Smaller of} \rightarrow \left| \begin{array}{l} 300\ mm \\ or \\ 0.35d_v = 0.35(0.9d) \\ = 0.35*\{0.9*(450-38-11-16/2)\} = 123.79\ mm \end{array} \right.$$

Therefore, single looped 10M stirrups will be provided @ 125 mm.

Longitudinal reinforcement:

$$\text{Required tension force } F_{lt} = \cot\theta \frac{0.45P_hT_f}{2A_{oh}} = \cot 35 \frac{0.45*2(713+363)*93.9*10^6}{2*258819}$$
$$= 219.62\ kN$$

$$A_s = \frac{219.62x10^3}{0.85*450} = 574.16\ mm^2$$

Therefore, use six 10M steel bars (A_s = 600 mm^2)

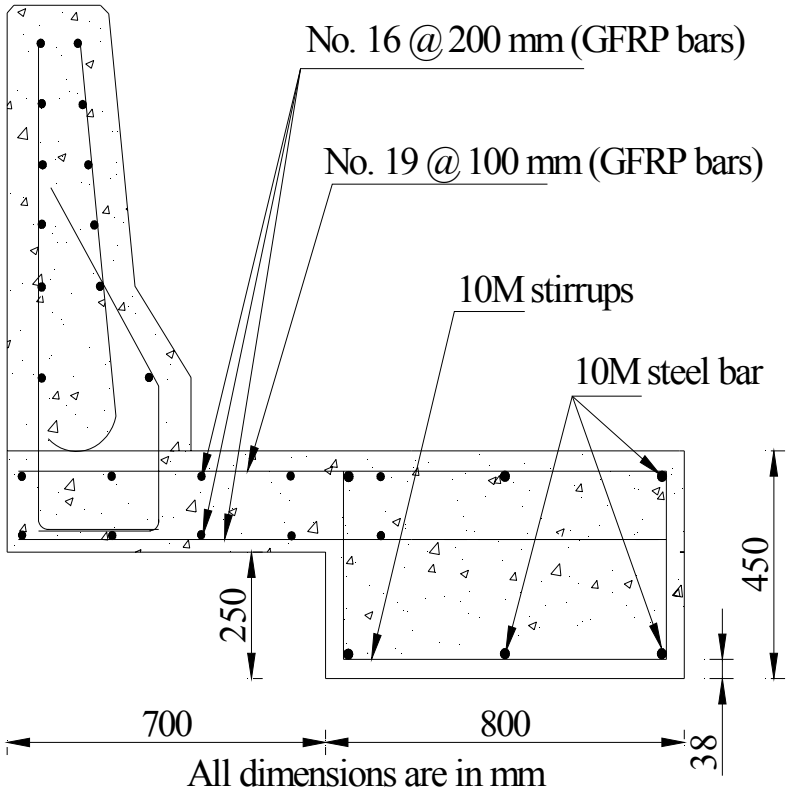

Figure (B-3): Reinforcement detail of prototype

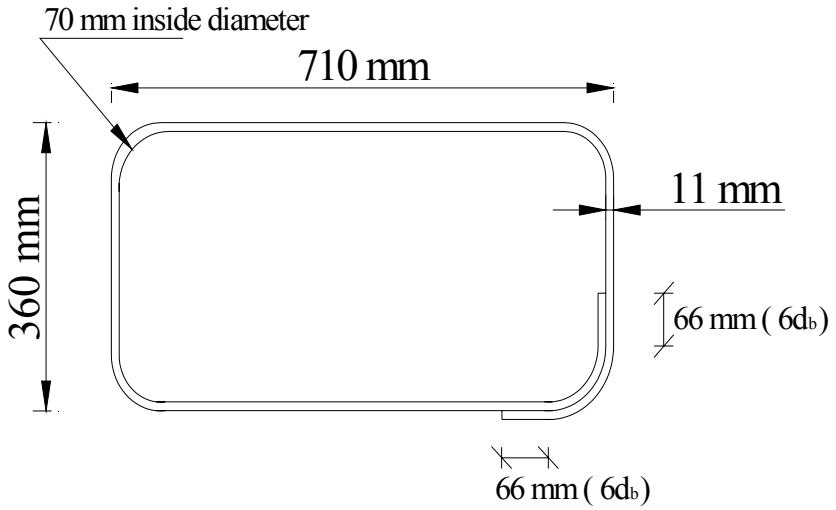

Figure (B-4): Detailing of 10M single looped stirrup

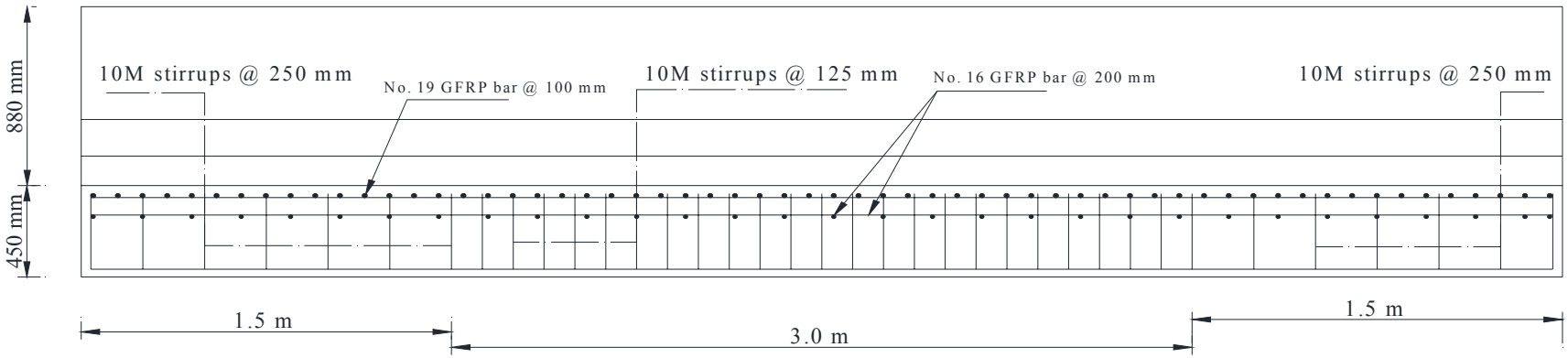

Figure (B-5): Spacing of stirrups along longitudinal direction while applying load at the middle portion of the barrier

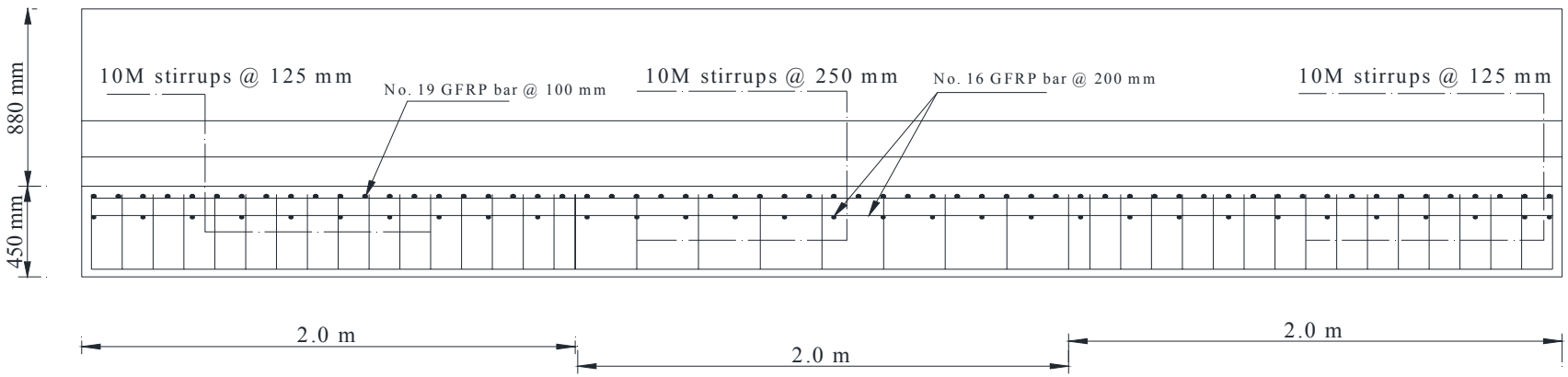

Figure (B-6): Spacing of stirrups along longitudinal direction while applying load at the edges of the barrier

APPENDIX C:

STRESSING FORCE ON RESTRAINING BAR

C.1. Overturning moment

Deal load of PL-2 concrete barrier: 0.2635 × 24 = 6.32 kN/m

Dead load of Concrete slab: 0.20 × 0.7 × 24 = 3.36 kN/m

Dead load of the supporting beam = 0.8*0.45*24 = 8.64 kN/m

Uniformly distributed overturning moment due to these loads

6.32*(0.7-0.157) + 4.8*0.7*(0.7*0.5) – 8.64*0.4 = 1.15 kN-m/m

Figure C-1 shows different components of overturning moment in the prototype.

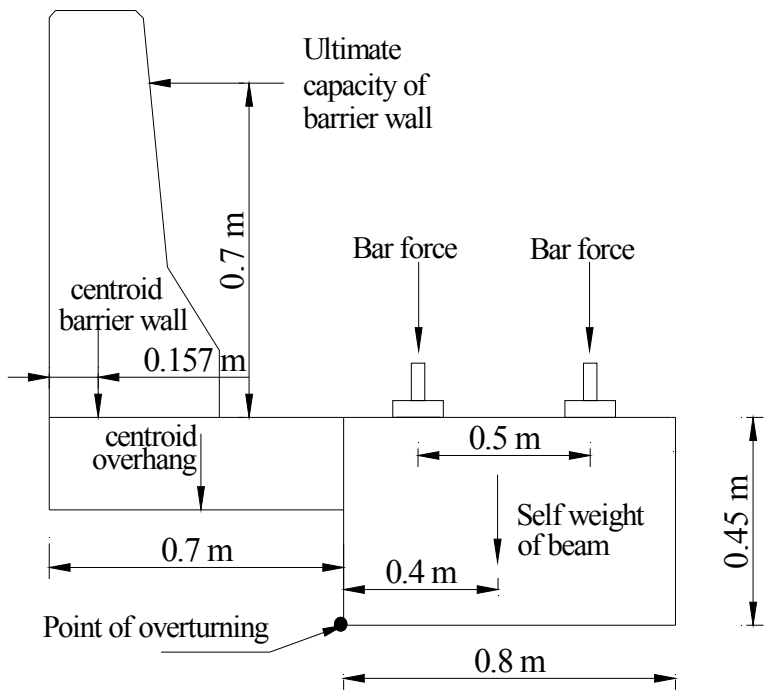

Figure (C-1): Different components of overturning moment

Overturning moment while applying load at middle:

Assume maximum load capacity of bridge barrier at middle 400 kN

Load is applied at 700 mm high from the top of the slab

Assuming failure load will spread over the critical length (3 m) of the barrier wall.

Overturning moment $M = \frac{400 * 0.7}{3} + 1.15 = 95\ kN - m$

Overturning moment while applying load at edge:

Assume maximum load capacity of bridge barrier at edge 300 kN

Load is applied at 700 mm high from the top of the slab

Assuming failure load will spread over the critical length (1 m) of the barrier wall.

Overturning moment $M = \frac{300 * 0.7}{1} + 1.15 = 211.15\ kN - m$

C.2. Bar stressing force

At middle:

In 1 m length there are 2 sets of bars; in each set two bars are spaced at 0.5 m away.

Required force on each bar = 95/(2*0.5) = 95 kN

Therefore, Apply force on each bar = 130 kN (Considering safety factor)

Using 100 mm X 100 mm steel plate in bar fixing.

Bar force will cause stress on concrete = 130*1000/ (100*100)
= 13 MPa < ($f'_c = 45$ MPa)
OK

At edge:

In 1 m length there are 2 sets of bars; in each set two bars are spaced at 0.5 m away.

Required force on each bar = 211.15/(2*0.5) = 211.15 kN

Therefore, Apply force on each bar = 325 kN (Considering safety factor)

Using 200 mm X 200 mm steel plate;

This force will cause stress on concrete = 325*1000/ (200*200)
= 8 MPa < (=(f'_c=45 MPa)

APPENDIX D:

CONCRETE CYLINDER TEST RESULTS

Table D-1: Concrete cylinder test results

Prototype ID	Age of Cylinders	Average Compressive Strength (MPa)	Average Tensile Strength (MPa)
M1	28 days	48	3.3
	130 days (test day)	50	3.4
M2	28 days	45	3.1
	105 days (test day)	45	3.1
RE	28 days	44	3.2
	128 days (test day)	45	3.2
LE	28 days	44	3.2
	121 days (test day)	45	3.2
M1-P	28 days	36	2.5
	46 days (test day)	37	2.5
M2-N	28 days	51	3.3
	30 days (test day)	51	3.3
RE-P	28 days	37	2.6
	48 days (test day)	38	2.6
LE-N	28 days	50	3.3
	45 days (test day)	51	3.3

APPENDIX E:

ESTIMATION OF GFRP BARS FOR PROTOTYPE CONSTRUCTION

Table E-1: Estimation of GFRP bars for prototype construction

Bar size	Bar designation	Bar location	Length (mm)	Total number
No. 19 GFRP bar Type-1		Top transverse assembly in deck slab and overhang	1420	180
No. 16 GFRP bar Type-1		Top longitudinal assembly in supporting beam and overhang	5920	15
		Bottom transverse assembly in supporting beam and overhang	1420	90
		Bottom longitudinal assembly in deck slab and overhang	5920	15
	H1	Barrier wall	5920	36
	V1	Barrier wall		120
	V2	Barrier wall		120
	V3	Barrier wall		120
10M steel bar	Single looped Stirrups	Supporting beam	710 X 360	120
10M steel bar	Longitudinal bar	Supporting beam	5920	18

APPENDIX F:

NO. OF HOLES AND GROOVES FOR REPAIRING AND ESTIMATION OF GFRP BARS

Table F-1: No. of holes for drilling

Hole diameter (mm)	Hole depth (mm)	Hole location	Total number
22	760	Top transverse assembly in overhang slab	49
19	640	Bottom transverse assembly in overhang slab	65
		Barrier wall	36

Table F-2: No. of grooves to cut

Groove width and depth (mm)		Groove length (mm)	Groove location	Total number
25		760	Top transverse assembly in overhang slab	50
Width (mm)	25	640	Barrier wall	36
Depth (mm)	50			

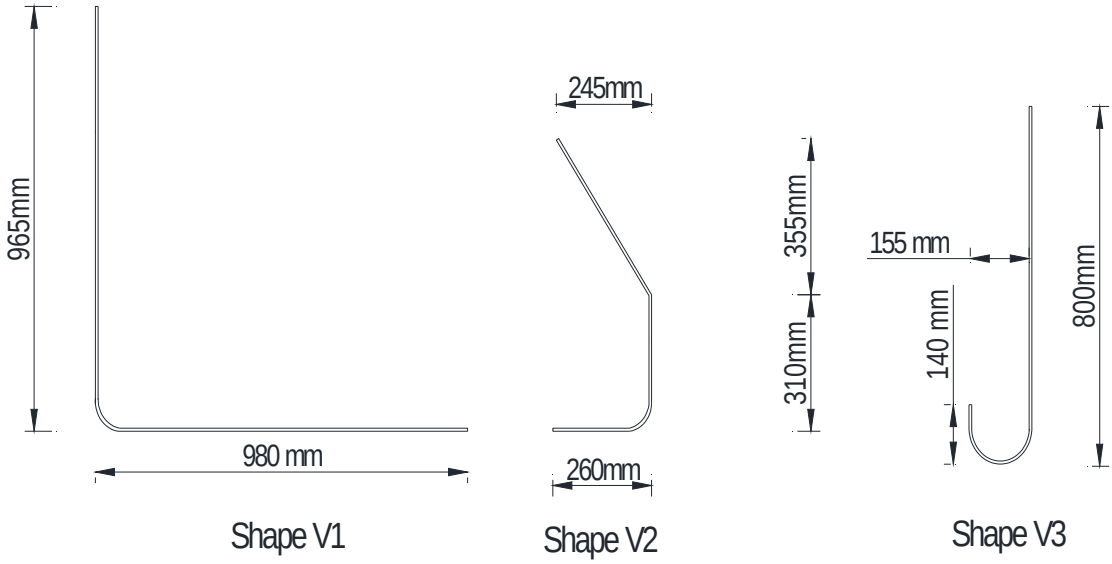

Figure (F-1): Shapes of vertical bars for repairing

Table F-3: Estimation of GFRP bars for repairing

Bar size	Bar designation	Bar location	Length (mm)	Total number
No. 19 GFRP bar Type-1		Top transverse assembly in overhang	1130	100
No. 16 GFRP bar Type-1		Top longitudinal assembly in overhang	3200	4
			1960	4
		Bottom longitudinal assembly in overhang	3200	4
			1960	4
	H1	Barrier wall	4480	12
			2560	24
			2600	24
	V1	Barrier wall		65
	V2	Barrier wall		65
	V3	Barrier wall		65

APPENDIX G:

LOAD-DEFLECTION AND LOAD-STRAIN RELATIONSHIPS FOR THE INDIVIDUAL TESTS

G.1. Graphs for M1 Test

G.1.1. Load-Deflection Graph

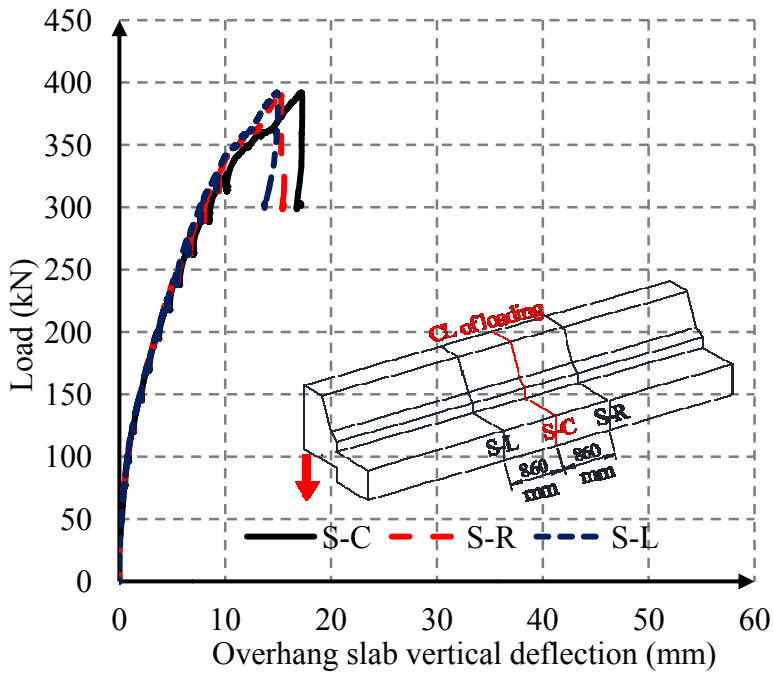

Figure (G-1): Overhang slab vertical deflection for M1 test

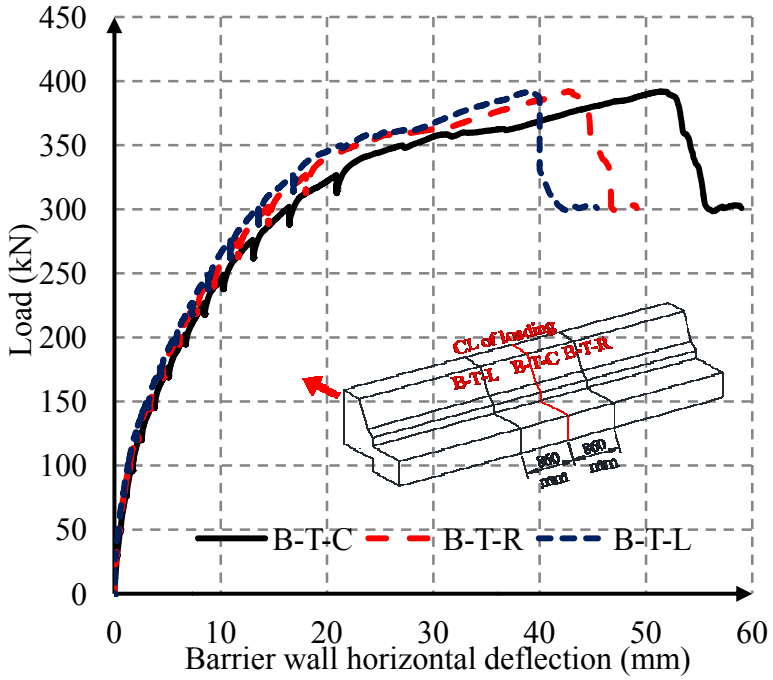

Figure (G-2): Barrier wall horizontal deflection for M1 test

G.1.2. Load-Strain Graph

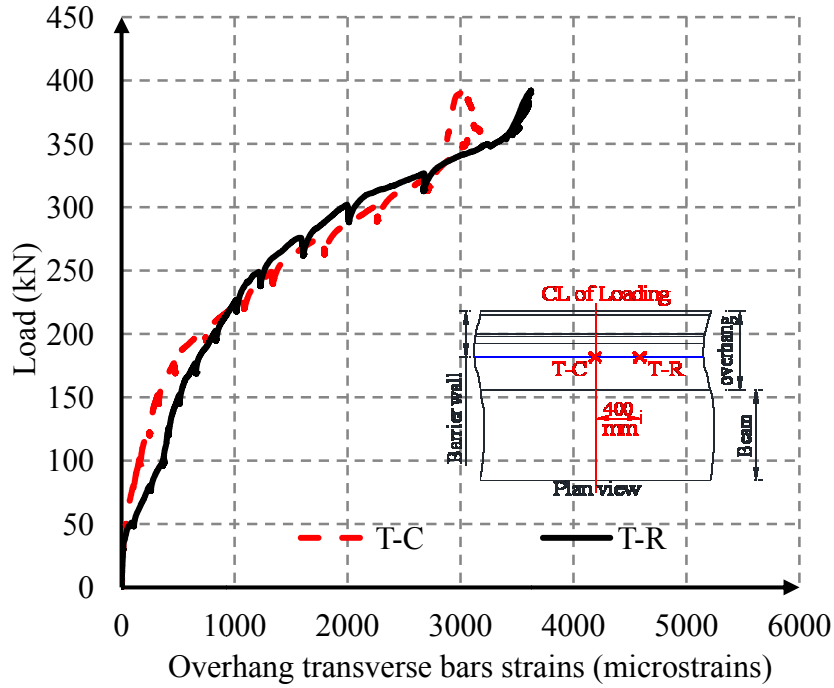

Figure (G-3): Overhang transverse bar strain for M1 test

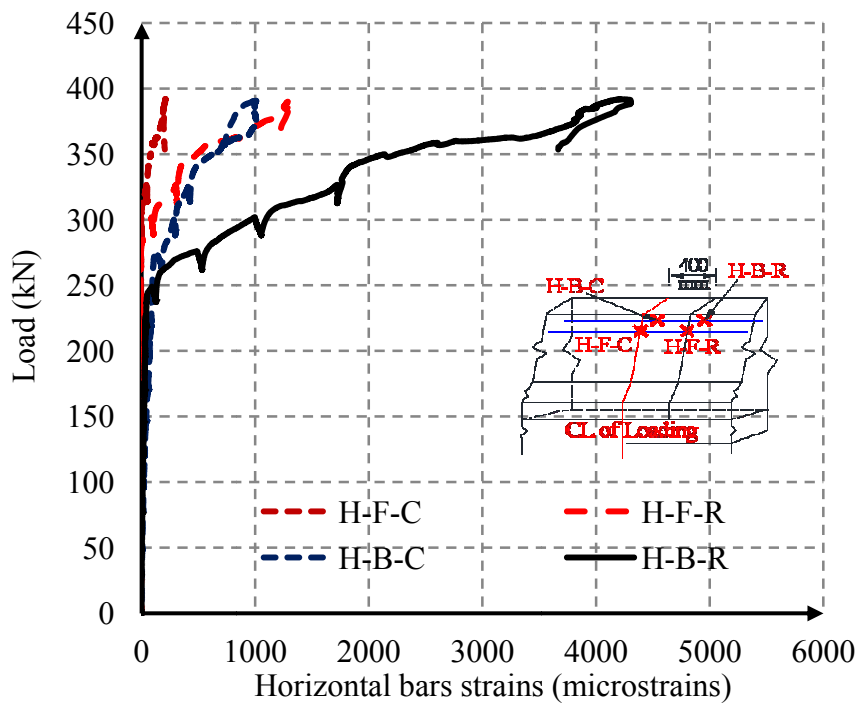

Figure (G-4): Barrier wall horizontal bar strains for M1 test

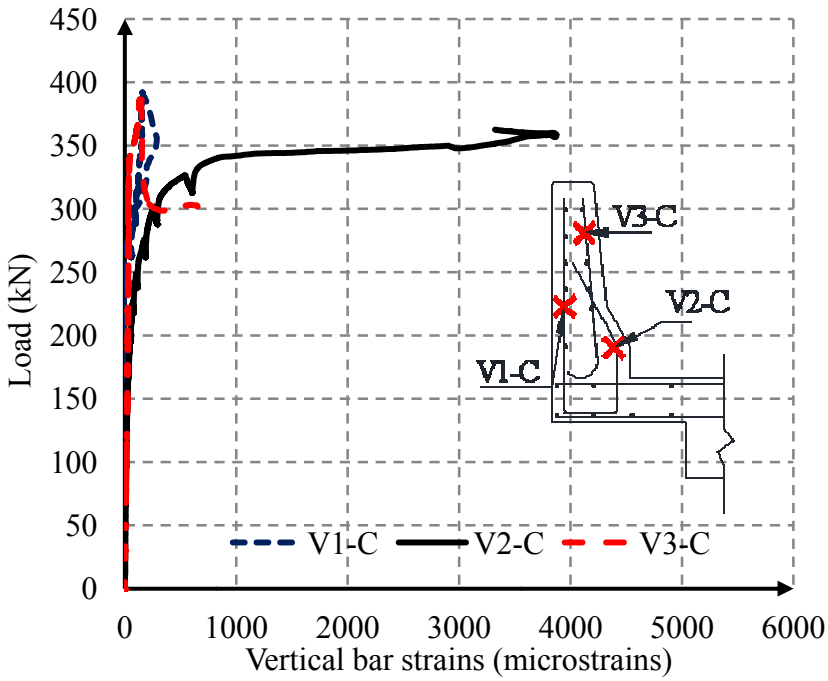

Figure (G-5): Barrier wall vertical bar strains at the centerline of loading for M1 test

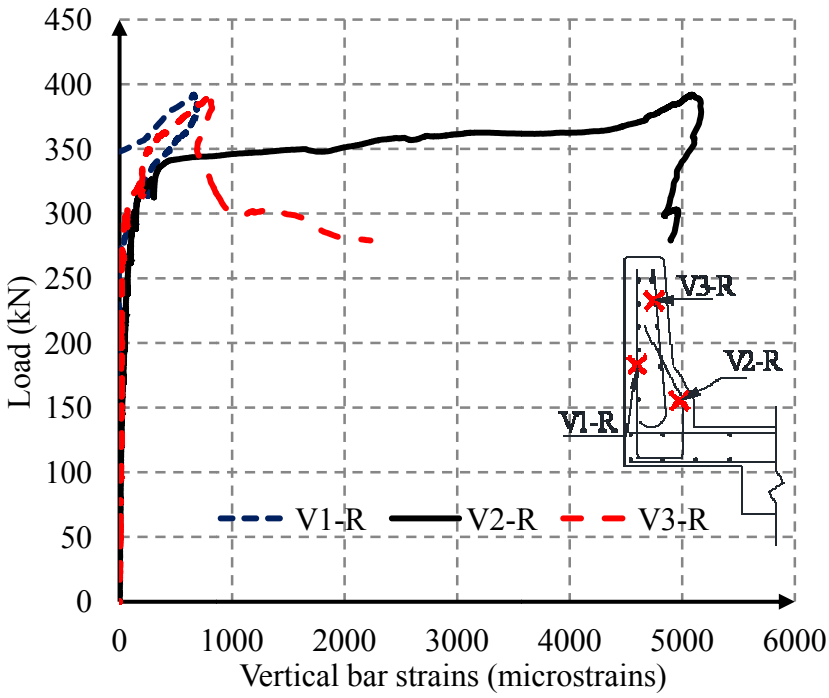

Figure (G-6): Barrier wall vertical bar strains 400 mm right to the centerline of loading for M1 test

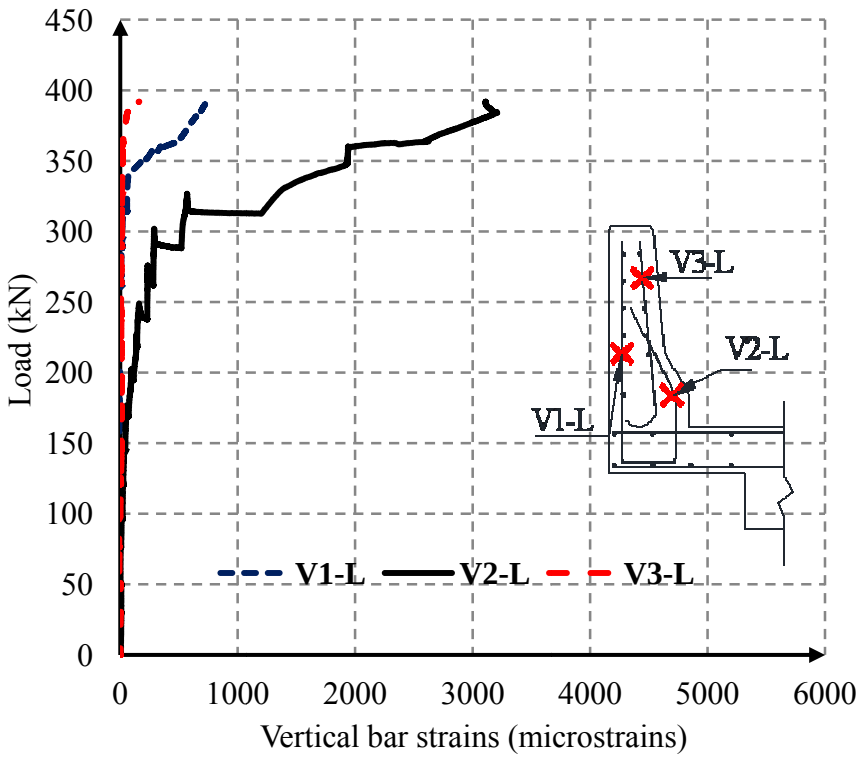

Figure (G-7): Barrier wall vertical bar strains 600 mm left to the centerline of loading for M1 test

G.2. Graphs for M2 Test

G.2.1. Load-Deflection Graph

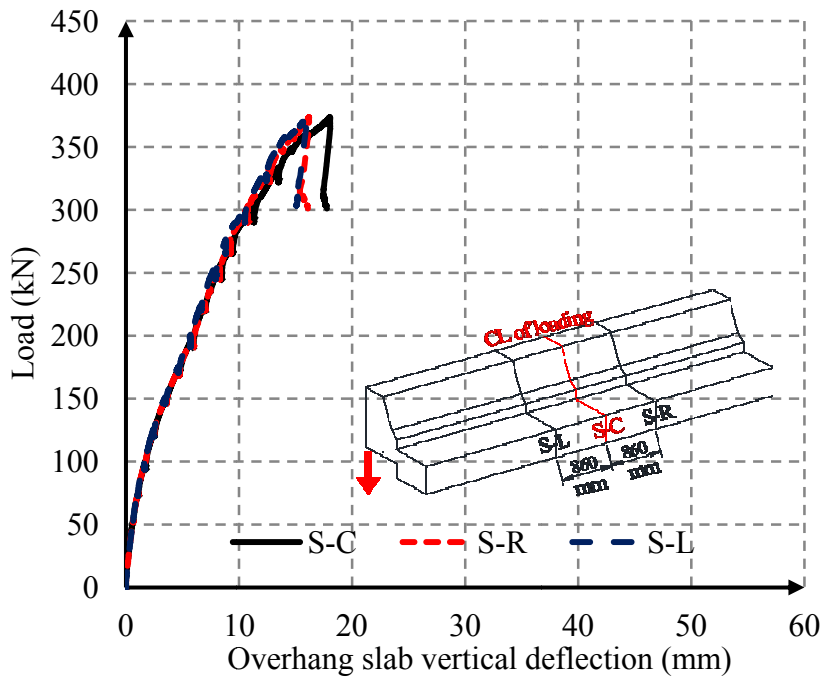

Figure (G-8): Overhang slab vertical deflection for M2 test

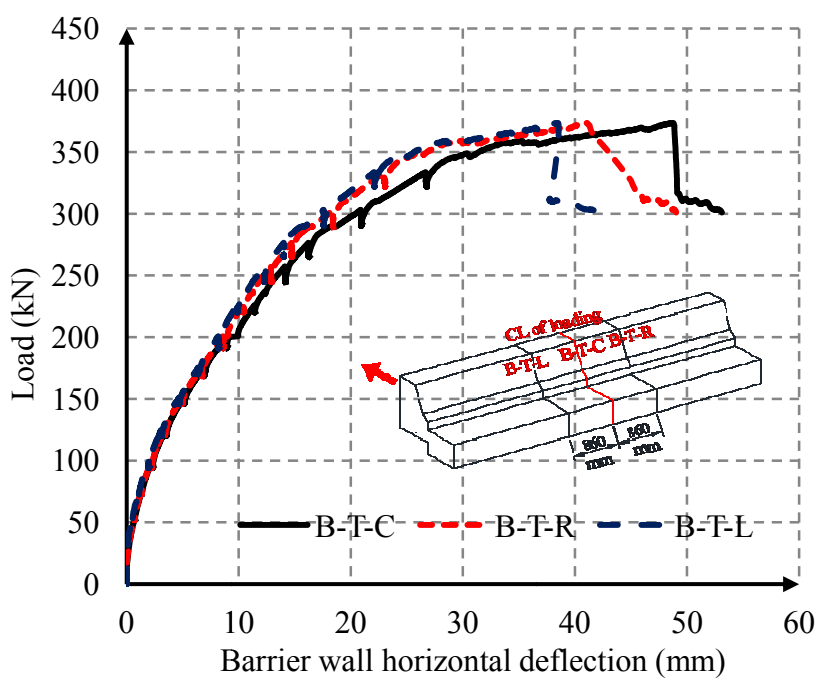

Figure (G-9): Barrier wall horizontal deflection for M2 test

G.2.2. Load-Strain Graph

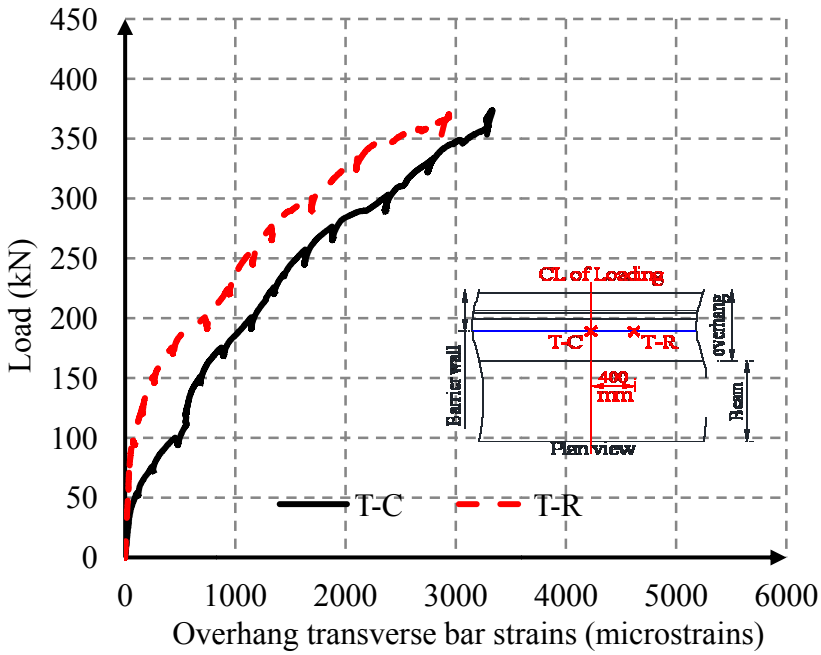

Figure (G-10): Overhang deck slab transverse bar strains for M2 test

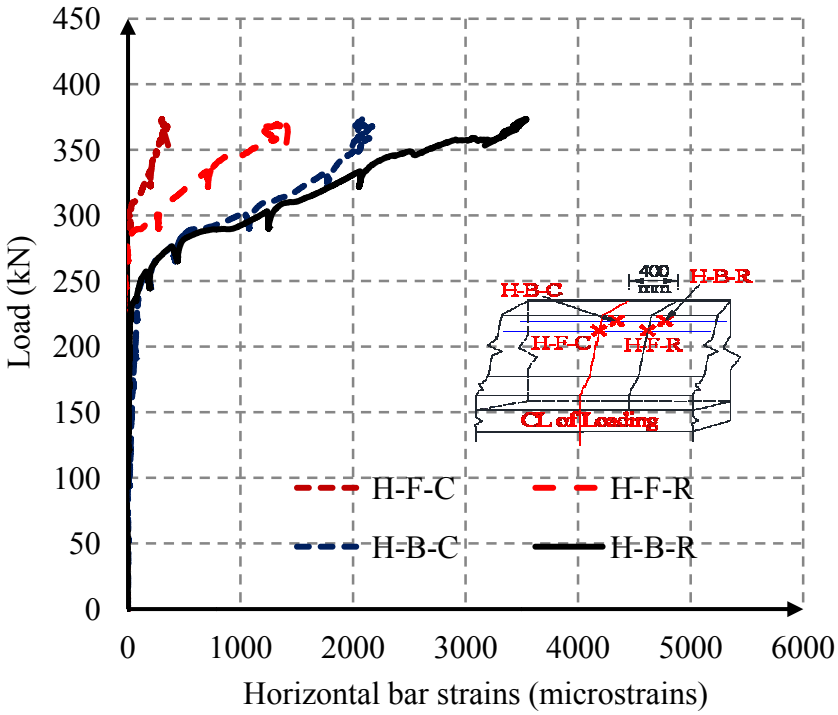

Figure (G-11): Barrier wall horizontal bar strains for M2 test

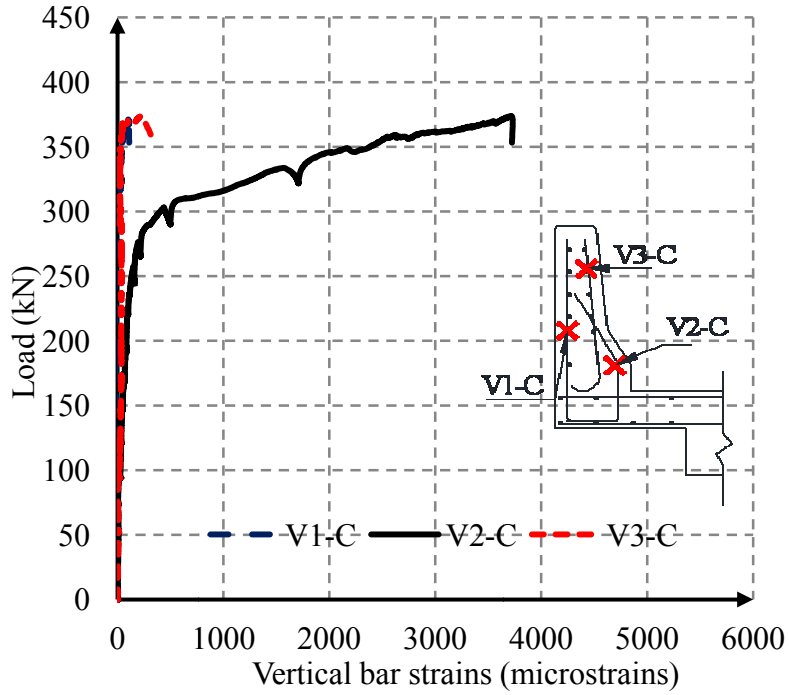

Figure (G-12): Barrier wall vertical bar strains at the centerline of loading for M2 test

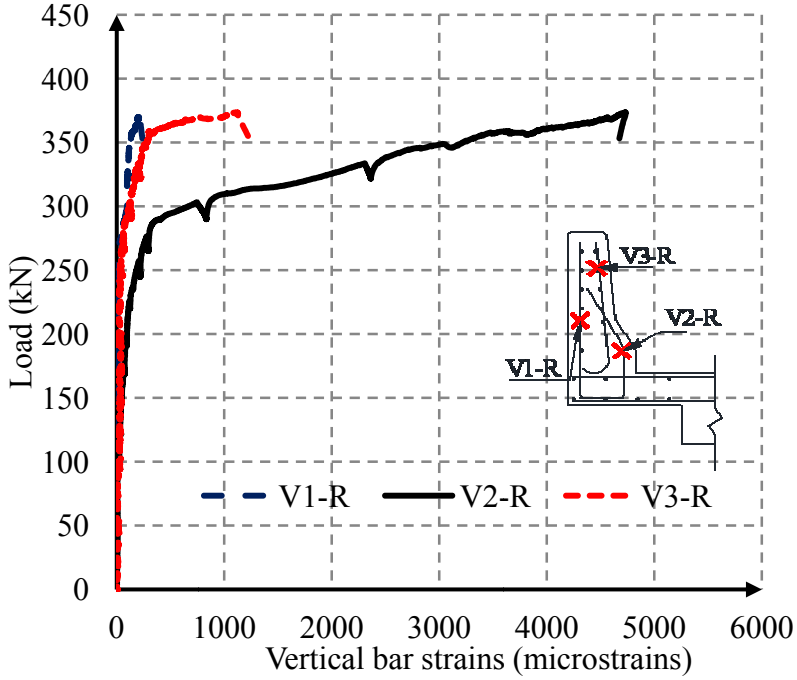

Figure (G-13): Barrier wall vertical bar strains 400 mm right to the centerline of loading for M2 test

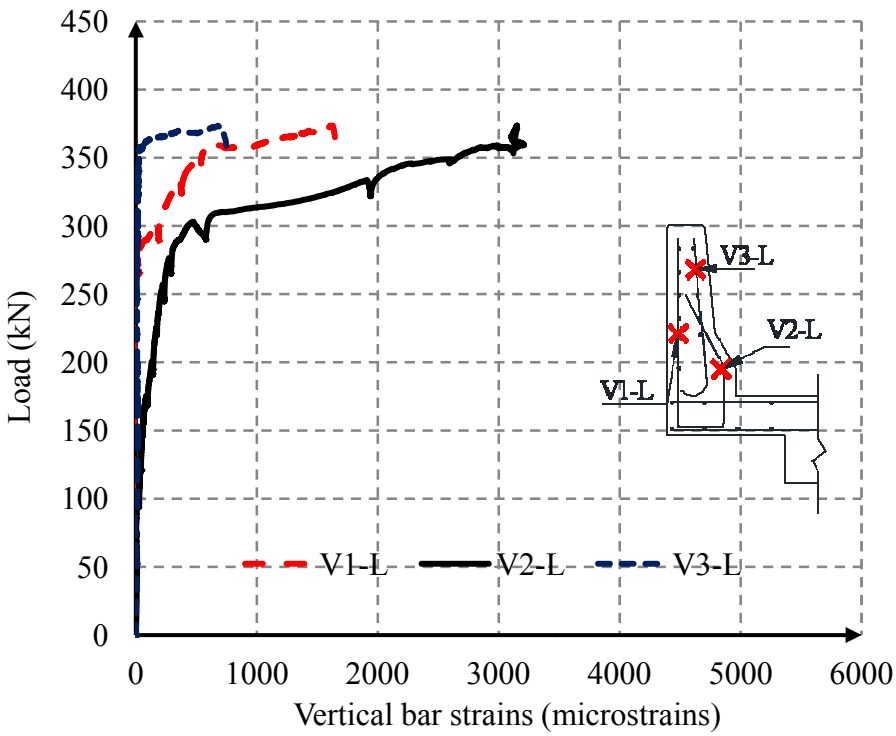

Figure (G-14): Barrier wall vertical bar strains 600 mm left to the centerline of loading for M2 test

G.3. Graphs for RE Test

G.3.1. Load-Deflection Graph

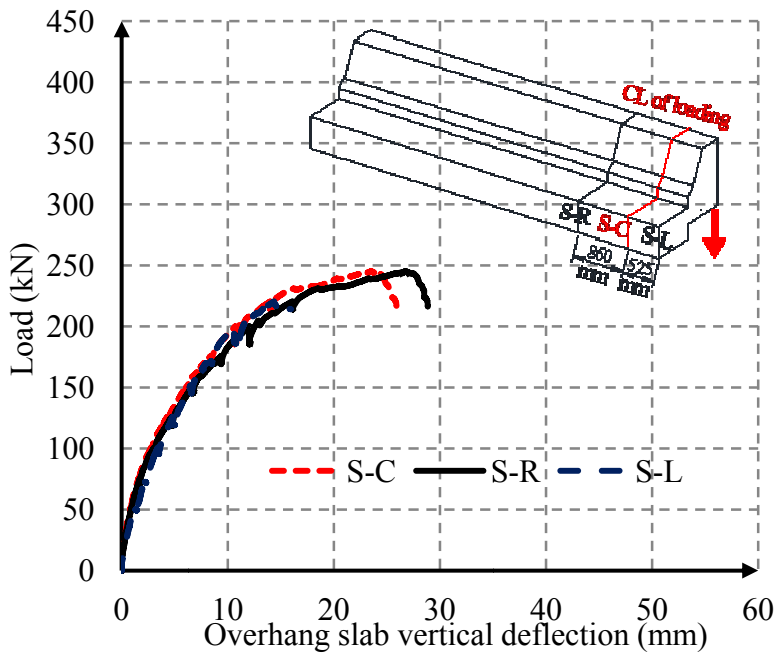

Figure (G-15): Overhang slab vertical deflection for RE test

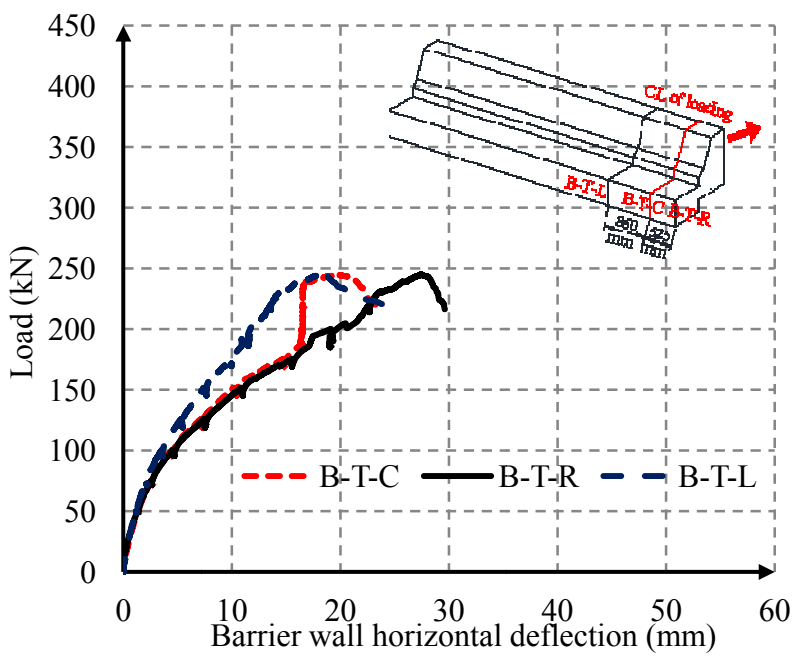

Figure (G-16): Barrier wall horizontal deflection for RE test

G.3.2. Load-Strain Graph

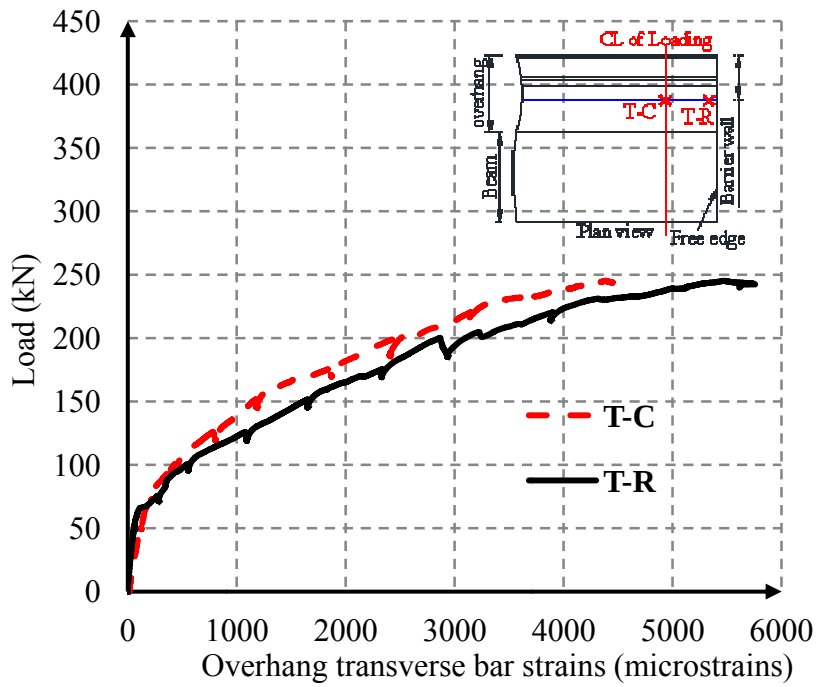

Figure (G-17): Overhang slab transverse bar strains for RE test

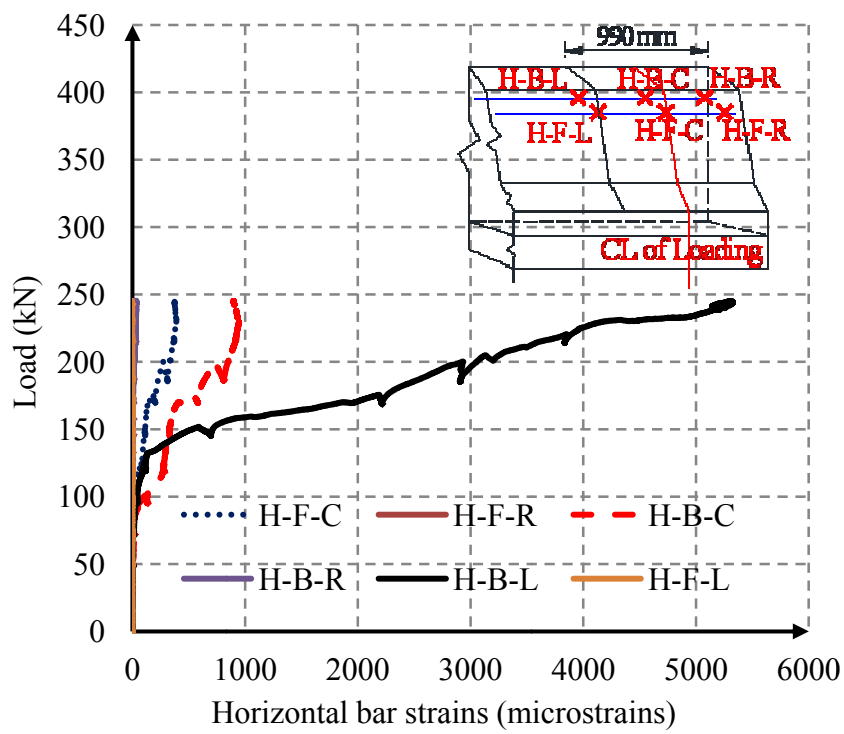

Figure (G-18): barrier wall horizontal bar strains for RE test

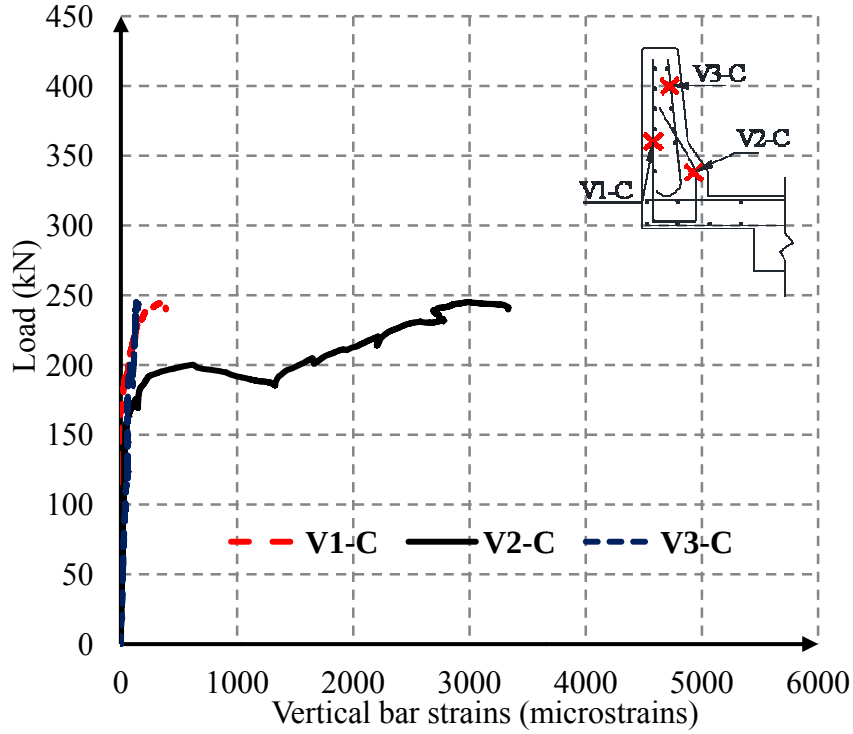

Figure (G-19): Barrier wall vertical bar strains at the centerline of loading for RE test

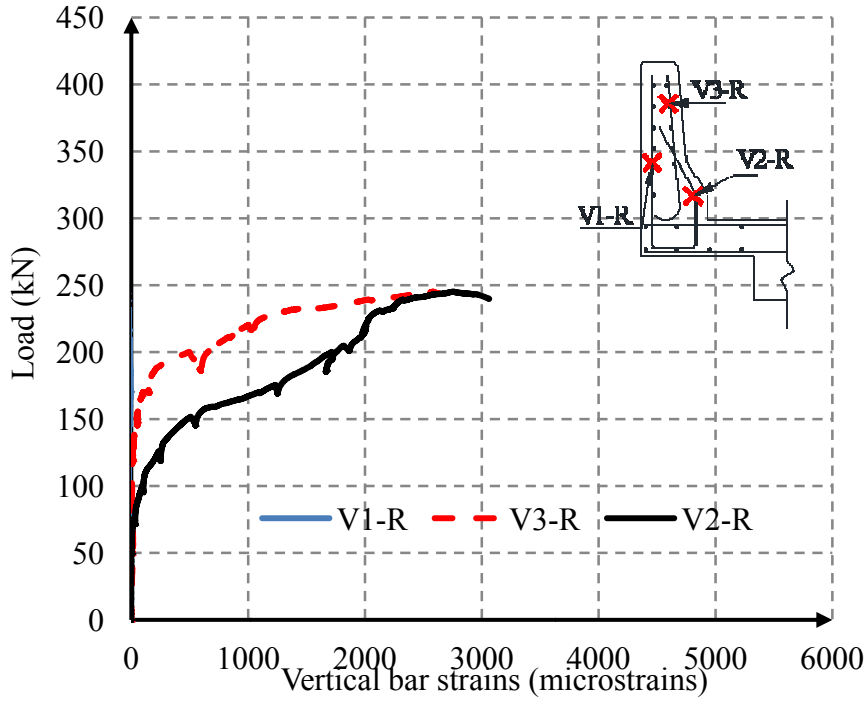

Figure (G-20): Barrier wall vertical bar strains at 400 mm right to the centerline of loading for RE test

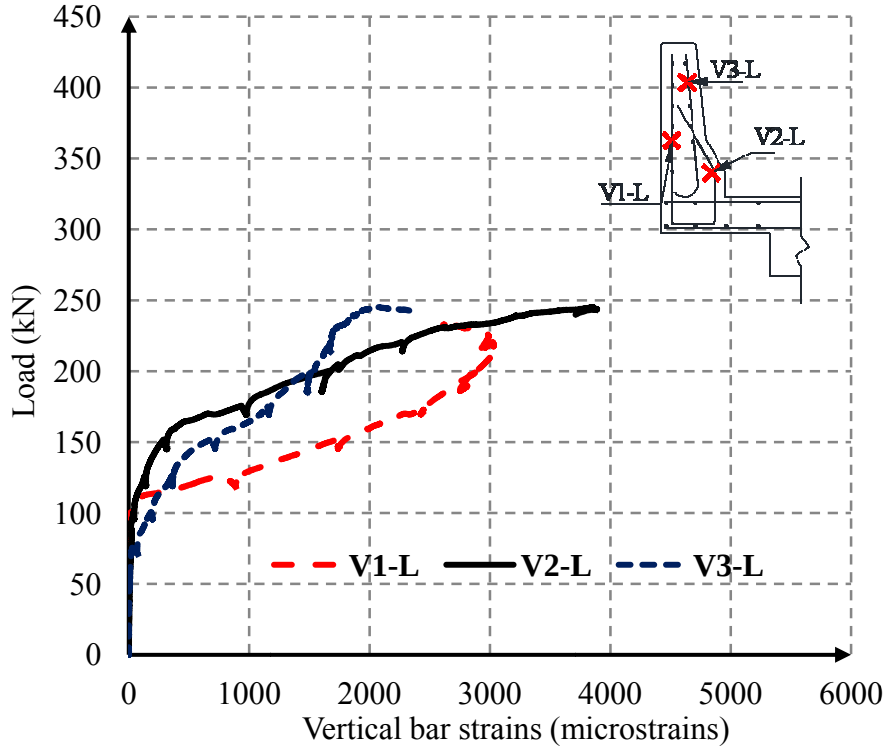

Figure (G-21): Barrier wall vertical bar strains at 600 mm left to the centerline of loading for LE test

G.4. Graphs for LE Test

G.4.1. Load-Deflection Graph

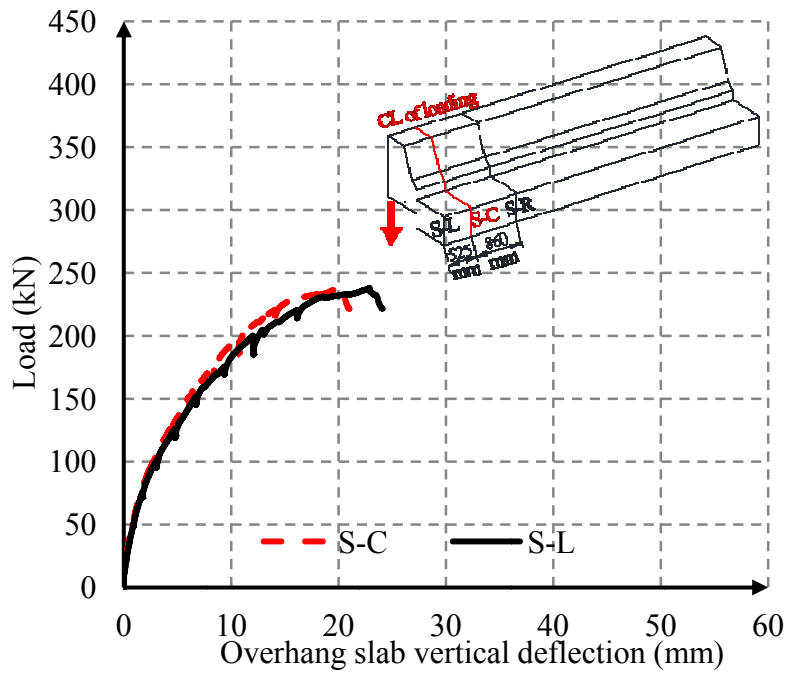

Figure (G-22): Overhang slab vertical deflection for LE test

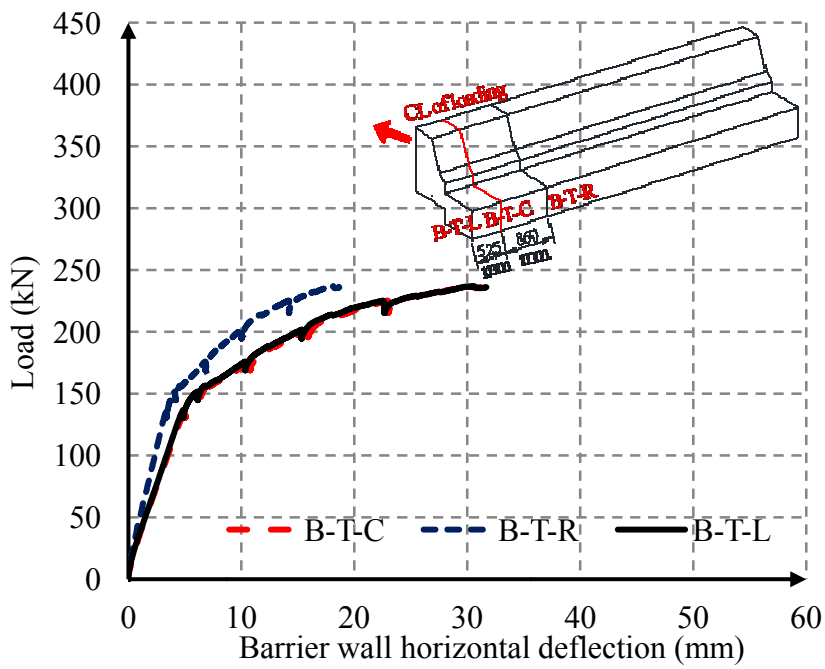

Figure (G-23): Barrier wall horizontal deflection for LE test

G.4.2. Load-Strain Graph

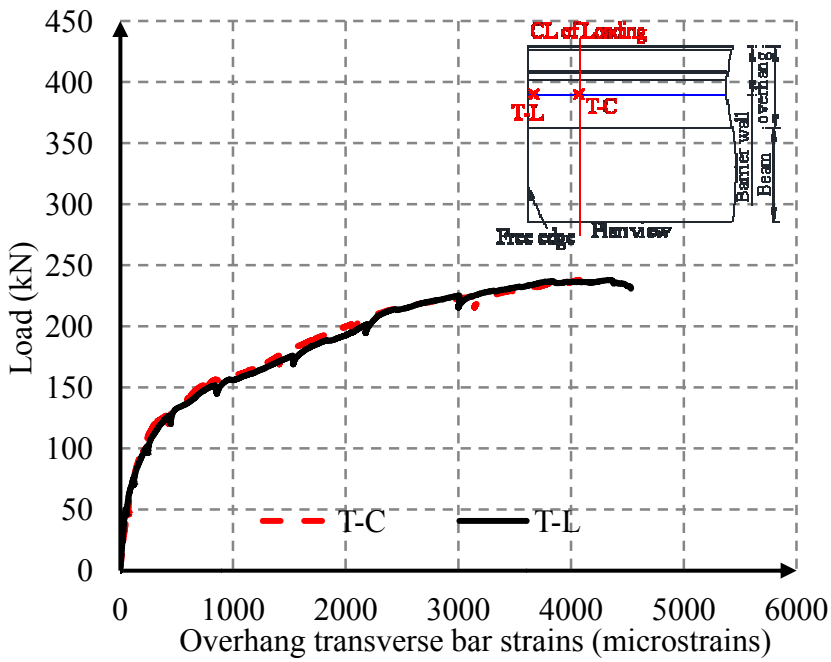

Figure (G-24): Overhang slab transverse bar strains for LE test

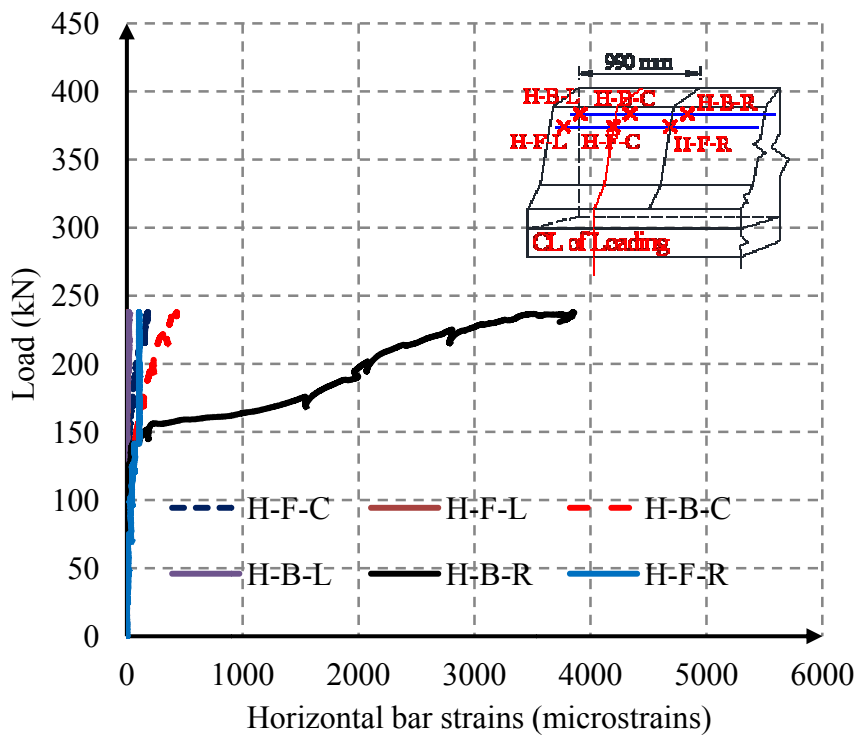

Figure (G-25) Barrier wall horizontal bar strains for LE test

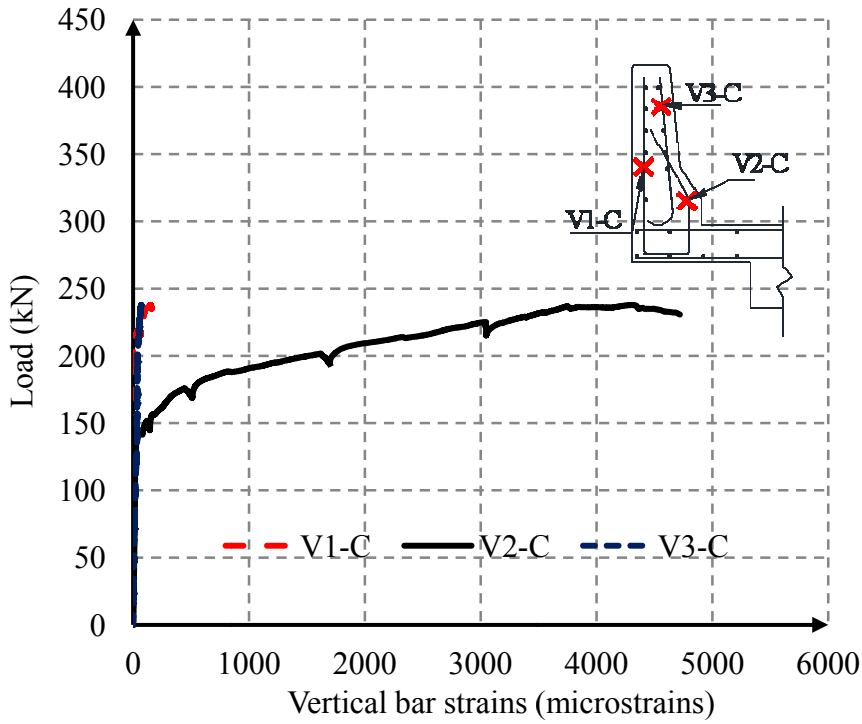

Figure (G-26): Barrier wall vertical bar strains at the centerline of loading for LE test

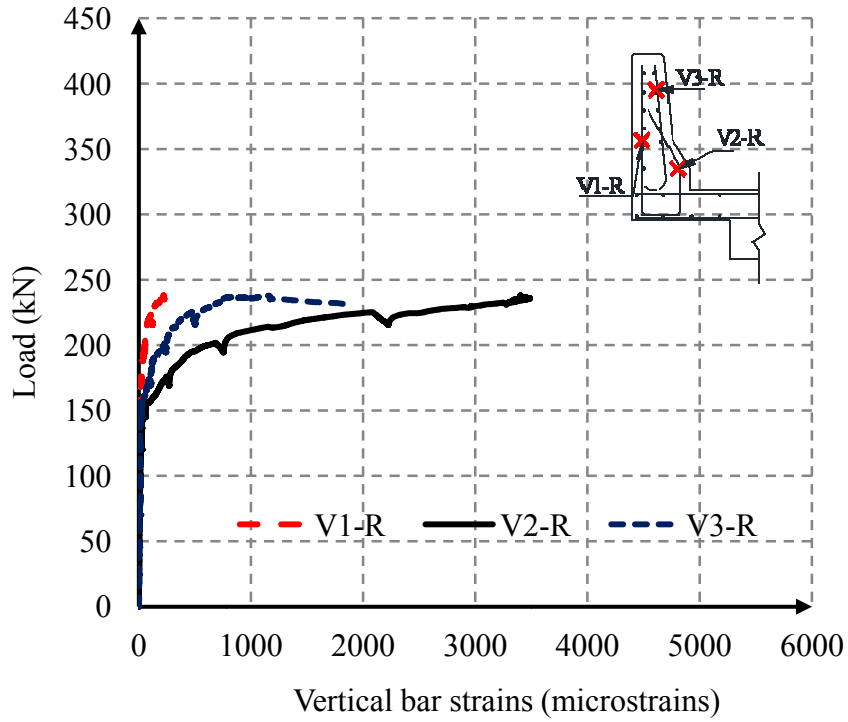

Figure (G-27): Barrier wall vertical bar strains at 400 mm right to the centerline of loading for LE test

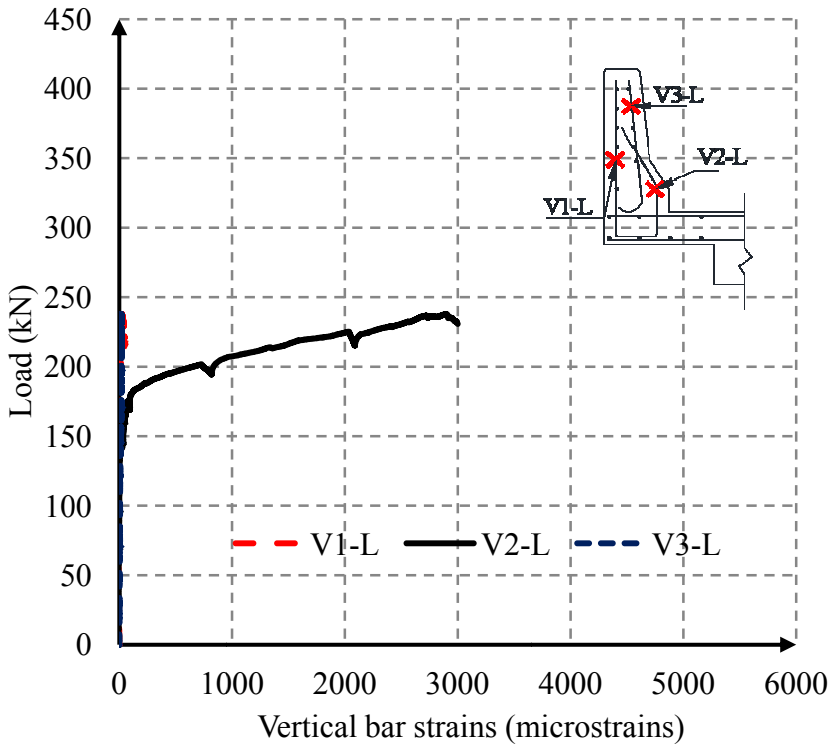

Figure (G-28): Barrier wall vertical bar strains at 600 mm left to the centerline of loading for LE test

G.5. Barrier Wall Vertical Bar Load-Strain Graphs for M1-P Test

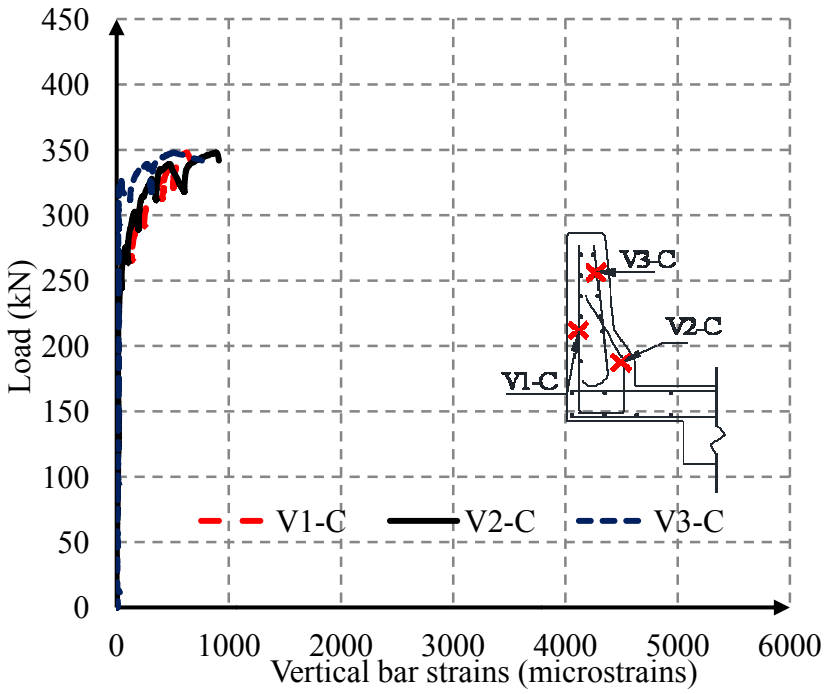

Figure (G-29): Barrier wall vertical bar strains at the centerline of loading for M1-P test

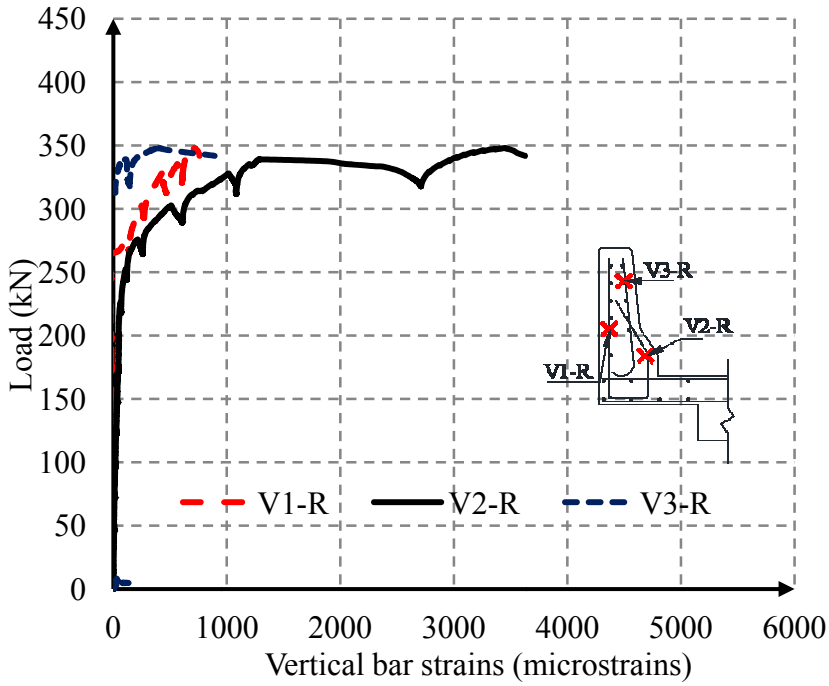

Figure (G-30): Barrier wall vertical bar strains at 400 mm right to the centerline of loading for M1-P test

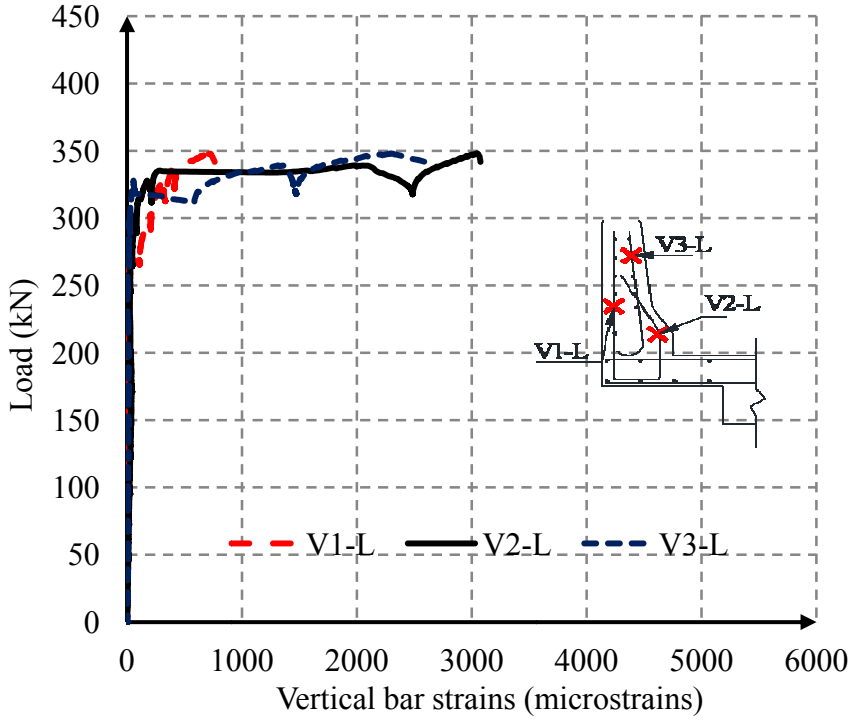

Figure (G-30): Barrier wall vertical bar strains at 600 mm left to the centerline of loading for M1-P test

G.6. Barrier Wall Vertical Bar Load-Strain Graphs for M2-N Test

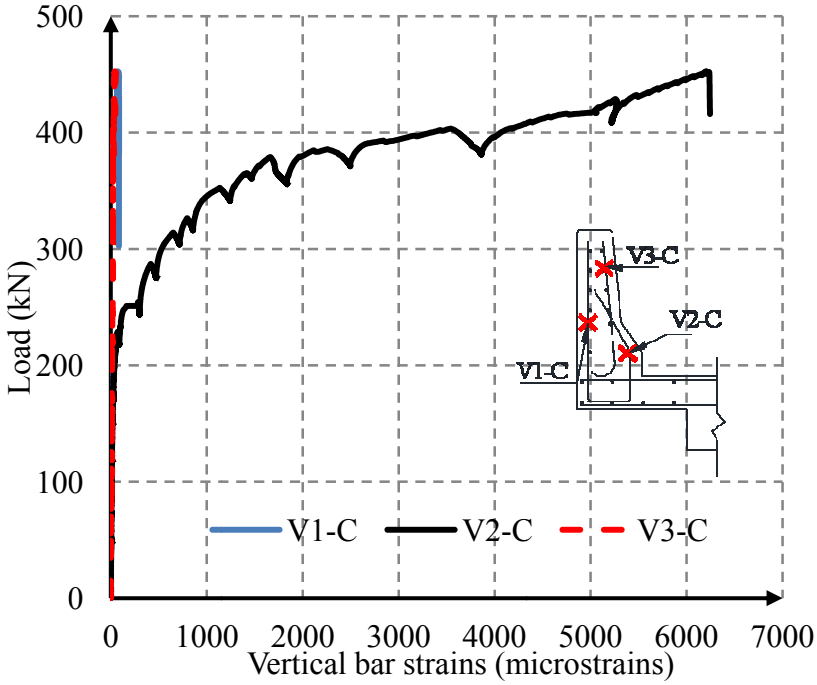

Figure (G-31): Barrier wall vertical bar strains at the centerline of loading for M2-N test

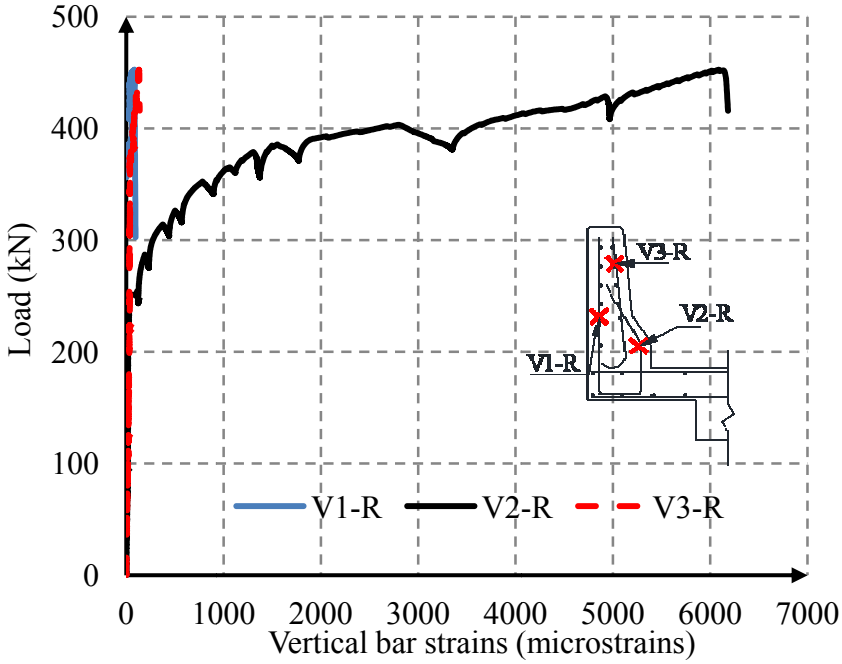

Figure (G-32): Barrier wall vertical bar strains at 400 mm right to the centerline of loading for M2-N test

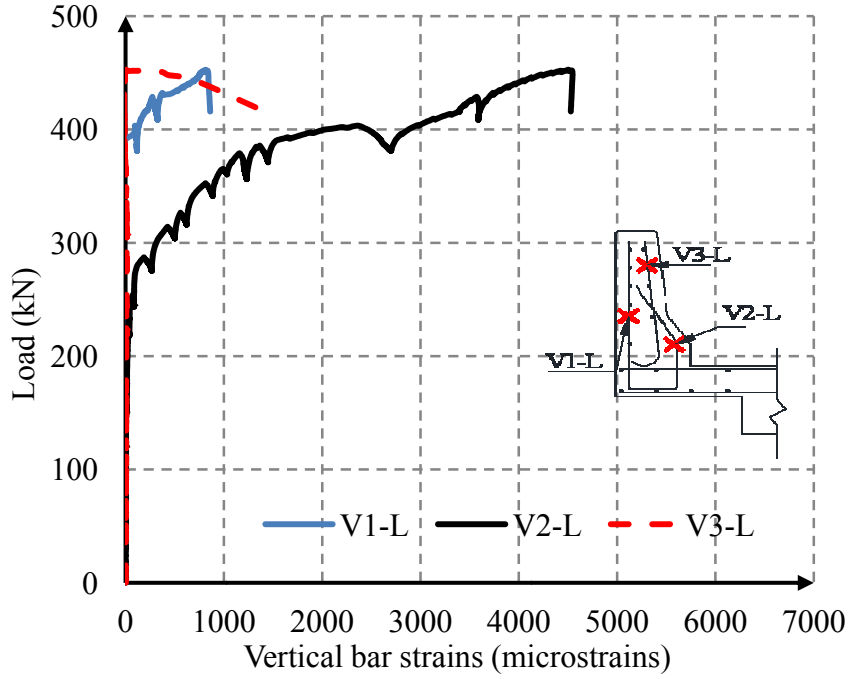

Figure (G-33): Barrier wall vertical bar strains at 600 mm left to the centerline of loading for M2-N test

G.7. Barrier Wall Vertical Bar Load-Strain Graphs for RE-P Test

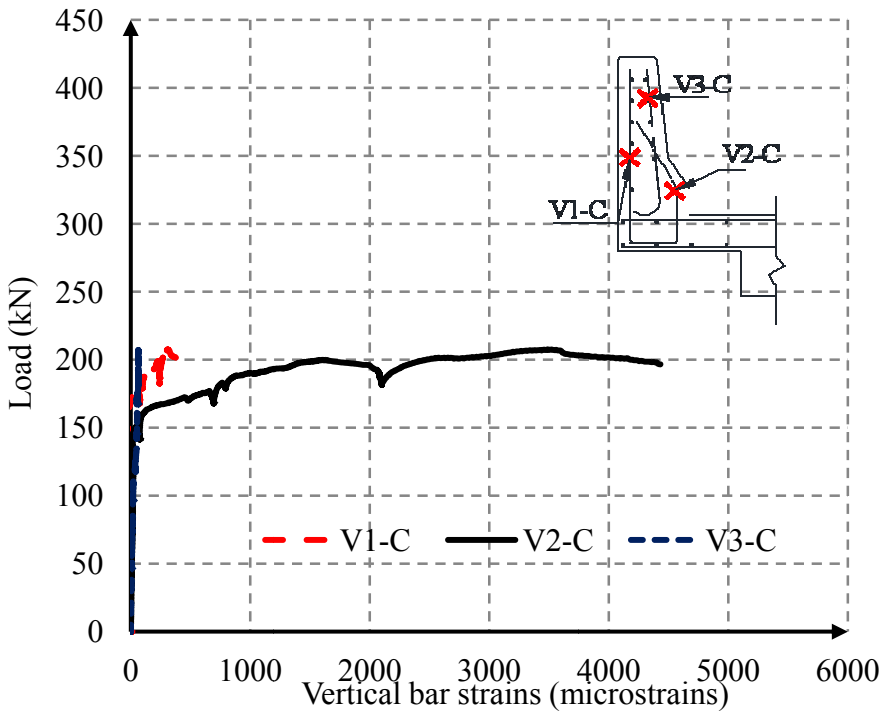

Figure (G-34): Barrier wall vertical bar strains at the centerline of loading for RE-P test

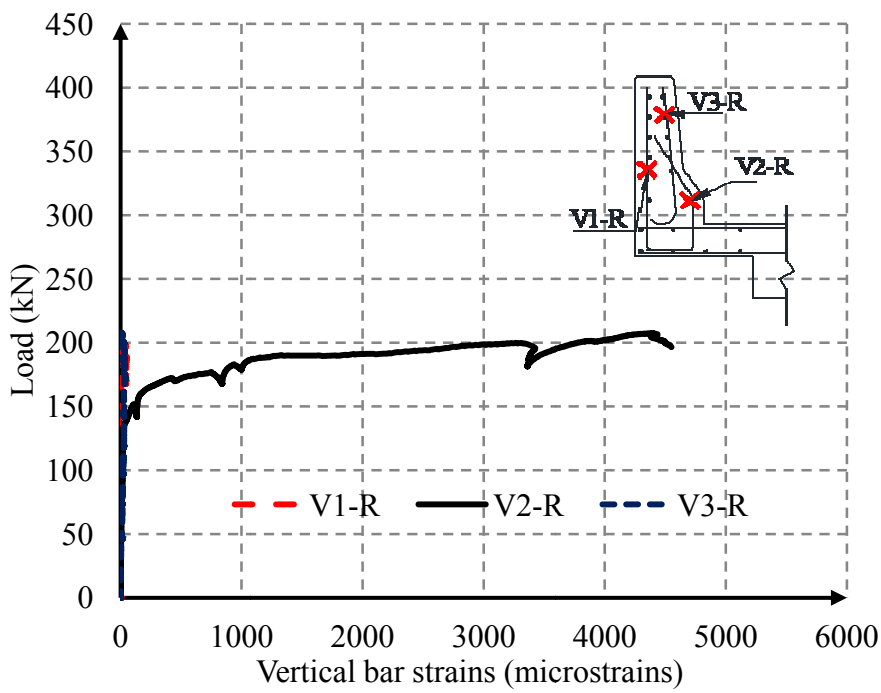

Figure (G-35): Barrier wall vertical bar strains at test side free edge for RE-P test

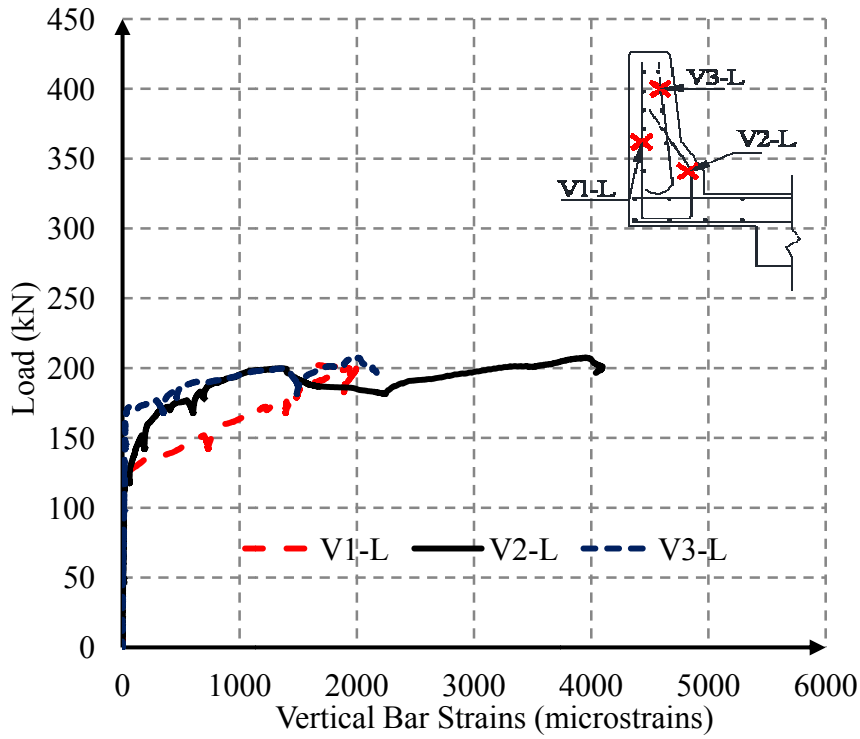

Figure (G-36): Barrier wall vertical bar strains at other side of the centerline of loading for RE-P test

G.8. Barrier Wall Vertical Bar Load-Strain Graphs for LE-N Test

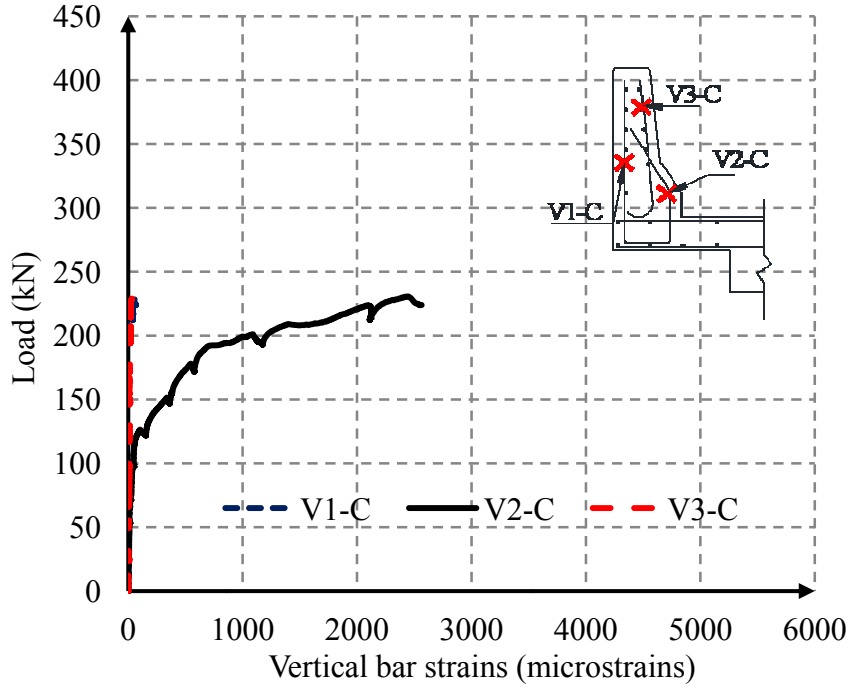

Figure (G-37): Barrier wall vertical bar strains at the centerline of loading for LE-N test

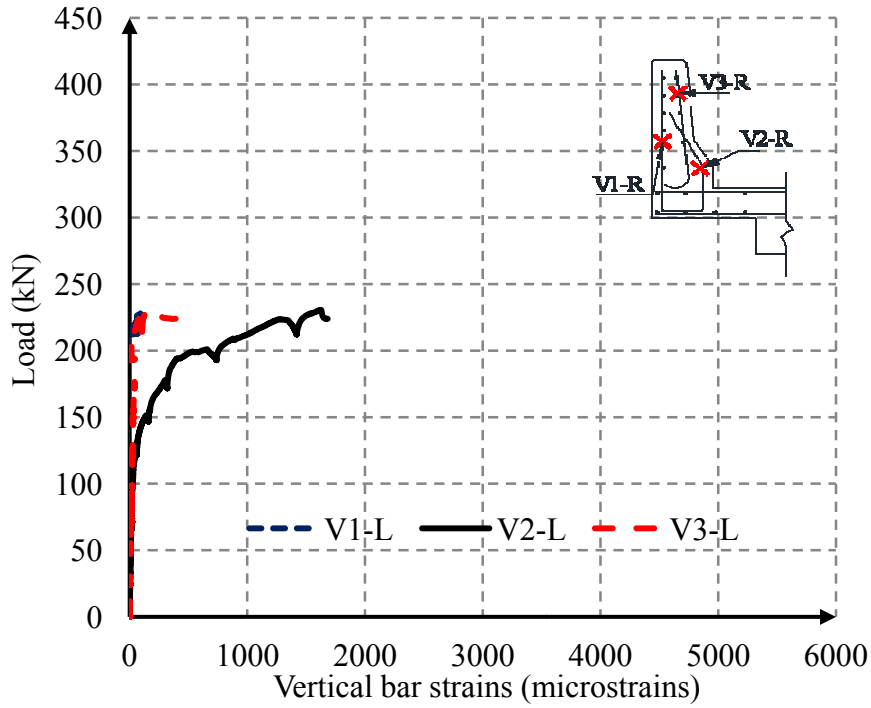

Figure (G-38): Barrier wall vertical bar strains at test side free edge for LE-N test

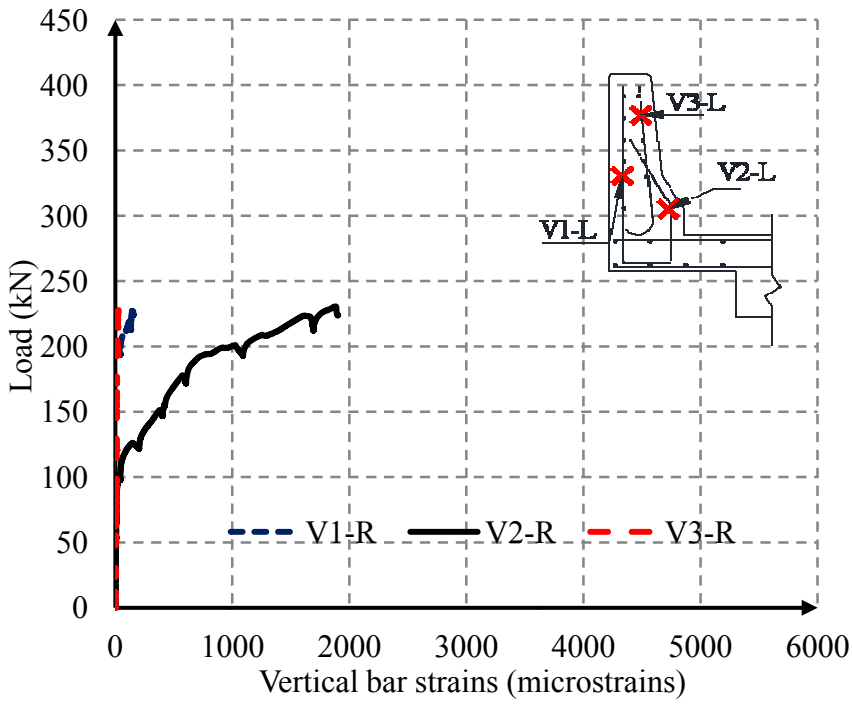

Figure (G-39): Barrier wall vertical bar strains opposite to the centerline of loading for LE-N test